A Critical Review on the Mechanisms of Fe^{2+} Regeneration in Electro-Fenton Process: Fundamentals and Boosting Strategies

Fengxia Deng [a,b], Hugo Olvera-Vargas [c], Minghua Zhou [d], Shan Qiu [a,*], Ignasi Sirés [b,*], Enric Brillas [b,*]

[a] *State Key Laboratory of Urban Water Resource and Environment, School of Environment, Harbin Institute of Technology, Harbin, 150090, P. R. China*

[b] *Laboratori d'Electroquímica dels Materials i del Medi Ambient, Departament de Ciència de Materials i Química Física, Secció de Química Física, Facultat de Química, Universitat de Barcelona, Martí i Franquès 1-11, 08028 Barcelona, Spain*

[c] *Instituto de Energías Renovables, Universidad Nacional Autónoma de México (IER-UNAM), Priv. Xochicalco S/N, Col. Centro, Temixco, Morelos CP 62580, México*

[d] *Key Laboratory of Pollution Process and Environmental Criteria, Ministry of Education, College of Environmental Science and Engineering, Nankai University, Tianjin, 300350, P.R. China*

*Corresponding author:

E-mail address: qiushan@hit.edu.cn (S. Qiu) ; i.sires@ub.edu (I. Sirés); brillas@ub.edu (E. Brillas)

Highlights

- Thorough revision of strategies for improving Fe^{3+} reduction in electro-Fenton
- Tailoring of active sites of carbon-based materials to improve electron transfer
- Development of new electron-rich metal-based materials to boost the Fe^{3+} reduction
- Effect of magnetic field, pulse electrolysis and interfacial Joule heating on mass transport
- Influence of UVA light and in-situ H^+ generation on the mass transport or iron ions

Graphical Abstract

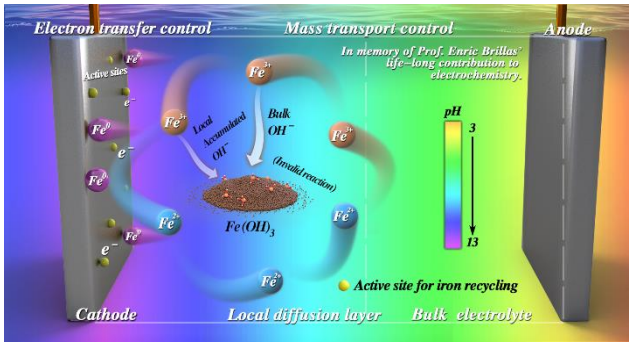

Abstract

This review presents an exhaustive overview on the mechanisms of Fe^{3+} cathodic reduction within the context of electro-Fenton (EF) process. Different strategies developed to improve the reduction rate are discussed, dividing them into two categories that regard the mechanistic feature that is promoted: electron transfer control and mass transport control. Boosting the Fe^{3+} conversion to Fe^{2+} via electron transfer control includes: (i) the formation of a series of active sites in both carbon- and metal-based materials, and (ii) the use of other emerging strategies such as single atom catalysis or confinement effects. Concerning the enhancement of Fe^{2+} regeneration by mass transport control, the main routes involve the application of magnetic fields, pulse electrolysis, interfacial Joule heating effect and photoirradiation. Finally, challenges are singled out and future prospects are described. This review aims to clarify the Fe^{3+}/Fe^{2+} cycling process in EF process, eventually providing essential ideas for smart design of highly effective systems for wastewater treatment and valorization at industrial scale.

Keywords: electron transfer; Fe^{3+} reduction; Fenton's reaction; hydrogen peroxide; mass transport enhancement

Contents

1. Introduction

In recent years, the electro-Fenton (EF) process has emerged as a potentially viable technology for wastewater treatment, owing to some remarkable results achieved. The target effluents under study, containing a great variety of pollutants of emerging concern,[1-3] belong to different industrial sectors such as pharmaceutical, textile, chemical, petrochemical, agricultural and food-processing, among others. In fact, because of its great efficiency and multiple advantages, EF has gained increasing popularity over the last years. In the conventional EF process, H_2O_2 is formed *in-situ* via the cathodic two-electron oxygen reduction reaction (ORR, reaction (1)), thereby being catalytically decomposed by soluble iron ions at acidic pH to produce $^{\bullet}OH$ (with $E°$ = 2.8 V vs SHE) via Fenton's reaction (2).[4-8] The need of external addition of Fe^{2+} catalyst is minimized because Fe^{3+} can be continuously reduced to Fe^{2+} at the cathode surface via reaction (3).[9-11] As a matter of fact, the cathodic regeneration of Fe^{2+} via reaction (3) is a major feature of EF process, since it ensures the continuous production of $^{\bullet}OH$ through reaction (2). The reaction (4) between H_2O_2 and Fe^{3+} also regenerates Fe^{2+}; however, it is much slower and produces the less powerful oxidant hydroperoxyl radical $HO_2^{\bullet}$. In the absence of an efficient Fe^{2+} regeneration, reaction (4) becomes rate-limiting as occurs in the chemical Fenton process. Accordingly, Fe^{2+} regeneration is a distinct characteristic of EF process that becomes the key step to control its efficiency.

$$O_2 + 2e^- + 2H^+ \rightarrow H_2O_2 \qquad (E^0 = 0.695 \text{ V vs. SHE at acid pH}) \qquad (1)$$

$$H_2O_2 + Fe^{2+} \rightarrow Fe^{3+} + {}^{\bullet}OH + OH^- \qquad (k_2 \approx 70 \text{ M}^{-1} \text{ s}^{-1}) \qquad (2)$$

$$Fe^{3+} + e^- \rightarrow Fe^{2+} \qquad (E^0 = 0.771 \text{ V vs. SHE}) \qquad (3)$$

$$H_2O_2 + Fe^{3+} \rightarrow Fe^{2+} + HO_2^{\bullet} + H_2O \qquad (k_2 \approx 0.02 \text{ M}^{-1} \text{ s}^{-1}) \qquad (4)$$

$2H_2O + 2e^- \rightarrow H_2 + 2OH^-$ (E^0 = -0.827 V vs. SHE) (5)

The efficiency of EF is largely dependent on both, H_2O_2 accumulation in the medium and the ability of Fe^{3+} reduction. As a result, in recent years, a growing body of investigations has focused on H_2O_2 production via two-electron ORR due to concerns about the low reactivity/selectivity related to oxygen mass transport limitations.[12-15] A series of reviews on cathodic H_2O_2 generation via 2-e^- ORR has been published, mainly concerning the development of novel cathodes and devices to increase the H_2O_2 accumulation.[16,17] In contrast to the considerable attention given to H_2O_2 production, little research has focused on the Fe^{3+} cathodic reduction, which constitutes a missing gap because Fe^{2+} regeneration is a crucial step in EF. To address this need, this review summarizes the mechanisms involved in Fe^{2+} regeneration during EF, as well as the strategies that have been developed to enhance the reaction.

It could seem that the Fe^{3+} cathodic reduction in the EF process is comparable to the homogenous iron reduction in chemical Fenton-based processes, which have been previously reviewed.[18,19] However, unlike these non-electrochemical processes, Figure 1a shows that the Fe^{3+} reduction through heterogeneous electron transfer in EF takes place at the cathode surface. This reaction is a function of the applied potential, which has a major effect on the double layer within the cathode/electrolyte region. The thermodynamic standard reduction potential of Fe^{3+} in solution (see reaction (3)), whereas the heterogeneous Fe^{3+} reduction in EF is driven by the external potential applied to the cell, which is the so-called overpotential.[20] Electron kinetics, diffusion, and hydrodynamics determine the rate of iron cathodic reduction. As shown in Figure 1b, the local cathode/electrolyte region includes the double layer (0.5-10 nm thick) and the diffusion layer (1-100 μm thick). The iron ions motion in the diffusion layer is driven by diffusion, while in the double layer (including the inner Helmholtz plane (IHP)

and outer Helmholtz plane (OHP)), it is dominated by the strong electrostatic field. Also, unlike conventional Fenton, in EF there appears a pH gradient between the bulk solution and the close vicinity of the cathode (the specific pH value in each volume portion denoted as microenvironment) (see Figure 1b). More precisely, the pH in the cathodic microenvironment could reach a value as high as 13, or even greater because of the continuous cathodic production of OH^- resulting from the HER (reaction (5)) or from ORR as dissolved O_2 in the vicinity of cathode becomes reduced.[21,22] Considering the abovementioned differences between the Fe^{3+} reduction in conventional Fenton (homogeneous reaction) and EF (mainly heterogeneous reaction), it is evident that there is still a knowledge gap to clearly elucidate the behavior observed in both processes. The understanding of the fundamentals of the Fe^{3+} cathodic reduction in EF is thus of great relevance to guide its efficient design and scale-up.

This review, for the first time, intends to systematically compile recent progress on the different approaches that have been developed to boost the Fe^{3+} cathodic reduction in the EF process for enhancing the Fe^{2+} regeneration. First, the basic mechanisms of the Fe^{3+}/Fe^{2+} cycling process during EF are discussed. The strategies to enhance the Fe^{2+} regeneration via Fe^{3+} cathodic reduction are subsequently detailed and examined, distinguishing between: (i) approaches for electron transfer acceleration, and (ii) designs for mass transport improvement. To sum up, a description of challenges and proposal of future prospects is presented.

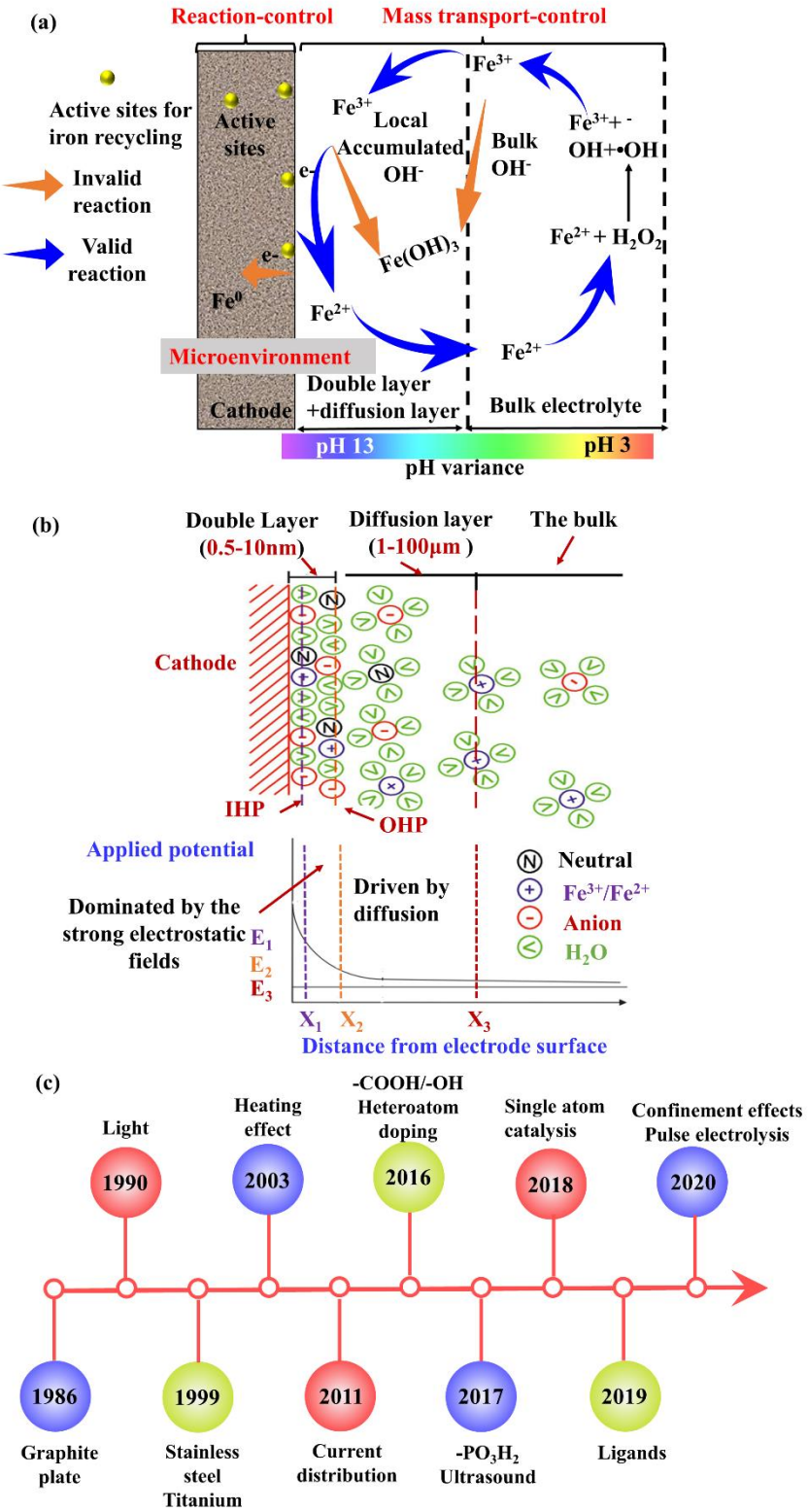

Figure 1. (a) Fe^{3+}/Fe^{2+} cycle in the electro-Fenton process (without considering the involvement of electrogenerated H_2O_2, for the sake of simplicity). (b) Scheme of the structure of the cathode/electrolyte interface, including the inner Helmholtz plane (IHP), outer Helmholtz plane (OHP), and diffusion layer. (c) Historical development of strategies for Fe^{3+} cathodic reduction in the EF process. X_1, X_2, X_3 account for the different distances to the electrode surface: IHP, OHP and diffusion layer. E_1, E_2, E_3 are the related potentials positioned at X_1, X_2 and X_3, respectively.

2. Fundamentals of Fe^{3+} cathodic reduction

2.1. Fe^{3+} cathodic reduction in EF

Prior to reviewing the strategies to increase the Fe^{3+}-to-Fe^{2+} conversion rate, this subsection presents the mechanistic fundamentals of Fe^{3+} reduction. Overall, once soluble Fe^{2+} is oxidized into Fe^{3+} in the bulk via the classical Fenton´s reaction (2), the metal ions diffuse through the solution until the active sites are reached on the cathode surface, where they receive the electrons to be reduced to Fe^{2+} via reaction (3). As can be seen in Figure 1a, the pH affects the Fe^{3+}/Fe^{2+} cycle. First, dissolved Fe^{3+} in the bulk solution precipitates in the form of insoluble hydroxide when pH is over 4 (H^+ concentration of 10^{-7}-10^{-8} M), not being further available for Fe^{2+} regeneration.[23] Fe^{2+} can co-precipitate with insoluble complexes, reducing the amount of soluble Fe^{2+} available for Fenton´s reaction (2).[24] Second, special attention must be paid to the pH in the close vicinity of the cathode, which increases due to the formation of OH^- through the HER by reaction (5) and ORR by reaction (1). The local pH could be as high as 13, which is much higher than that in the bulk, as previously modelled.[21] The local alkalinization of the volume near the cathode causes the Fe^{3+} precipitation as it approaches the electrode surface. This dynamic and alkaline microenvironment in the vicinity of the cathode could also impede the mass transport of iron ions. The iron precipitation can be partly minimized by promoting the mass transport of H^+ and OH^- from and toward the bulk solution, respectively, which can be achieved by means of enhanced convection. However, the continuous supply of H^+ from the bulk to the cathode vicinity via forced convection cannot be maintained owing to mass transport limitations, leading to concentration overpotentials.

The rate of Fe^{3+} cathodic reduction can be simply expressed as $r = k_1[Fe^{3+}]$ (where k_1 represents the heterogeneous rate constant for electron transfer and $[Fe^{3+}]$ is the local

Fe^{3+} concentration), also involving H^+ (acid pH) and e^-.[25] Therefore, there are two potential strategies to improve the reduction rate:

(i) The enhancement of electron transfer by regulating the kinetic rate constant through catalytic effects, as for example those emerging upon creation of active sites in carbon- or metal-based materials, use of single atom catalysts and confinement methods;

(ii) The enhancement of mass transport by increasing the concentration of Fe^{3+}/Fe^{2+} ions near the cathode surface through a physical effect such as a magnetic field, pulse electrolysis or interfacial Joule heating effect.

2.2. History of cathodic Fe^{3+}/Fe^{2+} cycling in EF

As can be observed in Figure 1c, the first investigation on the cathodic Fe^{3+}/Fe^{2+} cycling process in the field of wastewater treatment dates to 1986, when the Fe^{3+} reduction rate was optimized to obtain the maximum phenol degradation by an EF process involving the electrochemical generation of the Fenton´s reagent.[26,27] Nevertheless, note that the term "electro-Fenton" was first used by Prof. Brillas in 1996.[28] After their first publication, the Brillas' group has made significant progress in EF process, laying the foundations of the technology, especially on the aspects related to the use of carbon-based cathodes like carbon-PTFE gas-diffusion electrodes for H_2O_2 electrogeneration and Fe^{3+} reduction. At the initial stage of EF development, only commercial cathodes like lead, stainless steel, titanium, and graphite were used to assess the Fe^{3+}/Fe^{2+} cycle, with stainless steel cathode showing the highest initial current efficiency in an EF-like process with external H_2O_2 addition.[29] With the rapid progress in materials science, a series of new cathodes and surface modification methods were introduced into EF research. These novelties included oxygen-functional groups or heteroatom electrode doping,[30] the use of carbon-based nanomaterials such as graphene[31] and, more recently, emerging single atom catalysts[32] and confinement

effects[33] (see Figure 1c). Aside from the progress on cathode materials for improving the Fe^{3+} reduction, other phenomena have been implemented to enhance the Fe^{3+}/Fe^{2+} cycling, as for example photoirradiation, magnetic fields, pulse electrolysis and interfacial Joule heating effect.[34] In summary, the development of cathodic iron reduction in EF has taken two main directions: (i) the survey and fabrication of different cathode materials to boost the electron transfer to Fe^{3+}, and (ii) the application of external fields to enhance the mass transport of iron ions to the cathode surface.

3. Electron transfer improvement

The Fe^{3+}-to-Fe^{2+} cathodic conversion in EF is simultaneously controlled by electron transfer on the cathode (k_1) and the mass transport of iron ions to/from the cathode (closely related to the local Fe^{3+} concentration). This section is focused on the electron transfer process during the occurrence of the Fe^{3+}/Fe^{2+} cycle, determined by a catalytic effect. Since the nature and content of active sites on the cathode surface are the basis for such catalytic effect, different types of active sites and the involved mechanisms in the Fe^{3+} reduction are reviewed, along with the state-of-art of existing processes for increasing the number of active sites to improve the Fe^{2+} regeneration.

3.1. Electron-rich carbon-based materials

Carbon materials are prepared by thermochemical conversion of organic feedstock. They show excellent "electron shuttle" capacity to mediate electron transfer, as in the case of iron reduction. Consequently, carbon materials have been widely used to favor different redox reactions.[35] Carbon-based materials include carbon nanotubes, activated carbon, hydrothermal carbon, biochar, graphene, graphite, carbon black, fullerol and coal, among others.[36] Systematic reviews on the synthesis of the surface functional groups are available in the literature.[17,37-40] Even though the reduction mechanisms of

Fe^{3+} species on carbon materials in EF are not yet fully understood, three types of active sites on the surface of carbon materials have been reported to be directly involved in iron reduction (see Figure 2):

(i) The carbon backbone itself, which serves as electron donor via conjugated aromatic (sub-)structures, edge atoms and defects;[41-43]

(ii) oxygen-containing surface functional groups bonded to carbon atoms, giving rise to carbonyl, quinone, hydroquinone, hydroxyl and epoxy groups that act as active sites:[44,45]

(iii) heteroatom-based active sites introduced in the carbon structure.

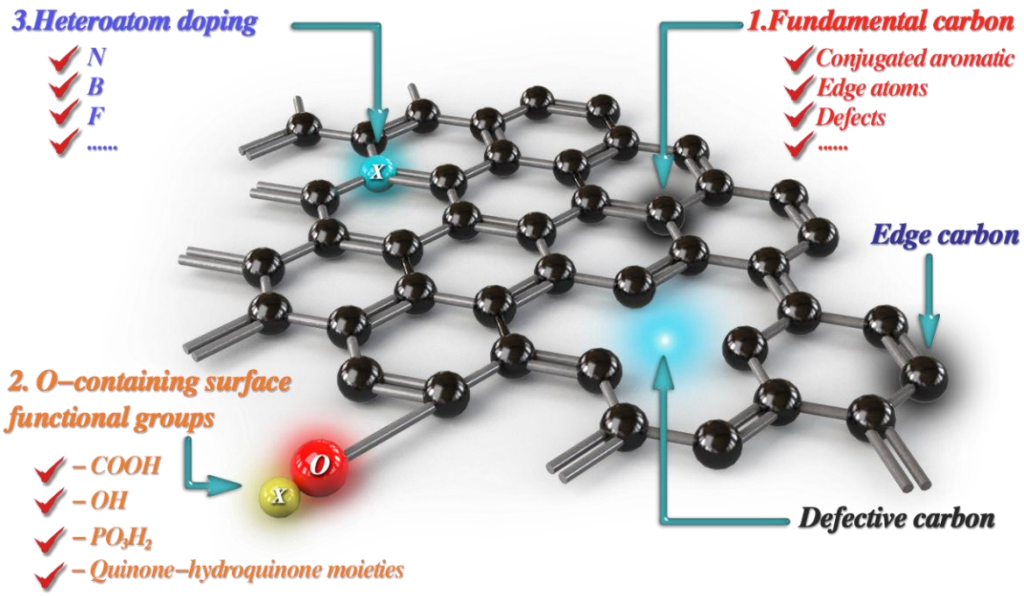

Figure 2. Classification of catalytic active sites in carbonaceous materials for Fe^{3+} reduction in EF.

3.1.1. Carbon-based structures as electron donor

Electron conductivity through the conjugated π-electrons in carbon materials is well known, being defined as an electron shuttling phenomenon.[51] In general, carbon materials are only the interface where electron transfer occurs (Fe^{3+} reduction, O_2 reduction or any other competing reactions), and their catalytic properties remain stable

as long as their structure is not altered by the chemical environment or exceedingly high electrode potentials.[45] However, it has been reported that the structure of some materials such as granular activated carbon, porous carbon and graphene aerogel may act as an electron donor to boost the Fe^{3+} reduction via reaction (6), where $(carbon\ material)^+$ and carbon material are their oxidized and reduced states, respectively. The reduced form can be recovered via reaction (7).[31,41,47]

$$Carbon\ material + Fe^{3+} \rightarrow (Carbon\ material)^+ + Fe^{2+} \quad (6)$$

$$(Carbon\ material)^+ + H_2O_2 \rightarrow Carbon\ material + HOO^{\bullet} + H^+ \quad (7)$$

A similar behavior has been observed on powdered activated carbon (PAC) and carbon nanotubes (CNTs), where CNTs presented a higher reduction capacity than PAC.[48] It should be noted that the difference in the Fe^{3+} reduction efficiency could also come from the disparity in the active surface areas (and thus the number of active sites) of the materials, as also verified when comparing the reduction ability of a planar-like gas-diffusion cathode and a 3D carbon felt,[49] but further research is needed to confirm the main phenomena involved. Cage-like C_{60} fullerene, rich in electrons and unsaturated bonds, can also provide electrons to boost Fe^{3+} reduction, as recently reported.[51] Worth mentioning, electron holes, defective sites and special edges (armchair and zigzag edges) may appear during the fabrication of carbon materials, and such sites can provide extra electronic states behaving as active sites for iron reduction. For example, Yoo et al.[39] found that the delocalized π-electrons of graphitic layers in porous carbon promoted Fe^{3+} reduction. These authors reported that the edge of the carbon plane bound with unsaturated carbon/heteroatoms (like oxygen) was enriched in unpaired electrons that were transferred to Fe^{3+} for reduction. Nanoscale carbon quantum dots (CQDs) derived from thermal decomposition of glucose also proved to accelerate the Fe^{2+} regeneration. Their reduction ability was utilized to reduce

chloroauric acid to form gold nanoparticles.[51] Zubir et al.[52] fabricated a graphene oxide (GO)-Fe_3O_4 composite and confirmed the continuous reduction of Fe^{3+} to Fe^{2+} from the unpaired π electrons of GO transferred to Fe_3O_4.

3.1.2. Surface functional groups

3.1.2.1. -COOH

The electron transfer rate of Fe^{3+} cathodic reduction has been found to be strongly dependent on the oxygen-containing functional groups on the cathode surface, as observed for carbonyl groups.[53,54] In general, a compound with a standard redox potential lower than $E°$ (Fe^{3+}/Fe^{2+}) could reduce Fe^{3+} into Fe^{2+}. O-containing functionalities with a low redox potential are then able to reduce Fe^{3+} in EF, as is the case of single-walled CNTs with E^o = 0.5 V/SHE,[55] and oxygen functional groups doped on carbon felt.[56] Yang et al.[44] reported that carboxyl groups (-COOH) instead of hydroxyl (-OH) and carbonyl groups (-C=O) were the active sites for Fe(III) complexation, which promoted the Fe(III) reduction. Fe complexation accelerated the homolytic cleavage of the formed Fe-OOH complexes by H_2O_2, which is the rate-limiting step for iron reduction ($k = 2.7 \times 10^{-3}$ s^{-1}). This acceleration was attributed to two aspects: (i) a much lower charge transfer energy from H_2O_2 to Fe(III) as the electron density of Fe(III) migrated to the -COOH groups, and (ii) a weaker Fe-O bond caused by the carbonyl group steric effect. The important role of -COOH in iron reduction was also reported for fullerol.[50] At low pH (< 5.0), the formation of carbonyl/carboxyl and an open-caged structure induced the formation of Fe(III)-fullerene surface complexes that experienced intramolecular electron transfer for iron reduction enhanced by visible light following reactions (8)-(10), where * denotes an excited state. At an extremely lower pH value, more protonated fullerol had less oxygen-binding sites for Fe^{3+}

complexation. In a word, -COOH served as iron anchor via complexation, which was a prerequisite for Fe(III) reduction. Note that despite the effective Fe^{3+} reducing capacity of O-bearing functional groups, from our perspective, more attention should be paid to the stability of such active sites in future investigations. For instance, it has been reported that -COOH tended to be reduced during electrolysis at negative potential.[57] Kou et al.[58] reported that Fe^{3+} was sufficient to oxidize carboxyl groups on graphene following a first-order reaction at a high temperature of 90 ºC via reaction (11), whereas it was negligible at low temperature.

$$\text{Fe(III)-}C_{60}(OH)_X^* \xrightarrow{\text{dark/slow}} [C_{60}(OH)_X]_{OX} + \text{Fe(II)} \quad (8)$$

$$\text{Fe(III)-}{}^3C_{60}(OH)_X{}^* \xrightarrow{\text{visible light/fast}} [C_{60}(OH)_X]_{OX} + \text{Fe(II)} \quad (9)$$

$$\text{Fe(III)-}C_{60}(OH)_X^{\bullet -} \rightarrow C_{60}(OH)_X + \text{Fe(II)} \quad (10)$$

$$Fe^{3+} + \text{-}COO^- \rightarrow \text{-}COO\bullet Fe^{2+} \rightarrow Fe^{2+} + CO_2 \quad (11)$$

3.1.2.2. -OH

On the surface of carbon prepared by hydrothermal carbonization (HTC), Qin et al.[45] suggested that hydroxyl groups bound with iron ions, instead of -COOH, favored the electron transfer from the hydroxyl moiety to Fe^{3+}. The controversy regarding the active sites on HTC-derived carbon and multi-walled carbon nanotubes is attributed to the differences in the redox properties of such materials that are determined by pyrolysis conditions including feedstocks, heat treatment temperature and pyrolysis time, among others. For instance, Klüpfel et al.[46] reported that the electron donating moieties (like phenolic structures) in both grass and wood-based chars varied with heat temperature (below 400 ºC). Phenolic structures in biomass-derived black carbon were observed as the dominant electron donating sites when heat temperature ranged from 200 to 500 ºC.

Even though a clear mechanism of iron reduction through the surface -COOH/-OH groups is still lacking, a possible pathway inspired by Sun and Skyllas-Kazacos[59] can be proposed. So, -COOH/-OH functional groups can be envisaged to provide H^+ to assist the transport of Fe^{3+} ions from the bulk to the close vicinity of the cathode where complex-assisted reduction takes place. The -COOH moieties release H^+ more easily than -OH counterparts, as verified by some researchers.[30,60]Another possible explanation is that Fe^{3+} might migrate toward -OH and then bind to it and form surface $[FeOH]^{2+}$ (see Figure 3), which is more prone to be reduced into Fe^{2+} as compared to Fe^{3+}, as reported by Xu et al.[30] In fact, surface -COOH/-OH tend to follow a similar mechanism in boosting iron reduction as chelating agents such as oxalate, citrate and ethylenediamine tetraacetic acid (EDTA), forming strong complexes with iron via ligand-to-metal transfer processes. These complexes have a strong influence on the redox potential of Fe^{3+}.[30]

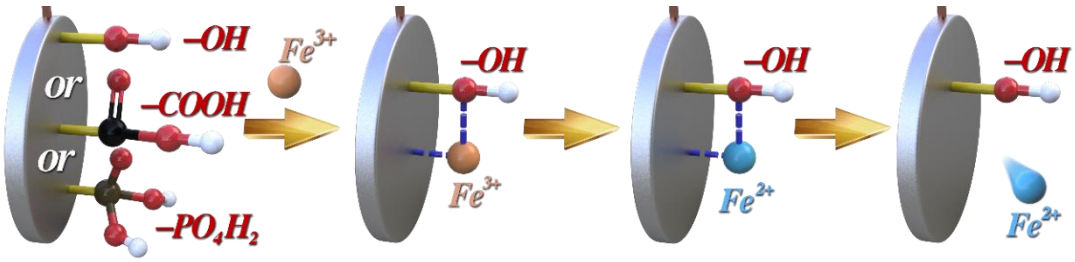

Figure 3. The plausible mechanism of various functional groups for cathodic Fe^{2+} regeneration.

3.1.2.3. Other functional groups

Aside from -OH/-COOH functional groups, the presence of a substantial concentration of quinone moieties is regarded as beneficial to facilitate the electron transfer during redox reactions, like Fe^{3+} reduction.[30] The mechanism of quinone-moieties-assisted Fe^{3+}/Fe^{2+} cycling might follow a similar pathway to homogenous quinone and quinone-like reducing compounds, transferring electrons to Fe^{3+}.[61]

Phosphate ions originated from reaction (12), similarly to -COOH and -OH, act as H^+ source, thereby increasing the local surface H^+ concentration. A high H^+ concentration may enhance the electron transfer, eventually boosting the iron cycling. In addition, it was reported that the energy barrier (37.2 kJ mol^{-1}) for proton transfer in phosphate is much lower as compared to that using sulfonate (69.6 kJ mol^{-1}).[62] This is because phosphate ions present a much higher affinity to Fe^{3+} with a low K_{sp} (= 10^{-36}), meaning that the phosphate Fe uptake capacity reached 246 $mg \cdot g^{-1}$.[63,64]

$$H_3PO_4 \rightarrow H^+ + H_2PO_4^- \rightarrow 2H^+ + HPO_4^{2-} \rightarrow 3H^+ + PO_4^{3-} \quad (12)$$

3.1.3. Active sites from heteroatom doping

Heteroatom doping has been confirmed as an efficient strategy to tune the electronic/surface structure of carbonaceous cathodes, thus endowing a greater reactivity and selectivity for the ORR.[65,66] Its role in iron reduction has drawn attention only recently.[67] Specifically, Liu et al.[67] clarified the mechanism of Fe^{3+} reduction on an N-doped carbon aerogel cathode (NDCA), including four pathways (see Figure 4a) that considered the different iron forms in solution at pH 3: Fe^{3+} (route I), $FeSO_4^+$ (route II), $Fe(OH)_2^+$ (route III), and $[FeOH]^{2+}$ (route IV). It is noticeable that the graphitic-/pyridinic-N groups on NDCA were found to act as complexing agents with iron ions to generate FeN_x, as confirmed by synchrotron-based X-ray absorption fine structure (XAFS). Pyrrolic N with unpaired electrons tends to donate electrons via intermolecular electron transfer to Fe(III)-complexes through the conductive carbon framework. A similar mechanism was proposed by Ma et al.,[68] as depicted in Figure 4b. The enhancement of Fe^{3+}/Fe^{2+} cycling was due to the improved electron transfer entailed by the coordination of Fe ions with N, and the synergistic effects of Ni and Al in graphene (see Figure 4b). Indeed, doped N atoms in graphene served as ligands to adjust the redox characteristics through ligand-field effects.

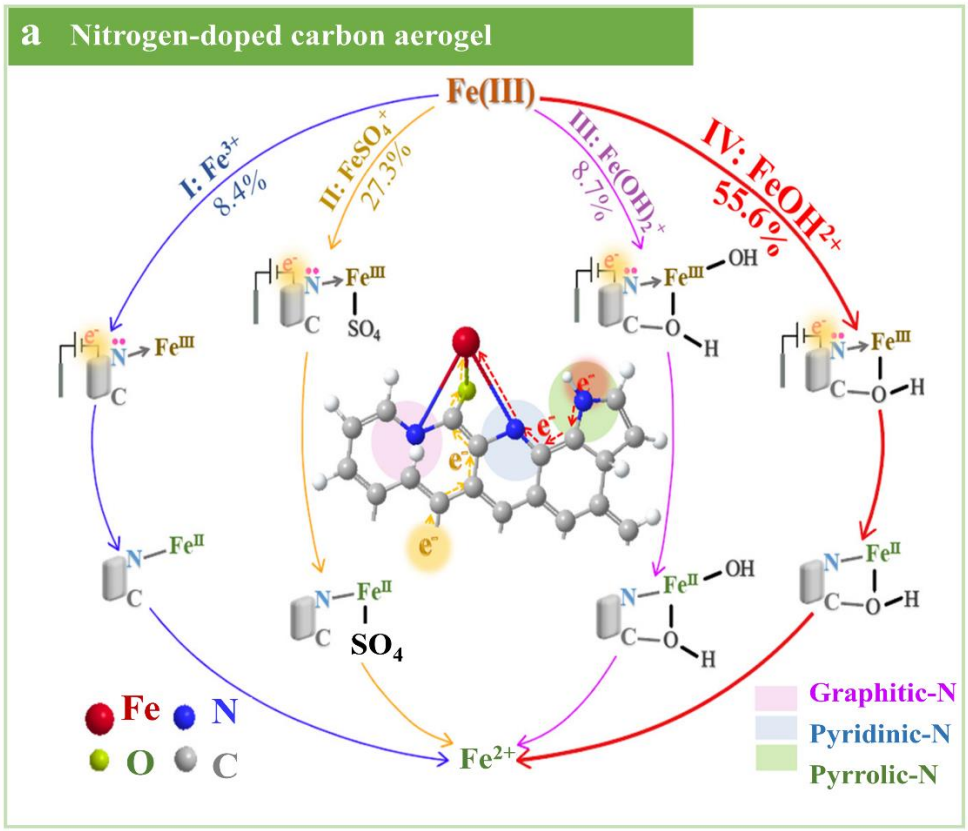
a Nitrogen-doped carbon aerogel
Fe(III)
I: Fe3+ 8.4%
II: FeSO4+ 27.3%
III: Fe(OH)2+ 8.7%
IV: FeOH2+ 55.6%
Fe2+
Fe N O C
Graphitic-N
Pyridinic-N
Pyrrolic-N

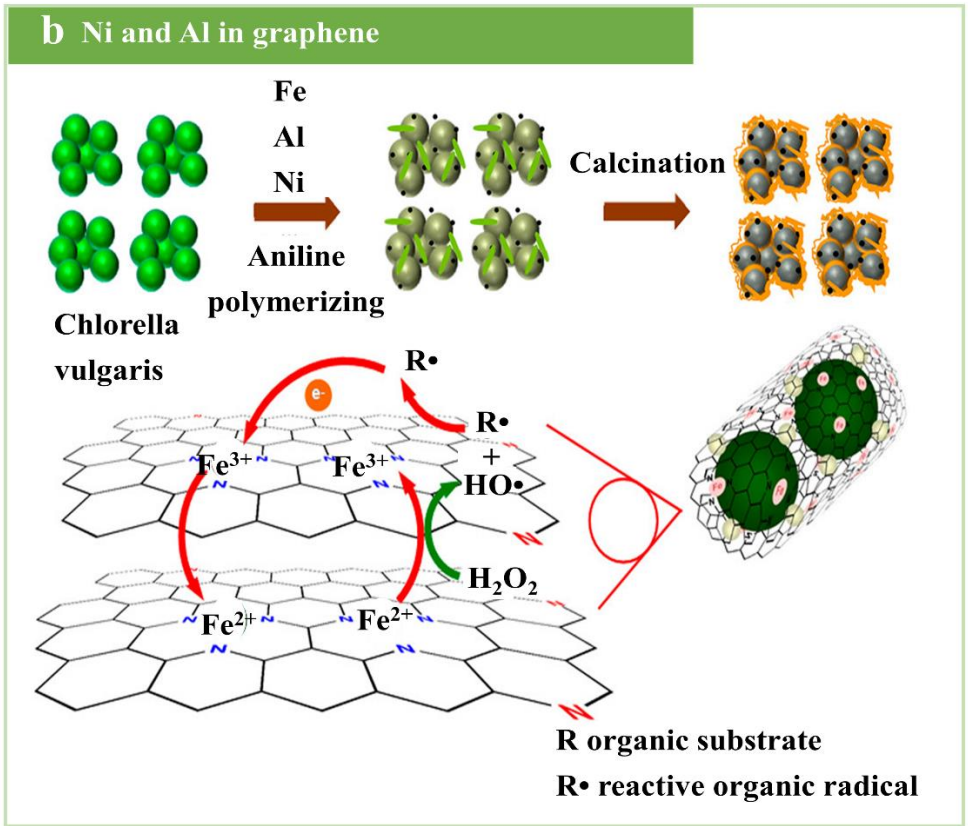
b Ni and Al in graphene
Fe
Al
Ni
Aniline polymerizing
Calcination
Chlorella vulgaris
R•
Fe3+
Fe2+
HO•
H2O2
R organic substrate
R• reactive organic radical

Figure 4. Possible mechanism of electrochemical Fe^{3+}-complex reduction on a nitrogen-doped carbon aerogel cathode. Reproduced with permission from ref 67 and 68. Copyright 2020 American Chemical Society

3.2. Electron-rich metal-based materials

In general, the Fe^{3+}-to-Fe^{2+} conversion in the EF process is driven by the electrochemical reduction via reaction (3), where electrons are supplied from the power source. From a boarder view, electron-rich metal-based materials can also provide electrons for Fe^{3+} reduction. Since the reduction potential of Fe(III) in iron-oxide surfaces is lower than that of aqueous Fe^{3+}, heterogeneous catalysts might be more suitable for boosting the Fe(II) regeneration.[69] In this subsection, electron-rich metal-based materials for Fe(III) reduction are presented, discussing the active sites involved in the reduction process. These materials can be used in EF to provide an additional electron source for cathodic iron reduction aside from the electrons supplied from the workstation.

The active sites in electron-rich metal-based materials can be divided into four types, as illustrated in Figure 5, based on their mechanisms: (i) exposed reductive metallic sulfides/phosphides, (ii) metallic centers (ZVI, ZVAl, etc.) or low-valence metal ions, (iii) exposed facets and (iv) other indirectly formed reducing reagents, like reductive H*, intermediate products of $O_2^{\bullet-}$ at the cathode, polyvalent metals or defects. Their corresponding mechanisms for boosting Fe^{3+} reduction are discussed below.

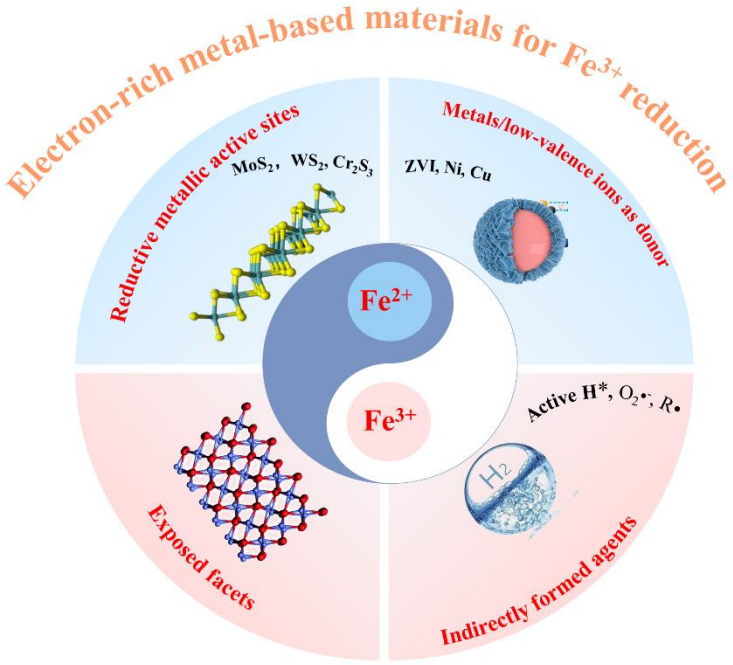

Figure 5. Classification of the electron-rich metal-based materials used for Fe^{3+} reduction.

3.2.1. Exposed reductive metallic active sites

A series of metal sulfide-based heterogeneous catalysts (MoS_2, WS_2, Cr_2S_3, CoS_2, PbS or ZnS) have been synthesized to alleviate the key limitation of Fe^{3+}/Fe^{2+} cycling.[70,71] In these novel systems, unsaturated S atoms add protons to form H_2S and then, the exposed reductive metallic active sites are available to accelerate iron reduction playing a co-catalytic effect in Fenton's reaction (2). Taking MoS_2 depicted in Figure 6a, the oxidation of surface Mo^{4+} to Mo^{6+} by Fe^{3+} from reaction (13) is possible once the unsaturated S atoms capture protons forming H_2S. The exposed Mo^{4+} allows the Fe^{3+} reduction and thus the limitation in EF can be substantially alleviated.[72] Mo^{4+} ions are regenerated with the aid of H_2O_2 to maintain the catalytic cycle (reaction (14)), whereas Mo^{4+} can also be formed from Mo oxidation with Fe^{3+} (see reaction (15)). The utilization of metal sulfide-based heterogeneous catalysts improved the organic decay rate by 18.5-fold, demonstrating first, the efficiency of the Mo-assisted Fe^{2+} catalytic regeneration process, and second, the importance of boosting Fe^{2+}

regeneration in EF. Since the release of H_2S gas poses potential harm, the researchers proposed MoO_2 to replace MoS_2 to avoid its formation. The mechanism of MoO_2 in iron reduction includes the following steps (Figure 6b): (i) Fe^{3+} is initially adsorbed on the surface of MoO_2, and (ii) Fe^{3+} is reduced to Fe^{2+} by Mo^{4+} via reaction (13), similarly to metal sulfides-based catalysts.[73] In addition to Mo^{4+}, Fe^{3+} ions can be reduced by the abundant defects in CoS_2 according to reactions (16)-(19).[74]

On the other hand, WO_3 was also used as electron donor to accelerate the reduction of Fe^{3+} through available W^{4+} active sites via reaction (20).[72,75] The use of other metals (M = Mn, Cu, Co, Zn, Ni, etc.) as catalysts in combination with iron is a promising option because they enhance the Fe^{3+} reduction following reaction (21) in concomitance with the formation of $^{\bullet}OH$ by Fenton-like reactions. Despite the high efficiency of the abovementioned powder catalysts, including metal sulfides-based heterogeneous catalysts, these systems still suffer from concerns about reuse in practical applications. To alleviate the continuous supply of catalysts with high cost and need for separation, a 3D-MoS_2 sponge loaded with MoS_2 nanospheres and graphene oxide (GO) (sponge@MoS_2@GO, Figure 6c) was developed.[72] The sponge@MoS_2@GO floated on the sewage and was used in a pilot-scale experiment with 150 L solution to remove aromatic organics. Fe^{2+} was regenerated by the reductive Mo^{4+}, achieving a 50-fold higher pollutant degradation as compared to the system in the absence of the co-catalyst.[72] Based on those works, MoS_2 as co-catalyst was introduced in the EF process to enhance the Fe^{3+}/Fe^{2+} cycle, confirming the improved Fe^{3+} reduction capacity of this system.[76]

$$Mo^{4+} + 2Fe^{3+} \rightarrow 2Fe^{2+} + Mo^{6+} \quad (13)$$

$$Mo^{6+} + H_2O_2 \rightarrow 2H^{+} + O_2 + Mo^{4+} \quad (14)$$

$$4Fe^{3+} + Mo^{0} \rightarrow 4Fe^{2+} + Mo^{4+} \quad (15)$$

$$O_2 + e^{-} \text{ (defect)} \rightarrow O_2^{\bullet -} \quad (16)$$

$$O_2 + 2e^{-} \text{ (defect)} + 2H^{+} \rightarrow H_2O_2 \quad (17)$$

$$O_2^{\bullet -} + Co^{4+}/Co^{3+} \rightarrow {}^1O_2 + Co^{2+} \quad (18)$$

$$Fe^{3+} + e^{-} \text{ (defect)} \rightarrow Fe^{2+} \quad (19)$$

$$W^{4+} + 2Fe^{3+} \rightarrow 2Fe^{2+} + W^{6+} \quad (20)$$

$$M^{n+} + Fe^{3+} \rightarrow Fe^{2+} + M^{(n+1)+} \text{ (M = Mn, Cu, Co, Zn, Ni, etc.)} \quad (21)$$

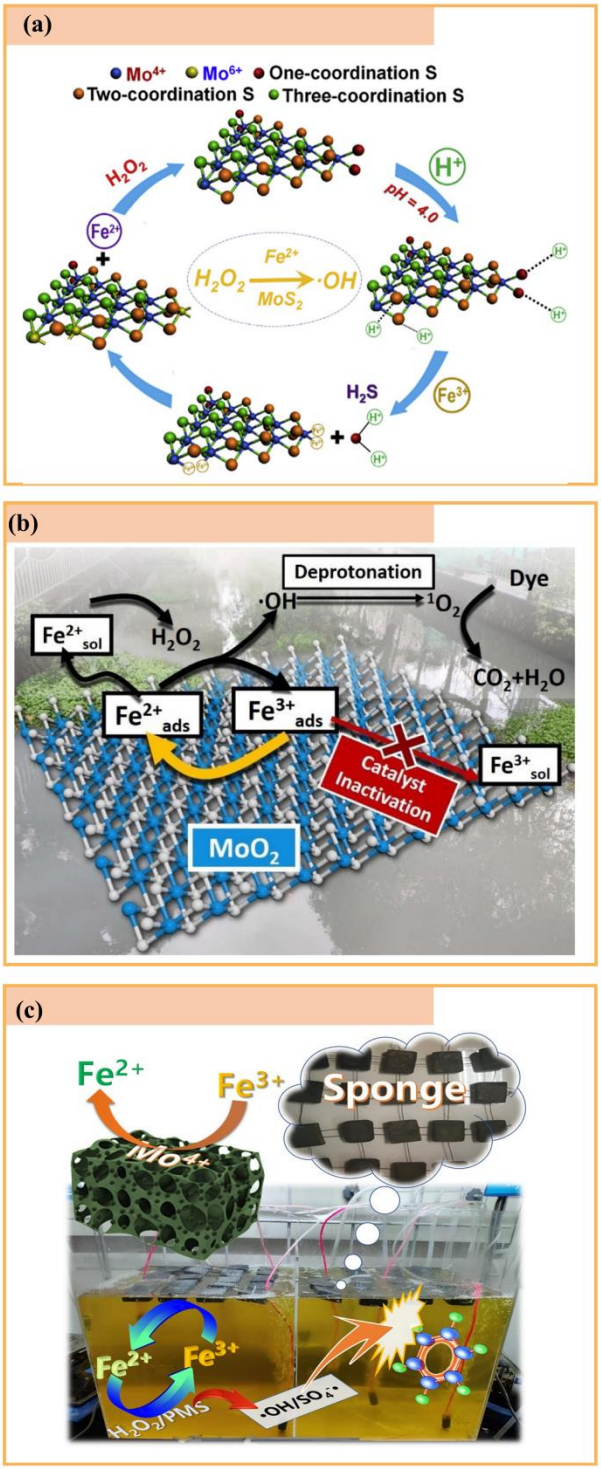

Figure 6. Mechanism of iron reduction through the Mo-based catalyst: (a) MoS_2. Reproduced with permission from ref 70. Copyright 2020 Elsevier). (b) MoO_2. Reproduced with permission from ref 73. Copyright 2019 Elsevier. (c) Sponge@MoS_2@GO. Reproduced with permission from ref 76. Copyright 2020 John Wiley and Sons.

3.2.2. Metals and their low-valence ions

Ni, Mn, Cu, Mo and Fe are electron-rich metals with multi-valences that could act as electron donors to boost the Fe^{3+} reduction. For instance, Fe involving its lowest valence (i.e., ZVI) plays two main roles in the EF process: (i) to become a source of iron ions for Fenton's reaction (2), via oxidation as shown in reactions (22)-(24), and (ii) to provide electrons for Fe^{3+} reduction from reaction (25), as also occurs with Ni in reaction (26).

$$Fe^0 - 2e^- \rightarrow Fe^{2+} \qquad (E^0 = -0.440 \text{ V vs. SHE for reduction}) \qquad (22)$$

$$Fe^0 + O_2 + 2H^+ \rightarrow H_2O_2 + Fe^{2+} \qquad (23)$$

$$Fe^0 + H_2O_2 + 2H^+ \rightarrow Fe^{2+} + 2H_2O \qquad (24)$$

$$2Fe^{3+} + Fe^0 \rightarrow 3Fe^{2+} \qquad (25)$$

$$2Fe^{3+} + Ni^0 \rightarrow 2Fe^{2+} + Ni^{2+} \qquad (26)$$

In the case of zero-valence metal, some of us[77] used a three-dimensional porous metallic iron-foam cathode to solve the issue of the low Fe^{2+} regeneration rate. It was found that the chemical regeneration of Fe^{2+} via reactions (25) and (26) on nickel-iron-foam was crucial for the continuous production of Fe^{2+} ions for phenol degradation (see Figure 7a). The utilization of ZVI along with carbon in EF has also been reported by Zhang et al.[78] The iron-carbon (Fe-C) micro-electrolysis system relies on the formation of numerous microscopic galvanic cells, where iron acts as anode and carbon serves as cathode. The modification of Fe-C particles catalyst with PTFE prevents iron releasing into the solution. In this system, Fe^{3+} reduction by Fe^0 via reaction (25) was reported as well.[78,79]

Although PTFE could prevent iron release from metal-based catalysts to some extent, a better strategy to alleviate the issue consists of a catalyst anchored into the cathode, in which chemical/electrochemical reduction can slow or even suppress Fe

dissolution. For example, a nickel-iron foam (Ni-F) cathode was used in EF for phenol degradation, as presented in Figure 7b.[80] In this system, the Ni-F composite cathode could provide Fe^{2+} ions in a controlled manner via complex chemical/electrochemical redox processes (chemical corrosion from reactions (23) and (24) and Fe^{3+} chemical/electrochemical reduction reactions (3) and (25). The Zhang's group[81,82] designed some novel $Fe@Fe_2O_3$ core-shell nanowires and confined them into multi-wall carbon nanotubes to obtain an oxygen-fed gas-diffusion electrode. This core-shell structure along with activated carbon fiber prevented the complete leaching of Fe^{3+} and Fe^{2+} into the bulk. In this way, the *in-situ* cycling of iron species ($Fe^0 \rightarrow Fe^{n+} \rightarrow Fe_2O_3$) was achieved. Zhao et al.[83] proposed a one-step metal-resin process to fabricate an iron-copper-carbon (FeCuC) composite aerogel cathode for EF, where Cu^0 acted as a reduction promoter for boosting electron transfer. One interesting finding was that Fe^0 particles were embedded in the 3D structure of the carbon aerogel and the surface iron was removed during activation treatment (CO_2/N_2). The metals in the FeCuC composite cathode were crosslinked with the carbon framework, being highly stable even in acid solution. Other metal oxides like CeO_2, with a redox cycle between 3+ and 4+ oxidation states, also favor the electron transfer rate in the Fe^{3+}/Fe^{2+} cycle in EF and thus, boost iron reduction through the interaction between Ce^{4+}/Ce^{3+} and Fe^{3+}/Fe^{2+} pairs. It was reported that the synergistic effect of Fe-Ce promoted the regeneration of Fe^{2+}/Ce^{3+} according to reactions (3) and (27)-(29).[84,85] Similar mechanisms were proposed for composite electrodes such as γ-FeOOH-graphene-polyacrylamide carbonized aerogel (γ-FeOOH GPCA) as shown in reaction (29),[86] $MnCo_2O_4$ loaded on carbon fiber ($MnCo_2O_4$-CF),[87]self-supporting carbon fiber paper (CFP) decorated with MnO_2-Fe_3O_4 CFP@MnO_2-Fe_3O_4/C,[88], and CuFeNLDH-CNTs modified graphite.[89]

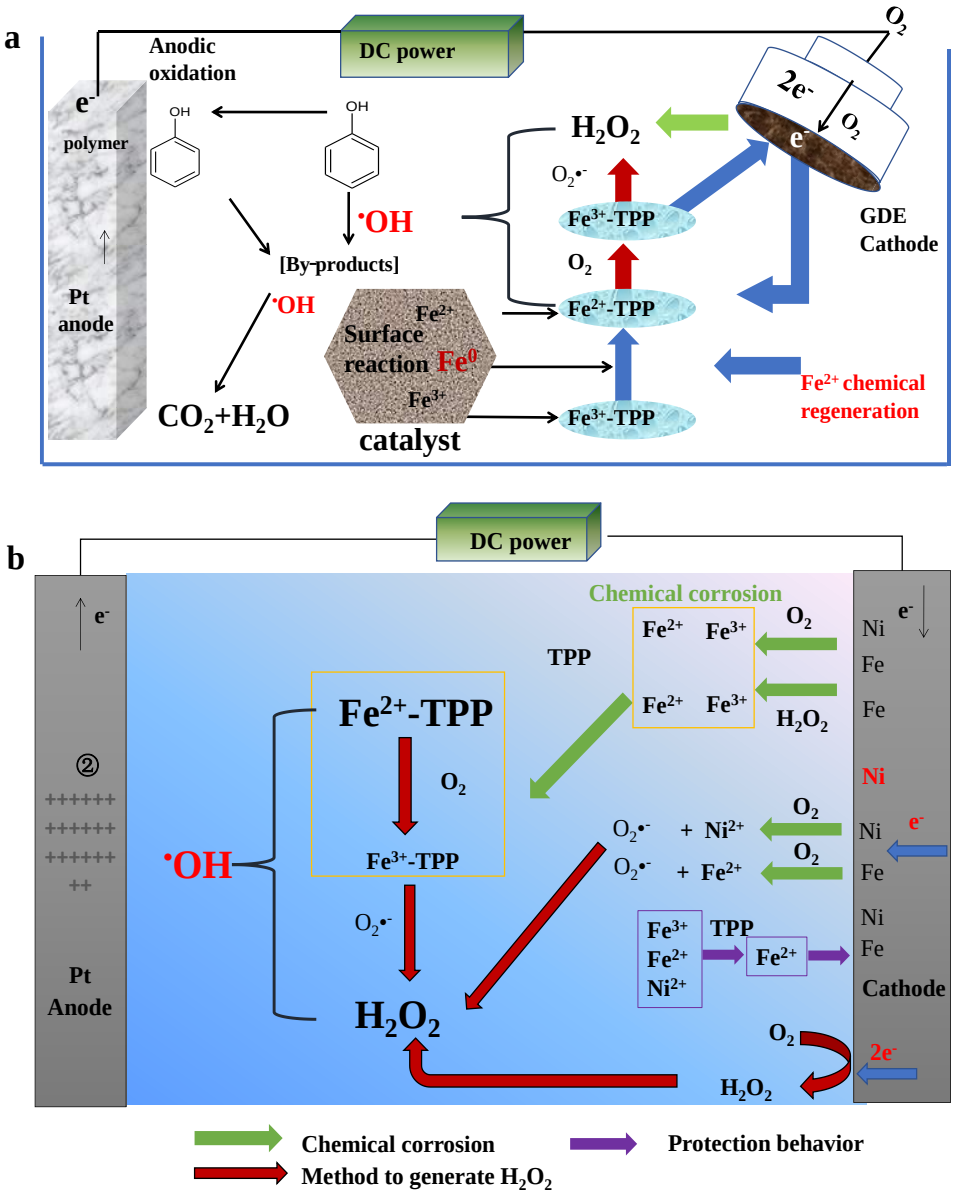

Figure 7. Mechanisms of zero-valent metal-catalyzed Fe^{3+} reduction in the electro-Fenton process: (a) nickel-foam. Reproduced with permission from ref 77. Copyright 2018 Elsevier. (b) Nickel-iron foam cathode. Reproduced with permission from ref 80. Copyright 2018 Elsevier.

$$Ce^{4+} + e^- \rightarrow Ce^{3+} \qquad (E^0 = 1.72 \text{ V vs. SHE}) \qquad (27)$$

$$Fe^{2+} + Ce^{4+} \rightarrow Fe^{3+} + Ce^{3+} \qquad (28)$$

$$\gamma\text{-FeOOH} + 3H^+ + e^- \rightarrow Fe_{ads}^{2+} \rightarrow Fe^{2+} \qquad (29)$$

The main concern with the use of these metal-based catalysts is the inevitable dissolution in the acidic or even neutral medium used in EF. Hence, stability needs to be taken into consideration for large scale applications. A strategy to improve this

consists in encapsulating the metal nanoparticles into carbon nanotubes and wash Fe particles remaining outside of the carbon shells, as investigated previously.[90,91]

3.2.3. Exposed facets

The reactivity of surface atoms varies at different facets.[92] In this regard, facet-dependent physicochemical properties such as redox potential and hydrophilicity could differ with exposed facets and hence, influence reactions occurring at the surface. It has been reported that adsorption was facet-dependent in hematite, where the {0 0 1} facet presented stronger adsorption than its {1 0 0} counterpart due to the abundant surface hydroxyl groups and adsorption site densities in the former.[93] A similar study showed that hematite {0 0 1} provided more reaction sites for interfacial electron transfer, thus promoting a larger electron transfer rate (19.6 s^{-1}) than hematite {1 0 0}.[93,94] The former facet, with a more positive redox potential, could facilitate iron cycling. Considering that Fe_3O_4 has a face-centered cubic crystal, its surface energy increases in the following order: {1 1 1} < {1 0 0} < {1 1 0}. Polyhedral Fe_3O_4 nanoparticles with exposed {1 1 0} facets account for 38.5%, and Fe^{3+} reduction can be boosted due to its higher surface.[95] Huang et al.[96] conducted a series of experiments about the variations of specific metals on various crystal planes at the molecular scale combining spectroscopic and theoretical calculations. They found that hematite {1 1 0} could confine Fe^{2+} in a five-coordination binding mode, while there was a six-coordinated bond in {0 0 1}. The difference in iron coordination not only controlled the efficiency of the Fe^{3+}/Fe^{2+} cycle, but also determined the formation of the $^{\bullet}OH$. This was explained in terms of the much lower activation energy for H_2O_2 decomposition in the five-coordination mode. Well-established synthesis methods for hematite with special facets, the related growth mechanisms, and the interactions between different facets and Fe^{2+} have been previously reviewed.[93]

Rational design of well-defined crystal surfaces for iron reduction is still challenging if the desirable planes are required because in general, high-energy planes vanish rapidly and are transformed into low-energy ones, minimizing the total surface free energy under equilibrium conditions.[97] Some excellent reviews have systematically discussed the synthesis methods for crystal facet engineering.[98] As reviewed by Wang et al.,[98] a substantial body of investigations have been focused on the facet-controlled synthesis of TiO_2, but there is a lack of work on other metals.

3.2.4. Other indirectly formed intermediates

3.2.4.1. Active hydrogen (H/[H]/H_2)*

Compared to other reducing agents like metal or metal sulfides-based catalysts, active hydrogen (abbreviated as H*/[H]/H_2) is a clean reagent that has become a hot topic in environmental application, although it is still underplayed.[99] H*, as a catalytic intermediate, is generally formed at the cathode during a two-electron transfer HER through either a Volmer-Heyrovsky or Volmer-Tafel mechanism. In HER, H_2O is reduced at the cathode and H* is produced via reactions (30)-(32).[100,101] H* is theoretically a strong reducing species (E^o = -2.106 V/SHE) and it could reduce species in the bulk, like Fe^{3+} from reaction (33) or nitrate.[102]

Regarding materials for improving the H* formation, as described in Figure 8, noble metals like Pd^0 enhance the adsorption/storage of H_2 and then activate it to form H* from reaction (34).[103] Georgi et al.[104] utilized H_2/Pd pairs to enhance Fe^{3+} regeneration via reaction (35).

$$H_2O + e^- \rightarrow H^* + OH^- \text{ (Volmer)} \quad (30)$$

$$H_2O + H^* + e^- \rightarrow H_{2(g)} + OH^- \text{ (Heyrovsky)} \quad (31)$$

$$2H^* \rightarrow H_{2(g)} \quad (32)$$

$[Fe(H_2O)_5(OH)]^{2+} + H^* \rightarrow$ $\triangle_r G^o$ = -87 kJ mol^{-1} (pH$\approx$ 3) (33)

$[Fe(H_2O)_6]^{2+}$

$\equiv Pd\text{-}H_2 \rightarrow 2 \equiv Pd\text{-}H^*$ (34)

$Pd\text{-}H^* + Fe^{3+} \rightarrow Pd + Fe^{2+} + H^+$ (35)

Figure 8. Different materials used for the formation of active H*.

Considering the Pd scarcity and its high cost, other abundant elements were incorporated into Pd-based catalysts to lower its concentration.[105] Zeng et al.[103] fabricated a three-dimensional catalyst, where Pd was loaded on the large surface area of Al_2O_3. They found that 360 μM Fe^{3+} could be completely reduced to Fe^{2+} within 1 min using $Pd@Al_2O_3$ catalyst (see Figure 9a). In another work, the presence of Ni promoted H* atoms owing to its strong metal-hydrogen (metal-H*) binding strength.[102] Some of us utilized a nickel-foam cathode to assist the Fe^{3+}/Fe^{2+} cycle with the help of H* atoms.[106] Liu et al.[107] introduced the use of atomic H* in the EF process to accelerate the regeneration of chemisorbed Fe(II)-complexes at a near-neutral pH using a Ni-deposited carbon felt cathode based on the *d*-band center theory. They observed the

formation of atomic H* on Ni-deposited carbon-felt cathode. The density functional theory (DFT) simulations showed that coordinated Ni atom at the Ni-deposited carbon-felt cathode could be the active sites for H_2O adsorption to be then reduced to atomic H* (see Figure 9b). Apart from metallic Ni, a Ni-based compound like $Ni(OH)_2$ was proven to be an excellent catalyst for H_2O dissociation as well, since it formed a metal/hydroxide interface that provided more active sites for active H* atoms formation (see Figure 9c).[108]

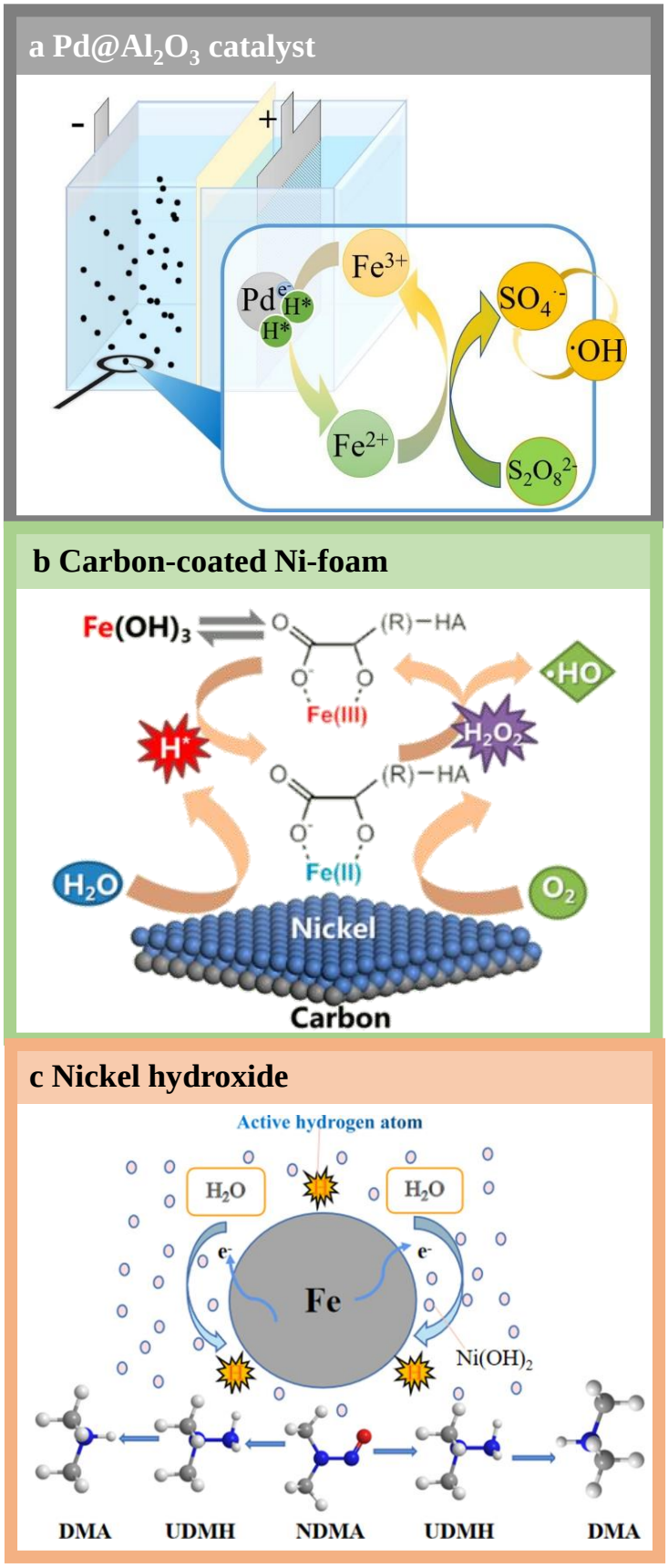

Figure 9. Generation of active hydrogen and its application in various configurations: (a) $Pd@Al_2O_3$ catalyst. Reproduced with permission from ref 103. Copyright 2020 Elsevier. (b) Carbon-coated Ni foam.

Reproduced with permission from ref 107. Copyright 2019 American Chemical Society. (c) Nickel hydroxide. Reproduced with permission from ref 108. Copyright 2021 Elsevier.

Liu et al.[107] elucidated the roles of active H*, electrons and electric field in the nitrate cathodic reduction. The *in-situ* produced active H* at the cathode was the responsible for nitrate reduction rather than the previously speculated H_2.[98] Attention should be paid over soluble H_2 dissolved at normal temperature/pressure that could also reduce Fe^{3+} back to Fe^{2+}. This suggests that it is needed to retain H_2 in the bulk solution.[99] From this assumption, metal-organic frameworks (MOFs) favoring H_2 adsorption were explored, which could be promising due to their high specific surface area, adjustable pore size and open metal sites. Tang and Wang[109] prepared a Pd/MIL-101(Cr) catalyst and found that the MOF could kept H_2 in the bulk. The reduction of Fe^{3+} through the solid Pd/MIL-101(Cr) catalyst was improved by 10-fold with the H_2-MIL-101(Cr) system and 5-fold with the H_2-Pd^0 one. Unsaturated iron sites (CUSs) in MOFs served as active sites to boost the cycling of the Fe(III)/Fe(II) couples. However, there was a concern about the proportion of Fe(III) in CUSs that was still too high, leading to a much higher electron density of iron centers, not good for Fe(III) reduction. To solve this drawback, Gao et al.[110] proposed the introduction of functional groups with strong electron-withdrawing ability such as -NH_2, -CH_3, H-, Br-, and -NO_2 to lower the electron density of iron centers. Among them, -NO_2 was confirmed to present superior catalytic activity in a wide pH range (4-8) with the highest electrophilicity, although organic ligands face issues for potential large-scale applications. In a different approach, Yang et al.[111] proposed a rational Fe(II) substitution to develop a mixed-valence MIL-53(Fe) catalyst (denoted as Fe^{II}-MIL-53(Fe)). The partial Fe(III) precursor was displaced by Fe(II) salts and the high portion of Fe(II) in CUSs favored iron reduction.

This subsection has discussed the high reactivity of active H* for cathodic Fe(III) reduction. H* detection is crucial to understand the fundamental mechanism involved. Among the several approaches to confirm the presence of active H*, KIO_3 as a non-volatile active H* scavenger deems as an effective method to capture this species according to reaction (36). A more intuitive analysis by NMR and ESR spectroscopy has also been applied.[112] More frequently, active H* has been monitored using electron paramagnetic resonance with 5,5-dimethyl-1-pyrroline N-oxide (DMPO) as the trapping agent. The interference of $^{\bullet}OH$ in ESR during the H* measurement was avoided by addition of the scavenger *t*-butanol (TBA) since it can selectively capture the $^{\bullet}OH$.[113] Protocols for the identification, quantification and generation methods of H* in electrocatalytic systems are described elsewhere.[110]

$$H^* + IO_3^- \rightarrow {}^{\bullet}OH + IO_2^- \quad (36)$$

3.2.4.2. Radicals

Superoxide ion ($O_2^{\bullet-}$) is formed through the reduction of O_2. Among various formation routes for this radical, the electrochemical reduction is potentially the most convenient, where O_2 accepts one electron to form it from reaction (37).[115] $O_2^{\bullet-}$ is a short-lived species in aqueous solution, but its lifespan could be extended when protons are absent because it disproportionates in water according to reaction (38). Considering its moderate redox potential (-0.32 V vs. SCE at pH 7.5) in front of that of Fe^{3+}/Fe^{2+} (reaction (3)),[19,115,116] the reduction of Fe^{3+} by $O_2^{\bullet-}$ following reaction (39) is more thermodynamically favored than the reduction with H_2O_2 from reaction (40) and $HO_2^{\bullet}$ from reaction (41). To investigate the reduction ability of $O_2^{\bullet-}$, some of us fabricated a novel carbon nitride graphite-based gas diffusion electrode (g-C_3N_4@GDE) and confirmed its role in cathodic iron reduction.[117] Moreover, we recently designed a novel microbubble-assisted rotary tubular titanium cathode (MRTTC) to alleviate the issue of

a low Fe^{3+} reduction rate in the EF process.[34] In this MRTTC, iron reduction attained a 200% enhancement as compared to the conventional EF process since the formation of $O_2^{\bullet-}$ provided an additional reduction pathway for Fe^{3+} cycle via reaction (39) aside from its direct cathodic reduction by reaction (3). A similar finding was reported by Zhang et al.[118] using a novel 3D anthraquinone/polypyrrole modified graphite felt (AQS/PPy-GF) cathode. The formation of $O_2^{\bullet-}$ has also been suggested in a three-dimensional EF system with nickel foam as particle electrode, which was said to promote reaction (42).[119,120] However, its role in iron reduction was not clearly demonstrated in this work. $O_2^{\bullet-}$could be detected by chemical reactions, spin trapping and direct measurement. More details can be found in the work of Hayyan et al.[115] Although $O_2^{\bullet-}$ favors the Fe^{3+} reduction via reaction (39), its formation through the monoelectronic reduction of O_2 competes with the two-electron ORR to yield H_2O_2 (reaction (1)). As a result, the balance between H_2O_2 and $O_2^{\bullet-}$ formation must be optimized to achieve the best degradation efficiency. Other strategies proposed in the review, for example, the introduction of surface functional groups, active sites from heteroatom doping, and mass transport methods, not only assist the electrochemical Fe^{3+}/Fe^{2+} cycle, but also boost the two-electron ORR to produce H_2O_2.

$$O_2 + e^- \rightarrow O_2^{\bullet-} \quad (37)$$

$$2O_2^{\bullet-} + H_2O \rightarrow O_2 + HO_2^- + OH^- \quad (38)$$

$$O_2^{\bullet-} + Fe^{3+} \rightarrow Fe^{2+} + O_2 \qquad k = 5 \times 10^7\ M^{-1}\ s^{-1} \quad (39)$$

$$H_2O_2 + Fe^{3+} \rightarrow Fe^{2+} + HO_2^{\bullet} + H^+ \qquad k = 0.02\ M^{-1}\ s^{-1} \quad (40)$$

$$HO_2^{\bullet} + Fe^{3+} \rightarrow Fe^{2+} + O_2 + H^+ \qquad k = 2 \times 10^3\ M^{-1}\ s^{-1} \quad (41)$$

$$Ni + 2O_2 \rightarrow Ni^{2+} + O_2^{\bullet-} \quad (42)$$

Apart from $O_2^{\bullet-}$, organic radicals such as $R^{\bullet}$ formed in a novel Fe-N-graphene wrapped Al_2O_3/pentlandite composite were also responsible for Fe^{3+} reduction, where $R^{\bullet}$ mainly acted as the electron donor.[69] This reduction mechanism occurred as follows: once $R^{\bullet}$ was formed, it was freely added to the graphene region resulting in an enhanced electron transfer from organic to iron ions. Transition metals can induce the formation of persistent free radicals (PFRs) via electron transfer from phenol/quinone moieties to metal atoms (e.g., CuO and Fe_2O_3). PFRs serve as electron donors for Fe^{3+}/Fe^{2+} cycling with half-lives of hours, days and even months unlike the short life of $^{\bullet}OH$.[121]

3.3. Other emerging strategies

As illustrated in Figure 10, other emerging strategies to boost Fe^{3+} cathodic reduction include: (i) single-atom catalysts to atomically disperse the active sites, (ii) unique microenvironments arising from confinement effect, and (iii) the introduction of reducing chelating agents.

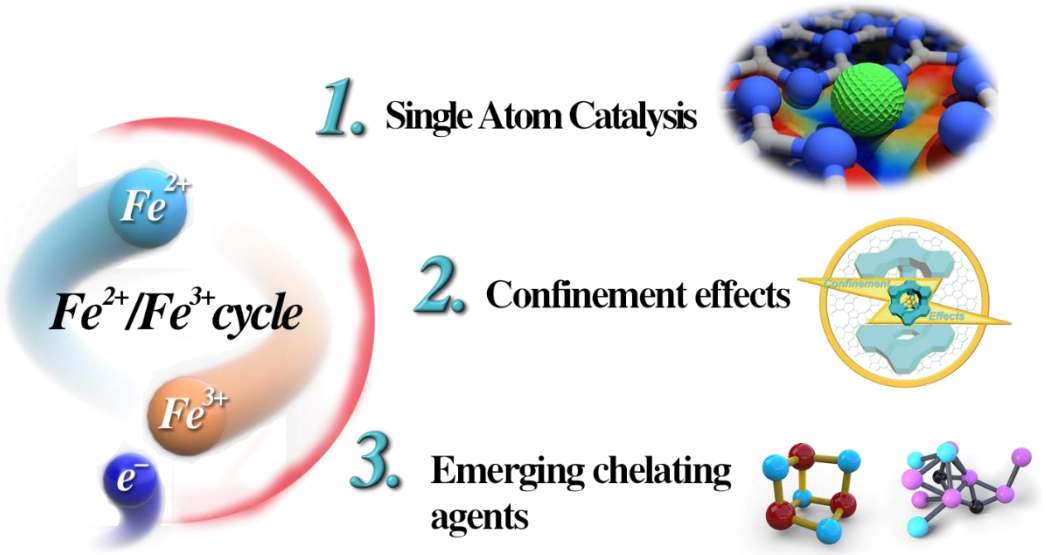

Figure 10. Other emerging strategies to enhance cathodic reduction.

3.3.1. Single-atom catalysts

Single-atom catalysts (SACs) with isolated metal atoms are deemed as a new frontier in heterogeneous catalysis science, tracing back to the investigation of Maschmeyer et al.[122] in 1995. SACs can maximize the dispersion of active sites and thus, improve the catalytic atom-utilization efficiency. The energy level/electronic structure and unsaturated coordination environments suffer fundamental alterations when they are reduced to atomic scale. In this way, SACs could significantly improve the corresponding activity.[123]

The utilization of SACs for iron reduction was, for the first time, reported by Yin et al.,[124] who revealed that the decay of $Fe(NO_3)_3$ in the confined nanopores of a support with abundant Si-OH groups promoted Fe sites dispersed at an atomic level, as can be seen in Figure 11. The atomic Fe catalytic sites anchored on a sandwich structure avoided acid leaching and Fe agglomeration using the layered structure. So, the high-density N atoms and "six-fold cavities" in g-C_3N_4 firmly encapsulated Fe at the atomic level.[125-127] To improve the exposed metal active sites, single Fe atom anchored in pyridinic-N-dominated and defect-enriched graphene (N-DG) nanosheets were created, as shown in Figure 11a, in which defect-rich graphene favored the Fe immobilization. The synergistic effects of the Fe-N and Fe-O sites promoted the two-electron ORR in the Fe/N-DG catalysts as well. Considering that SACs are still in their infancy, most of the work has focused on the promotion of the two-electron ORR. In our opinion, iron cycling can also be enhanced in the presence of SACs. On the other hand, constructing the atomic dispersed catalysts is still challenging since the obtention of atoms involves high surface energy and they tend to aggregate to form nano nanoparticles.[32] Chen et al.[32] systematically summarized innovative fabrication methods related to wet-chemistry approaches to obtain atomic dispersion of metal centers, which include defect

engineering strategy, spatial confinement strategy, coordination design strategy and other sacrificial template approaches.

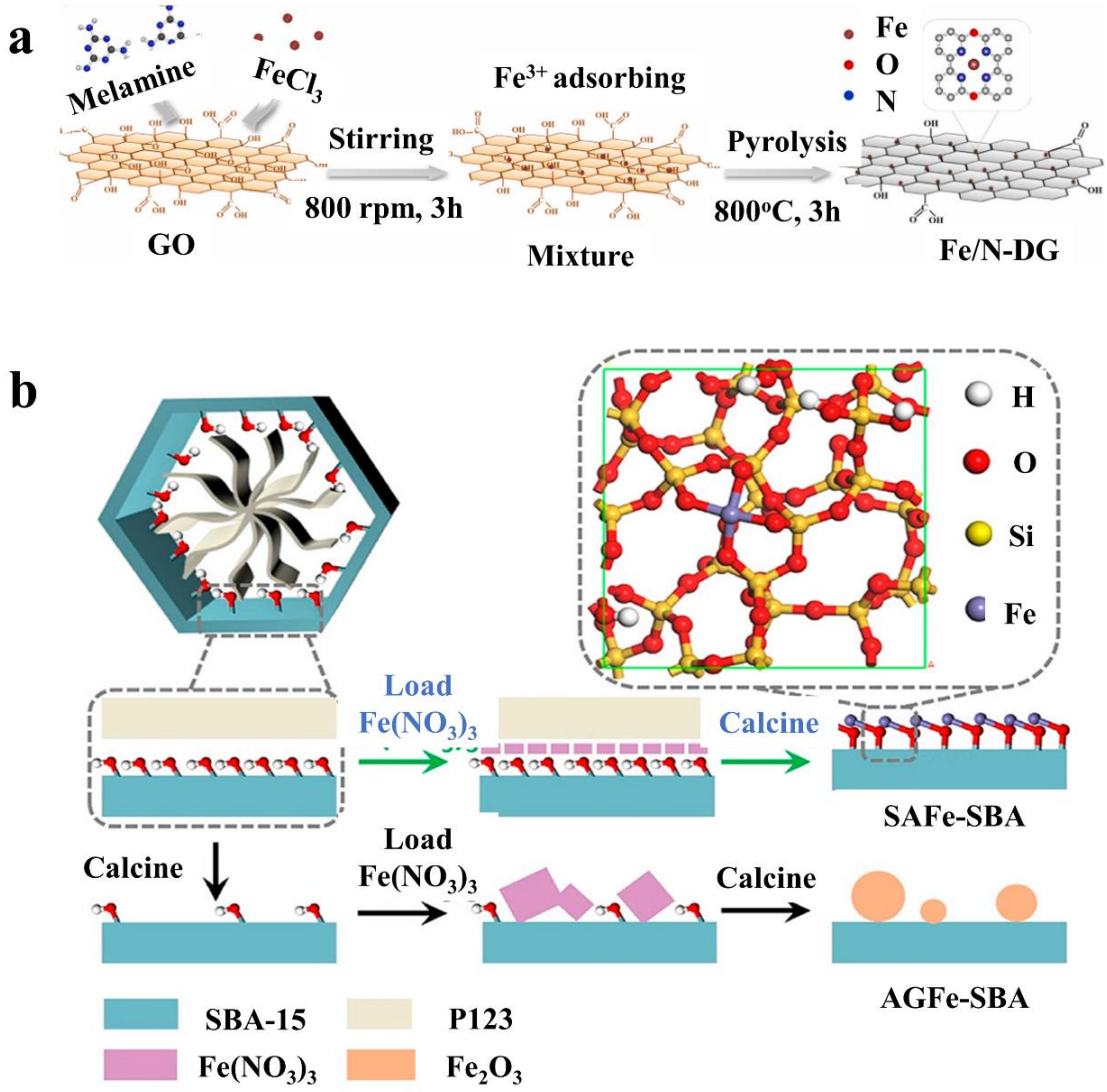

Figure 11. (a) Schematic illustration of the preparation methodology to obtain Fe/N-DG catalysts. Reproduced with permission from ref 127. Copyright 2021 Elsevier. (b) Single atom Fe sites on SBA-15. Reproduced with permission from ref 124. Copyright 2019 American Chemical Society.

3.3.2. Confinement effects

Cavities of nanostructured materials offer a special environment that confines/entraps the reactant molecules, eventually enhancing their electrocatalyst efficiency. These properties derive from their nanosized spatial morphology termed as

nanoconfinement effects.[128,129] In 1987, Derouane[131] was the first to define confinement effects and postulated a general theory over the van der Waals physisorption energy *W* of a molecule within a "confined environment" according to Eq. (43):

$$W(s) = \frac{-C}{4d^3(1-\frac{s}{2})^3} \quad (43)$$

where *d* is the distance between the molecule and the pore wall, $s = l/a$ is the curvature indicator, a is pore radius, *l* is the radius of the molecule, and *C* is a constant.

It can be deduced from Eq. (43) that the *W* value in the confined pore is approximately 8-fold higher than that in the plane. As reviewed in ref [129] and [131], the confinement in nanospace can substantially change the physicochemical properties of encapsulated substances, including hydrogen bond network, water flow rate, phase transition, and even the alteration of energy barriers, kinetics, and pathways of chemical reactions. Once the molecules are encapsulated into nanometer-sized confinements, some interesting phenomena can take place. For example, Yang et al.[132] observed the formation of singlet oxygen ($^1O_2$) rather than the commonly observed $^{\bullet}OH$ from Fenton's reaction (2), which was catalyzed by 2 nm Fe_2O_3 nanoparticles confined inside multiwalled carbon nanotubes (MWCNTs) with inner diameter of 7 nm. Similarly, the melting point of ionic liquids inside CNTs reached 473 K, much higher than the melting temperature in unconfined state (279 K).[133] In this regard, confinement not only ensures better interaction between reactants and active species, but also presents a synergetic effect provided by the unique microenvironments. This favors a series of catalytic reactions, including the Fe^{3+}-to-Fe^{2+} conversion.[134]

Recently, Su et al.[134] took advantage of CNTs unique hollow and tubular nanostructure to confine Fe^0. The study confirmed the confinement effects on tuning the iron valences, where Fe^0 instead of iron oxide was observed inside CNTs and the

conversion of Fe^{3+} to Fe^{2+} assisted by Fe^0 was achieved. The confined Fe^0 inside CNTs favored the two-electron ORR and less iron was released from this cathode material. Zhang et al.[135] recently found that the degradation rate was enhanced one order of magnitude when the reaction occurred in a channel smaller than 20 nm because a larger amount of •OH was confined for fast organic oxidation avoiding parasitic reactions due to •OH limited lifespan. The research of Shermukhamedov et al.[136] analyzed the influence of confinement effects on the Fe^{3+}/Fe^{2+} redox couple in single wall carbon nanotubes. They found that the electron transfer rose with decreasing nanotube diameter from 3.5 to 0.8 nm since the solvent reorganization energy was lower in smaller nanotubes.

3.3.3. Introducing emerging chelating agents

Zhang and Zou[23] have reviewed the application of chelating agents in Fenton and Fenton-like reactions at high pH values in a systematic manner. In this subsection, only the emerging chelating agents with the ability to enhance the Fe^{3+}/Fe^{2+} cycle will be analyzed, especially inorganic chelating agents since the organic ones increase total organic carbon (TOC) load along with the potential toxicity effects. They can act as quenching agents and consume reactive species, thus decreasing the oxidizing ability.[137] Some inorganic ligands have been used in the EF process, including sodium disilicate (SD), tetrapolyphosphate (4-TPP), tripolyphosphate (3-TPP), pyrophosphate (PP), Na_3PO_4, HSO_3^- ion, SO_3^{2-} ion, and hydroxylamine sulfate,[137,139] which are discussed in detail below.

Cui et al.[140] reported that a low-cost sodium disilicate (SD) chelating agent could extend the operation of the EF process at neutral pH (from 6 to 8), where Fe(II)-DS activated O_2 to form additional H_2O_2, enhancing the efficiency according to reactions (44)-(47). Disilicate ions were then removed via the addition of CaO or $CaCl_2$. Guan et

al.[141] compared the performance of various ligands (PO_4^{3-}, humic acid (HA) and SiO_3^{2-}) on the transformation of Cr(VI) and iron reduction, reporting a similar trend.

$$Fe^{2+} + \text{disilicate} \rightarrow [\text{disilicate-Fe(II)}] \quad (44)$$

$$[\text{disilicate-Fe(II)}] + O_2 \rightarrow [\text{disilicate-Fe(III)}] + O_2^{\bullet-} \quad (45)$$

$$[\text{disilicate-Fe(II)}] + O_2^{\bullet-} \rightarrow [\text{disilicate-Fe(III)}] + H_2O_2 + 2OH^- \quad (46)$$

$$[\text{disilicate-Fe(II)}] + H_2O_2 \rightarrow [\text{disilicate-Fe(III)}] + {}^{\bullet}OH + OH^- \quad (47)$$

Following the pioneer work of Wang et al.[142] describing the chelating properties of tetrapolyphosphate, we used polyphosphates like tetrapolyphosphate (4-TPP), tripolyphosphate (3-TPP) and pyrophosphate (PP) as supporting electrolytes to circumvent the pH limitation in the EF process (see reactions (48)-(50)).[143,144] As an interesting result, it was found that the addition of TPP accelerated the cathodic cycle of Fe^{3+}/Fe^{2+} via decreasing the redox potential, also promoting the oxidation of Fe^{2+} to form ${}^{\bullet}OH$. Figure 12 shows that the ${}^{\bullet}OH$ generation ability decreased in the order: Fe^{2+}-4-TPP > Fe^{2+}-3-TPP > Fe^{2+}-PP $\approx$ Fe^{2+}-PO_4, which was in good agreement with charge transfer calculations by DFT and ultraviolet photoemission spectroscopy (UPS, Figure 12c).[106,143] The potential eutrophication concern derived from the presence of polyphosphate supporting electrolytes was addressed by $CaCl_2$ precipitation, and a promising high value-added compound was obtained after treatment.[145]

$$O_2 + Fe^{2+}\text{-TPP} \rightarrow Fe^{3+}\text{-TPP} + O_2^{\bullet-} \quad (48)$$

$$Fe^{2+}\text{-TPP} + O_2^{\bullet-} + 2H_2O \rightarrow Fe^{3+}\text{-TPP} + H_2O_2 + 2OH^- \quad (49)$$

$$Fe^{2+}\text{-TPP} + H_2O_2 \rightarrow Fe^{3+}\text{-TPP} + {}^{\bullet}OH + OH^- \quad (50)$$

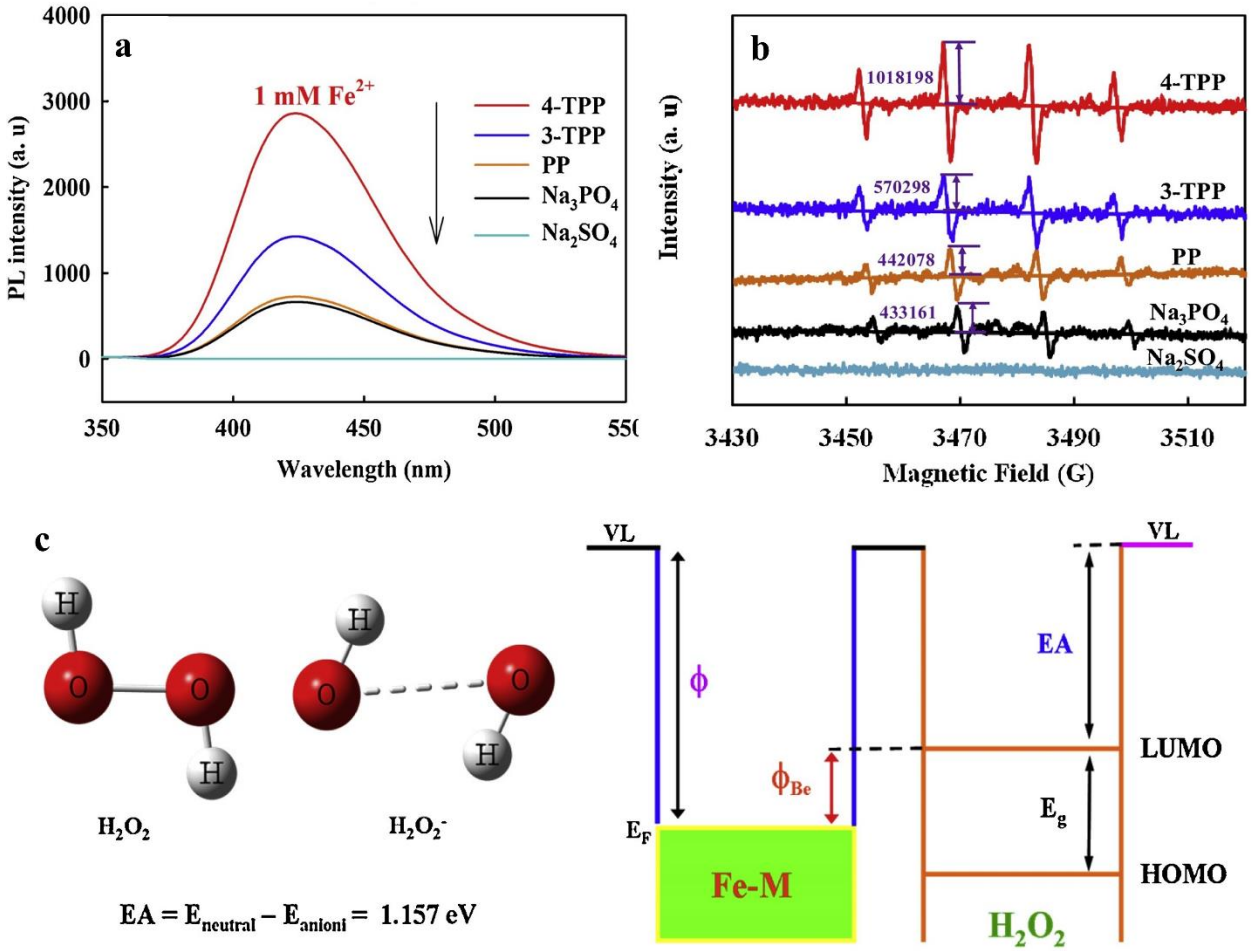

Figure 12. (a) PL spectra of 2-hydroxyterephthalic acid (TAOH) for different ligands, (b) ESR spectra of various Fe^{2+}-ligand complexes, and (c) energy level diagram of the Fe^{2+}-ligands and target molecule in contact and following the Schottky-Mott vacuum level alignment, in which VL, Φ, E_F, $Φ_{Be}$, E_g, EA, LUMO and HOMO stand for vacuum level, work function, Fermi level, electron injection barrier, energy gap, electron affinity, the lowest unoccupied and highest occupied molecular orbitals, respectively. Reproduced with permission from ref 143. Copyright 2019 Elsevier.

3.3.4. Microbial electro-Fenton systems

In recent years, bioelectrochemical and electro-Fenton systems (i.e., bio-electro-Fenton or bio-EF) have been merged by some scholars, giving rise to an EF process that can be self-powered by a microbial fuel cell. Usually, in bio-EF systems, the anodic chamber contains a bioanode colonized by microorganisms that converts the chemical energy stored in organic feed into electricity (Figure 13a). Thus, the performance of bio-EF is largely dependent on the electroactive bacteria that transfer electrons to the electrode surface upon oxidation of the organic matter contained in the anolyte. The

cathodic compartment generally consists of a conventional EF half-cell equipped with an electrode material capable of producing H_2O_2 (reaction (1)) that is further employed in Fenton's reaction (reaction (2)). A great advantage of bio-EF is its capacity to deal with refractory pollutants or wastewater in the catholyte in the absence of external power supply, since such wastes are generally toxic for the bioanode microorganisms. There are several types of bio-EF processes, depending on the biocell configuration, which include microbial fuel cells (MFCs)-EF, microbial electrolysis cells (MECs)-EF, microbial reverse electrodialysis cells (MRECs)-EF and MFC-powered MEC-EF. Such systems have been systematically described in recent review papers.[146-147] In bio-EF systems, microbial cultures are not directly involved in the degradation of pollutants on the cathodic chamber because the microorganisms are isolated in the anodic compartment.[149] As such, Fe^{2+} regeneration mainly depends on the cathodic Fe^{3+} reduction, following the mechanisms that have been described throughout the text. The efficiency of such iron reduction powered by the harvested bio-electrons has been demonstrated using *Shewanella decolorationis S12*,[150] *Shewanella putrefaciens SP200*, [151] Pseudomonas,[152] and mixed bacterial cultures from sludge.[153-155] Recently, a novel bio-EF system (Figure 13b) was proposed, in which Fe^{2+} mainly converted by *Pseudomonas* and *Geobacter* at anode chamber transported into cathodic part via cation exchange membrane for Fenton's reaction (2).[152] However, the low current output from the bio-EF process is still a concern for quantitative cathodic iron reduction.[156] Because of the oxidative environment generated in the EF half-cell of bio-EF systems, it is preferable to keep microorganisms in the anodic half-cell.

Whatsoever, it has been reported that microbial communities constituting a biocathode are promising options to remove toxic metals via microbial reduction.[157] As for the iron reduction, the first study on biocathodes to improve the regeneration rate of

dissolved Fe^{2+} in MFC was reported by Zhang's group (Figure 13c),[158,159] who used the iron-reducing bacterium (IRB) *Geobacter sulfurreducens*. This study was aimed at regenerating Fe^{2+} from ferric sludge derived from a neutral Fenton process. The regenerated Fe^{2+} solution was then used as catalyst for the Fenton treatment of domestic wastewater polluted with pharmaceuticals. Other IRBs include *Rhodoferax ferriredueens, Geothrix fermentans, Desulfobulbus propionieus, Shewanella futrefaciens,* and *Geobacter metallireducens*. Among them, *Geobacter* and *Shewanella*, whose whole genome sequencing has been completed, have been widely investigated.[160] For instance, it was reported that a *Geobacter sulfurreducens*-enriched biocathode enhanced the Fe^{2+} generation rate three-fold as compared to the cathode without biofilm. The authors outlined that the electrons used for Fe^{3+} reduction were originated from two sources: (i) the external circuit that connected with the bioanode, where microbial degradation of organics takes place, and (ii) the anaerobic metabolism of IRBs forming the biofilm, which are believed to be produced from a complex trans-periplasmic electron transfer chain involving a variety of c-type cytochromes (Figure 13d).[161] Hence, in the metabolic route, electrons are collected from the oxidation of the quinone pool by the tetraheme *c*-type cytochrome (CymA) located in the inner-membrane.[162] The small tetraheme cytochrome (STC) serves as redox shuttle to mediate electron transfer between CymA and other enzymes. This process culminates with the electrons arriving at the outer membrane, where they are transferred to Fe^{3+} to trigger its reduction. Overall, three ways for electron transfer from the outer membrane to dissolved Fe^{3+} can be distinguished (Figure 13c**)**: (i) electron transfer mediators such as outer-membrane CymA,[163] (ii) direct contact with Fe^{3+} ions,[164] and (iii) through adhered conducting structures such as highly conductive monolateral pili.[165]

As final consideration, the exploration of bio-EF processes incorporating biological half-cells in multiple stack cell reactors to boost Fe^{2+} regeneration can be envisaged as a novel research opportunity.

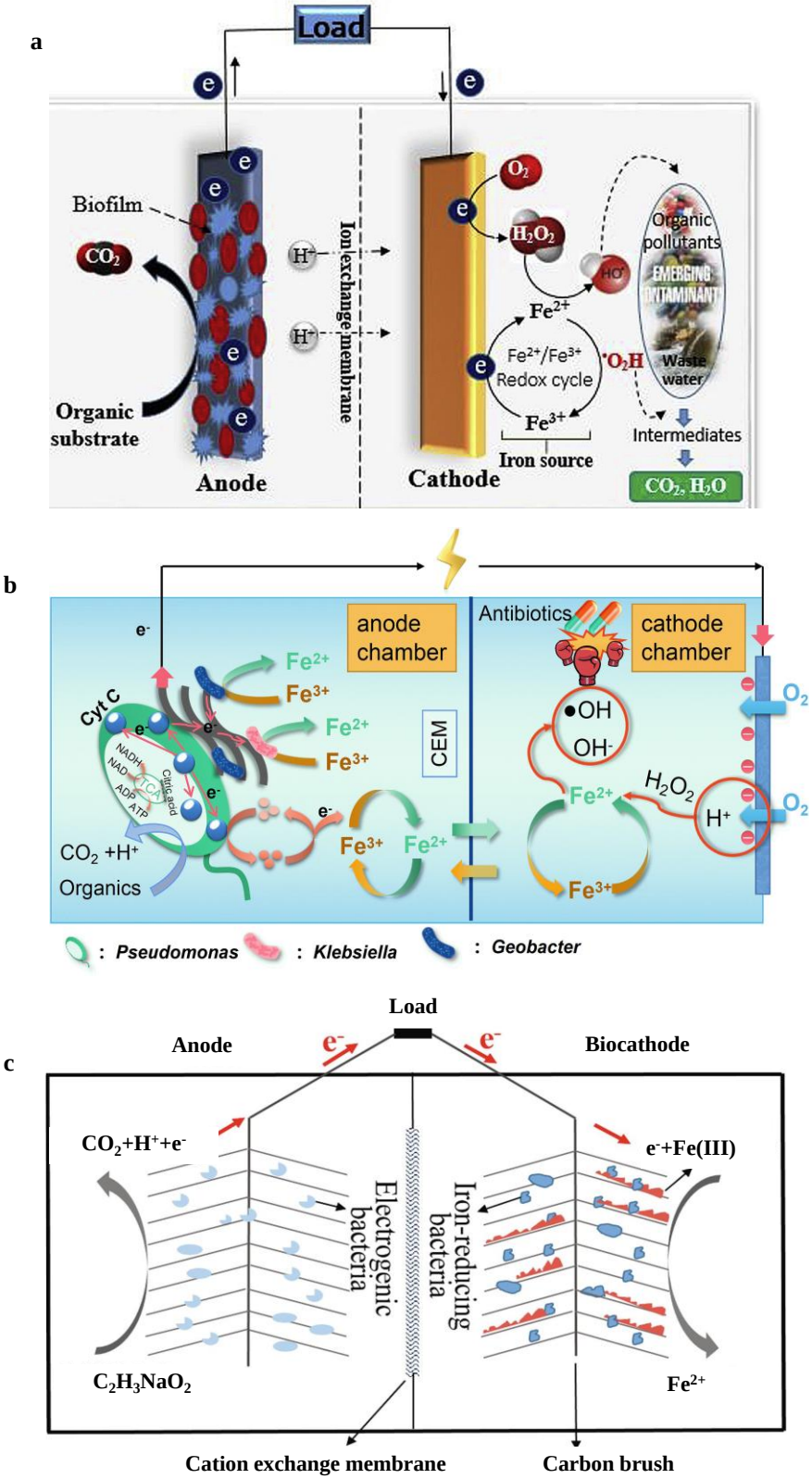

Figure 13. (a) Mechanism of the bio-EF system with a bioanode to supply electrons for cathodic iron reduction. Reproduced with permission from ref 148. Copyright 2019 Elsevier. (b) A novel double-chamber bio-EF with iron transported between anode and cathode chambers. Reproduced with permission from ref 152. Copyright 2022 Elsevier. (c) A two-chamber microbial electrolysis cell (MEC) with iron-reducing bacteria supported on a biocathode. Adapted with permission from ref 159. Open Access.

4. Mass transport improvement

In EF, the pH distribution in the cathode vicinity is different from the bulk pH (see Figure 1a). Theoretical calculations can be performed from Eqs. (51)-(53):

$$M(OH^-)=\frac{It}{zF} \tag{51}$$

$$[OH^-]=\frac{It}{250zF\pi d^2\delta} \tag{52}$$

$$pH=14+\log\left(\frac{It}{250zF\pi d^2\delta}\right) \tag{53}$$

where δ is the thickness of local layer (m), t is the electrolysis time (s), I is the applied current (A), z is the number of transferred electrons, F is the Faraday constant (96485 C mol^{-1}), and d is the diameter of the cathode (m).

The results obtained with the above equations coupled with local pH sensor allow establishing that the pH in the vicinity of cathode can reach values as high as 13 with continuous production of OH^- via HER/ORR and a relative slow supply of H^+ from the bulk. The pH in the cathode vicinity has been reported to keep high despite strong mechanical mixing.[21] Inevitably, the local cathodic alkaline environment leads to the formation of $Fe(OH)_3$ and reduces the amount of soluble iron ions, as confirmed by previous investigations, especially in EF with gas-diffusion electrodes.[166] Effective strategies are then required to modulate the cathodic local alkaline environment to boost iron mass transport and prevent its precipitation, which is detrimental for Fe^{3+} reduction.[167,168] This subsection discusses the approaches to improve iron mass transport in local environment, including:

(i) The application of physical phenomena such as magnetic fields to produce additional forces on iron ions and favor their local mass transport;

(ii) the use of pulse electrolysis instead of conventional continuous signals;

(iii) the promotion of interfacial Joule heating effect to increase the temperature in the close vicinity of cathode.

4.1. Magnetic fields (magnetization)

Magnetic fields have attracted great attention and present an interesting effect on physicochemical processes in electrochemical systems.[169,170] The introduction of magnetic fields in EF is attractive because of their availability, efficiency, and relatively low cost.[171] In general, there are two forces involved when applying magnetic fields to electrochemical systems: the Lorentz force (F_L) given by Eq. (54) and the magnetic field gradient forces or Kelvin forces ($F_{\nabla B}$) defined by Eq. (55):[172,173]

$$F_L = j \times B \tag{54}$$

$$F_{\nabla B} = \frac{X}{\mu_0} B \frac{dB}{dx} \tag{55}$$

where j is the current density, B is the magnetic field, X is the volume susceptibility of magnetic species, μ_0 is the permeability of free space (usually its value is $4\pi\times10^{-7}$ H m^{-1}), and $\frac{dB}{dx}$ is the time change rate of the magnetic field (T m^{-1}).

$F_{\nabla B}$ arises from the magnetization of species with different magnetic properties in the applied nonuniform magnetic fields, including those with paramagnetic/diamagnetic/ferromagnetic nature.[173,174] According to Eq. (55), $F_{\nabla B}$ is proportional to the susceptibility of magnetic species (closely related to the paramagnetic/diamagnetic/ferromagnetic nature of the species), the magnetic field, and its gradient. The formed $F_{\nabla B}$ would be lower than the external applied magnetic field if species are antimagnetic ions. On the contrary, $F_{\nabla B}$ could be intensified for the

paramagnetic ions, such as O_2 and NO_3^-. This enhancement can be largely boosted with ferromagnetic species such as Fe, Co and Ni ions,

Several reviews on the combined effects of magnetic fields in electrochemistry, involving kinetics, mass transport and double layer, among others, have been published during the last decades.[175] The magnetic field was proven to accelerate the Fe^{3+} reduction as well,[176,177] and the boosting mechanism has been described as follows:[178]

(i) It enhances the convection and thus reduces the thickness of the diffusion layer by complex micro-magnetohydrodynamic (MHD) phenomena derived from the Lorentz Force imposed on the positively charged iron ions ($X = 14750 \times 10^{-9}\ M^{-1}$) (see Figure 14a);[174]

(ii) it alters the accumulation of paramagnetic species (Fe^{2+} and Fe^{3+}) at the cathodic interface due to formed forces acting on iron ions.[179,180] These paramagnetic species tend to accumulate along the magnetic lines with a higher magnetic flux intensity owing to the magnetic field gradient force $F_{\nabla B}$ that is induced.[173,175]

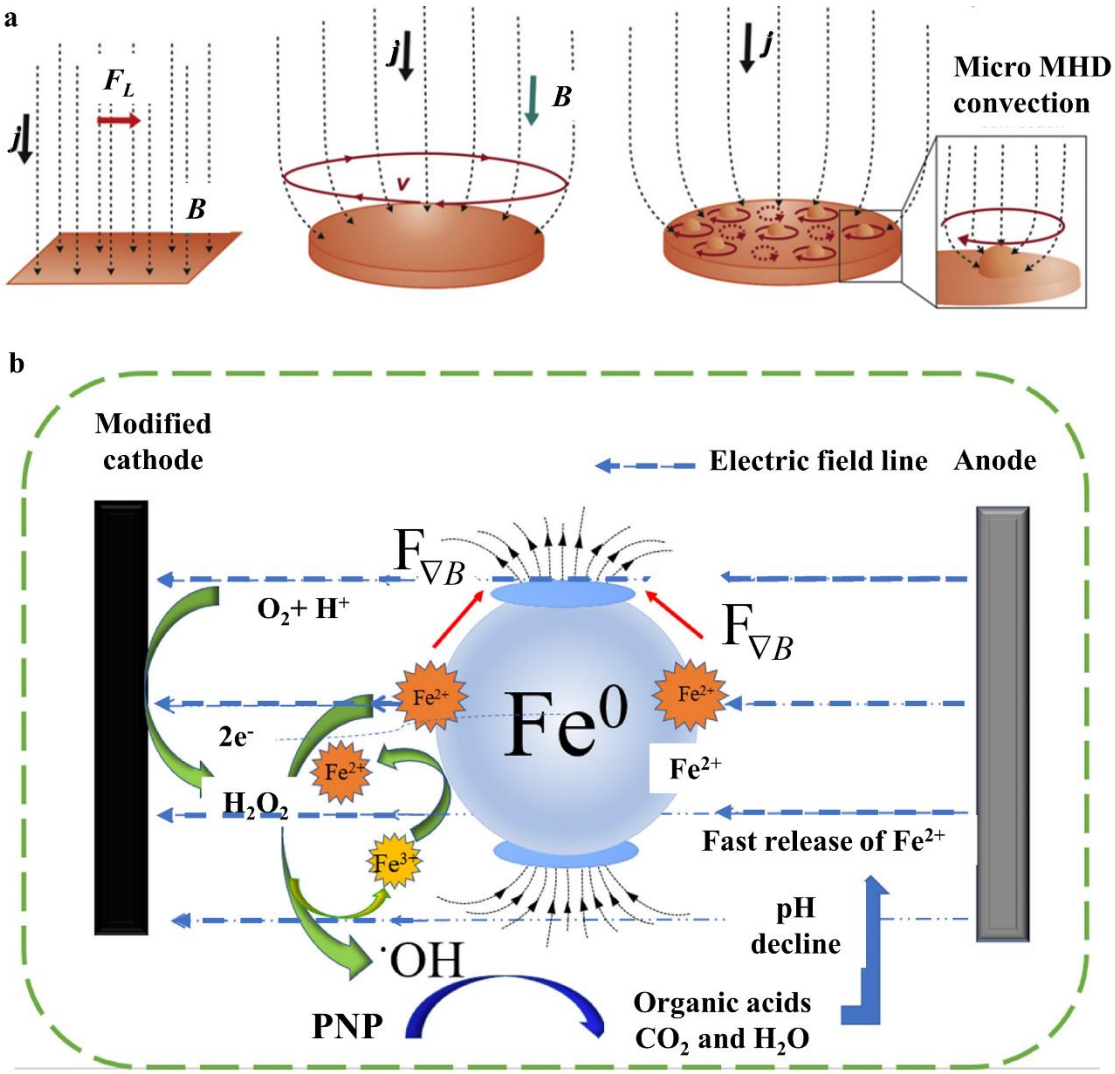

Figure 14. (a) Magnetically-induced micro-magnetohydrodynamic (MHD) convection. Reproduced with permission from ref 174. Copyright 2014 Elsevier. (b) Mechanism of pre-magnetized iron for enhancing the Fe^{3+} reduction in the EF process. Reproduced with permission from ref 181. Copyright 2020 Elsevier.

The influence of the magnetic field on cathodic iron reduction dates back to 1954, when Yang and co-workers reported the use of a magnetic field placed perpendicularly to the cathode, favoring the accumulation of a larger concentration of paramagnetic Fe^{2+} near the cathode region as compared to the trial in the absence of the magnetic field.[182] Very recently, Tian et al.[181] introduced a weak magnetic field in EF from ferromagnetic Fe^0 and paramagnetic Fe^{2+}/Fe^{3+}. $F_{\nabla B}$ induced the corrosion of magnetized Fe^0 and generation of paramagnetic ions (especially Fe^{2+}) responsible for

the Fenton's reaction (2). An enhancement of the mass transport of iron ions to the cathode was also observed, which can be explained by the movement of Fe^{2+} towards the magnetic lines with higher magnetic field flux intensity, as shown in Figure 13b. A similar phenomenon was also observed for the paramagnetic Cu^{2+} ($X = 1460 \times 10^{-9}$ M^{-1}).[183]

4.2. Pulse electrolysis

Compared to conventional galvanostatic or potentiostatic modes in electrocatalytic processes, pulsed current/potential was reported as a novel strategy to boost iron reduction. Pulse electrolysis induces not only periodic changes in the cathode potential, but also local changes in the environment of the electrode surface. Our groups developed a dual-cathode pulsed current EF system to assist iron reduction thanks to the minimization of cathode surface alkalization,[166] as shown in Figure 15a. By using this system, the low H^+ concentration in the vicinity of the cathode resulting from the ORR and H_2 evolution was avoided with the current pulses, which allowed abundant H^+ in the bulk migrate toward the cathode surface during the current off-time (2 s). Similarly, the accumulated OH^- diffuses out and thus, the mass transport of iron ions is enhanced. Aside from regulating the iron mass transport via pulsed current, reactivity/selectivity of other reactions like ORR or the electrochemical CO_2 reduction (CO_2RR) can also be tuned. Ding et al.[184,185] (Figure 15b) found that pulsed potential also tuned the charge/discharge process of the electric double layer, modifying in turn the adsorption of reaction intermediates like *OOH, $*O_2$ and *H, as confirmed by DFT stimulations. The boosted reactivity/selectivity might be due to the suppressed HER via a dynamic rearranging of such surface intermediates. A comprehensive review of pulse electrolysis was summarized by Liu et al.[186], who concluded that both modified surface states along with induced chemical environments of the formed intermediates were the

dominant factors to tune the corresponding selectivity. From the enhancement of ORR/CO_2RR reactivity/selectivity, one can suggest that the chemical state of iron ions along with the kinetic rate of iron reduction could be tuned simultaneously to the mass transport enhancement. However, limited attention has been given to pulse electrolysis and further research is needed to go deeper into the mechanistic understanding of iron reduction enhancement by the dynamic chemical microenvironments generated.

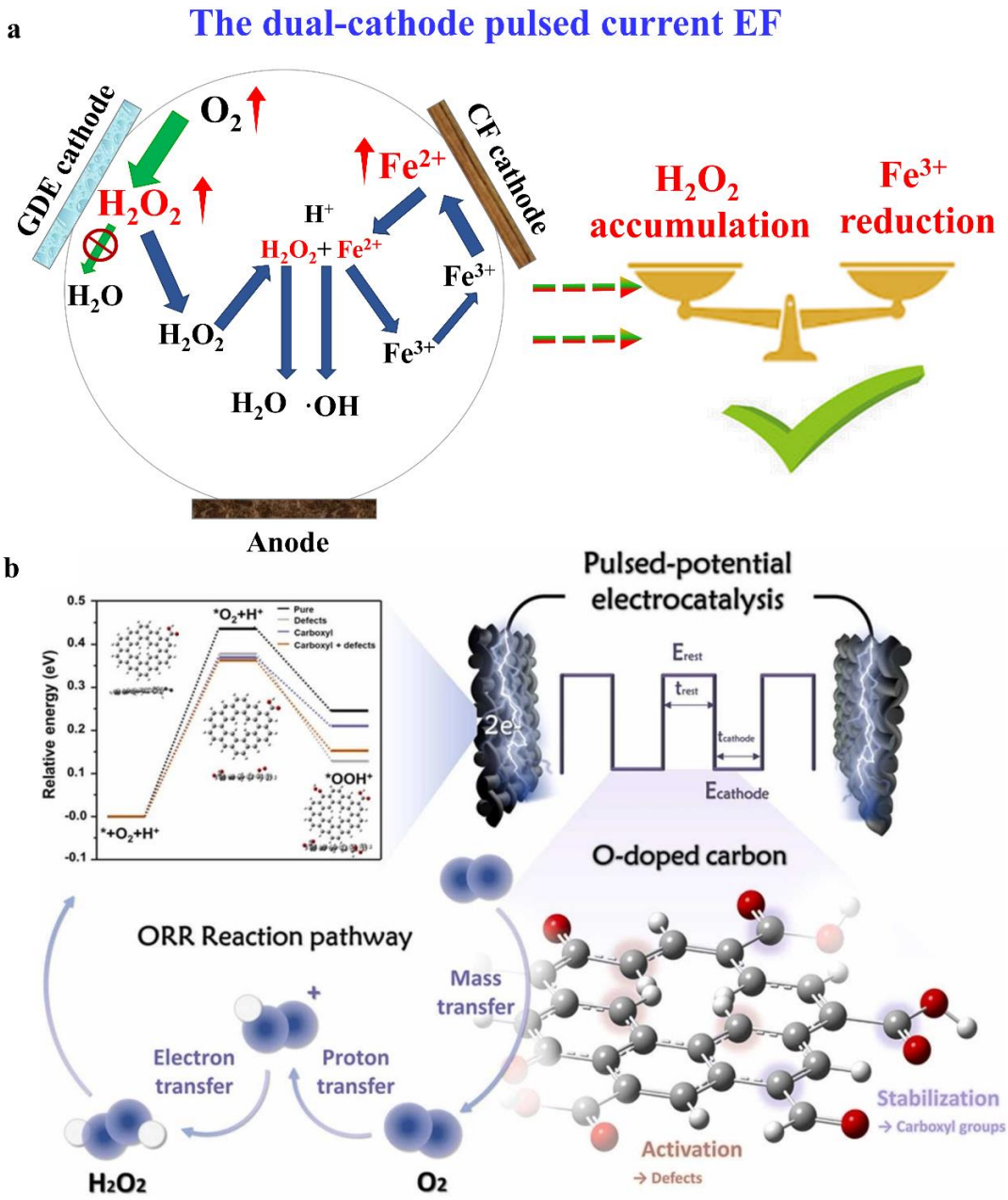

Figure 15. (a) Plausible mechanism in a two-electrode pulsed current system for EF process. Reproduced with permission from ref 166. Copyright 2020 Elsevier. (b) Pulsed current system. Reproduced with permission from ref 185. Copyright 2022 Elsevier.

4.3. Interfacial Joule heating effect

Although the electrochemical Fe^{3+}/Fe^{2+} cycling is a function of applied potential, as stated in section 2.1, it is also influenced by temperature. An early investigation by Qiang et al.[187] showed that a rise in bulk solution temperature significantly improved the Fe^{2+} electrochemical regeneration rate, increasing from 48% at 10 ºC to 80% at 46 ºC. This phenomenon was in good agreement with the Arrhenius equation, corroborating that the Fe^{3+} reduction rate is temperature-dependent. More important, increased mass transport can be expected as well, since the diffusion coefficients (*D*) of iron ions are a function of temperature.

However, it is not feasible to heat the whole solution to the desired temperature, not only because an energy input with a specific heat capacity as high as 4.2 kJ kg^{-1} C^{-1} is needed, but also because the electrochemical Fe^{2+} regeneration takes place mainly in the cathodic double layer, not in the bulk. Therefore, the "interfacial Joule heating" (IJH) effect could be used to increase the temperature within the double layer itself. The IJH is known as the heat released from current dissipation to the surrounding environment, according to Joule's law. Pei et al.[188] demonstrated the existence of a temperature gradient between the double layer and the bulk through the IJH effect, increasing the temperature from 23.6-28.2 ºC in the bulk to 59.8 ºC at the surface of the electrode. The temperature gradient was more pronounced at higher current density and only existed in the boundary layer of the electrode. The rate constant (*k*) and diffusion coefficients (*D*) of Fe^{3+}/Fe^{2+} within the boundary layer were then increased, boosting the mass transport as shown in Eqs. (56) and (57). Although the IJH effect could increase the temperature and boost the mass transport of Fe^{3+}/Fe^{2+}, the electrodes

themselves could undergo some damage if the temperature rises too high. As can be seen in Figure 16, the highest temperature reached by the IJH effect on the surface of a titanium suboxide (TiSO) plate (x = 0 cm) working at 10 mA cm^{-2} was 70 ºC. The electrode had a surface area of 105 cm^2 and high resistance of 25 ± 2 Ω. In this case, no damage to the electrode surface was reported.[189] On the contrary, it was reported that the localized current-induced IJH effect rose the temperature up to 500 ºC to locally melt the microstructure of an Au electrode with a potential as high as 100 V.[190] This was due to the high resistance of the Schottky barrier at the Au-ZnSe nanowire contact. Hence, the temperature increase induced by the IJH effect is largely dependent on the electrode/catalysts' resistance, applied potential/current density, cell configuration and electrolysis time. If is therefore necessary to control the local temperature generated by the IJH effect in order to avoid damage to the electrode structure.

$$k(t) = k_0 \exp\left\{-\frac{E_a}{\mathrm{R}}\left[\frac{1}{T(t)+273.15}-\frac{1}{T_0+273.15}\right]\right\} \tag{56}$$

$$D_\mathrm{t} = \frac{D_0\mu_0}{T_0+273.15}\frac{T_\mathrm{t}+273.15}{\mu_\mathrm{t}} \tag{57}$$

where E_a is the activation energy, T is the temperature in ºC, and μ is the kinematic viscosity.

The thermodynamics and kinetics of Fe^{3+} ions reduction within the boundary layer can be modified by the IJH effect. The boosted molecular thermodynamic movement coupled with lower kinematic viscosity can drive Fe^{3+}/Fe^{2+} ions to move faster to/from the electrode. This can be related to theoretical calculations based on the collision theory and the Maxwell function given by Eqs. (58)-(62) for average values of speed v_m, kinetic energy $E_{\mathrm{K-m}}$, rotational energy $E_{\mathrm{R-m}}$ and internal energy $E_{\mathrm{I-m}}$.

$$f(v)= 4\pi\left(\frac{m}{2\pi kT}\right)^{1.5}\exp\left(-\frac{mv^2}{2kT}\right)v^2 \tag{58}$$

$$v_{\mathrm{m}} = \int_0^{\infty} vf(v)dv = \sqrt{\frac{8RT}{\pi M}} \tag{59}$$

$$E_{\mathrm{K\text{-}m}} = \frac{i_{\mathrm{K}}}{2}kT \tag{60}$$

$$E_{\mathrm{R\text{-}m}} = \frac{i_{\mathrm{R}}}{2}kT \tag{61}$$

$$E_{\mathrm{I\text{-}m}} = \frac{i_{\mathrm{I}}}{2}kT \tag{62}$$

where k is the Boltzmann constant (1.38×10^{-23} J K^{-1}), v (m s^{-1}) is the molecular speed, T is the temperature (K), and m is the molecular mass (kg), and M is the molar mass (g/mol).

Considering the commonly used high current density in the EF process, the IJH effect-based EF could show an impact on Fe^{3+} reduction as well. However, more investigation is needed, especially to attain a trade-off between the current efficiency for desirable reactions and the IJH effect.

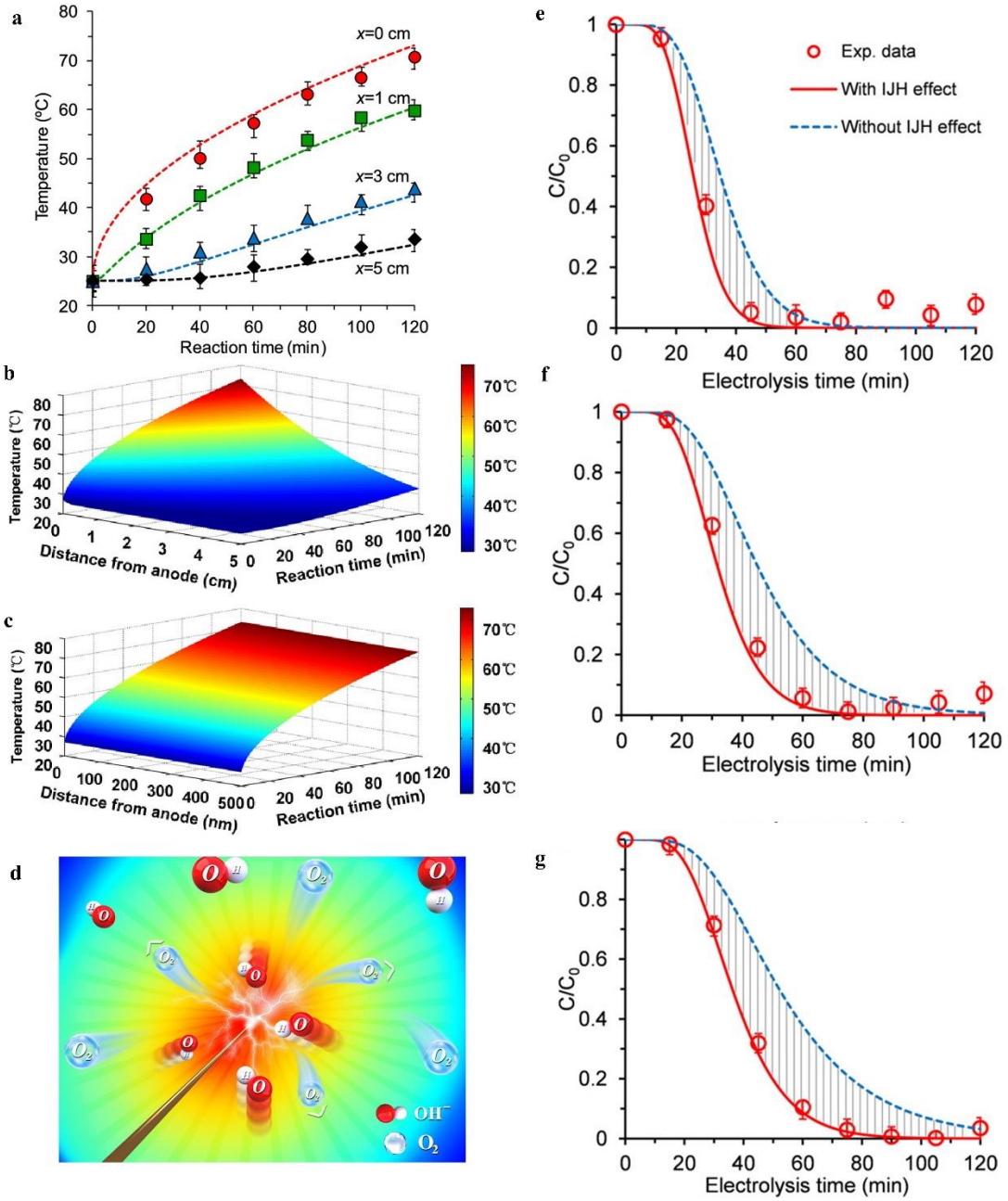

Figure 16. (a) Temperature on the surface of a TiSO anode (x = 0 cm) detected with thermocouples at locations of x = 0-5 cm. (b-c) Temperature field modeled at the location on scales of x = 0-5 cm and x = 0-500 nm. Reproduced with permission from ref 191. Copyright 2019 American Chemical Society. (d) Nanotip-enhanced local temperature. Reproduced with permission from ref 189. Copyright 2022 Elsevier. (e-g) Electrochemical oxidation of phenol, *p*-CP, and 2,4-D at low temperature, in which the shadow zones indicate decoupled contribution of the IJH effect. Reproduced with permission from ref 188. Copyright 2020 American Chemical Society.

4.4. Photo-assisted electrolysis

The photo-assisted EF process is known as photoelectro-Fenton (PEF), in which electrochemistry and photocatalysis are combined. In PEF, the solution is irradiated with UVA light (λ = 315-400 nm, λ_{max} = 360 nm) or visible-light. A higher Fe^{3+} reduction rate is found because of the following photolytic reactions:[192-194]

(i) Photosensitive Fe^{3+} ions are directly reduced to Fe^{2+} via photon absorption according to reaction (63) for Fe^{3+} and reaction (64) for $[Fe(OH)]^{2+}$, the predominant form in acidic medium at pH 2.5-3.5 (Figure 17a);[195]

(ii) photolysis of Fe(III)-carboxylate complexes ($[Fe(OOCR)]^{2+}$) to Fe^{2+} by reaction (65). These complexes are formed with short-chain acids, which are the final degradation by-products during EF prior to total mineralization to CO_2. The most commonly formed carboxylic acid is oxalic acid, which originates Fe(III)-oxalate complexes like ($Fe(C_2O_4)^+$, $Fe(C_2O_4)^{2-}$ and $Fe(C_2O_4)_3^{3-}$) via the general reaction (66) (Figure 17b);[196]

(iii) photoinduced electrons (e_{CB}^-) by UV/Vis illumination over a semiconductor (e.g., TiO_2) could also assist the Fe^{3+}/Fe^{2+} cycle at its surface by reactions (67) and (68).[196]

$$Fe^{3+} + H_2O + h\nu \rightarrow Fe^{2+} + {}^{\bullet}OH + H^+ \quad (63)$$

$$[Fe(OH)]^{2+} + h\nu \rightarrow Fe^{2+} + {}^{\bullet}OH \qquad k = 0.0012\ s^{-1} \quad (64)$$

$$[Fe(OOCR)]^{2+} + h\nu \rightarrow Fe^{2+} + CO_2 + R^{\bullet} \quad (65)$$

$$2[Fe(C_2O_4)_n]^{(3-2n)} + h\nu \rightarrow 2Fe^{2+} + (2n-1)C_2O_4^{2-} + 2CO_2 \quad (66)$$

$$\text{Semiconductor} + h\square \rightarrow e_{CB}^- + h_{VB}^+ \quad (67)$$

$$\equiv Fe(III) + e_{CB}^- \rightarrow \equiv Fe(II) \quad (68)$$

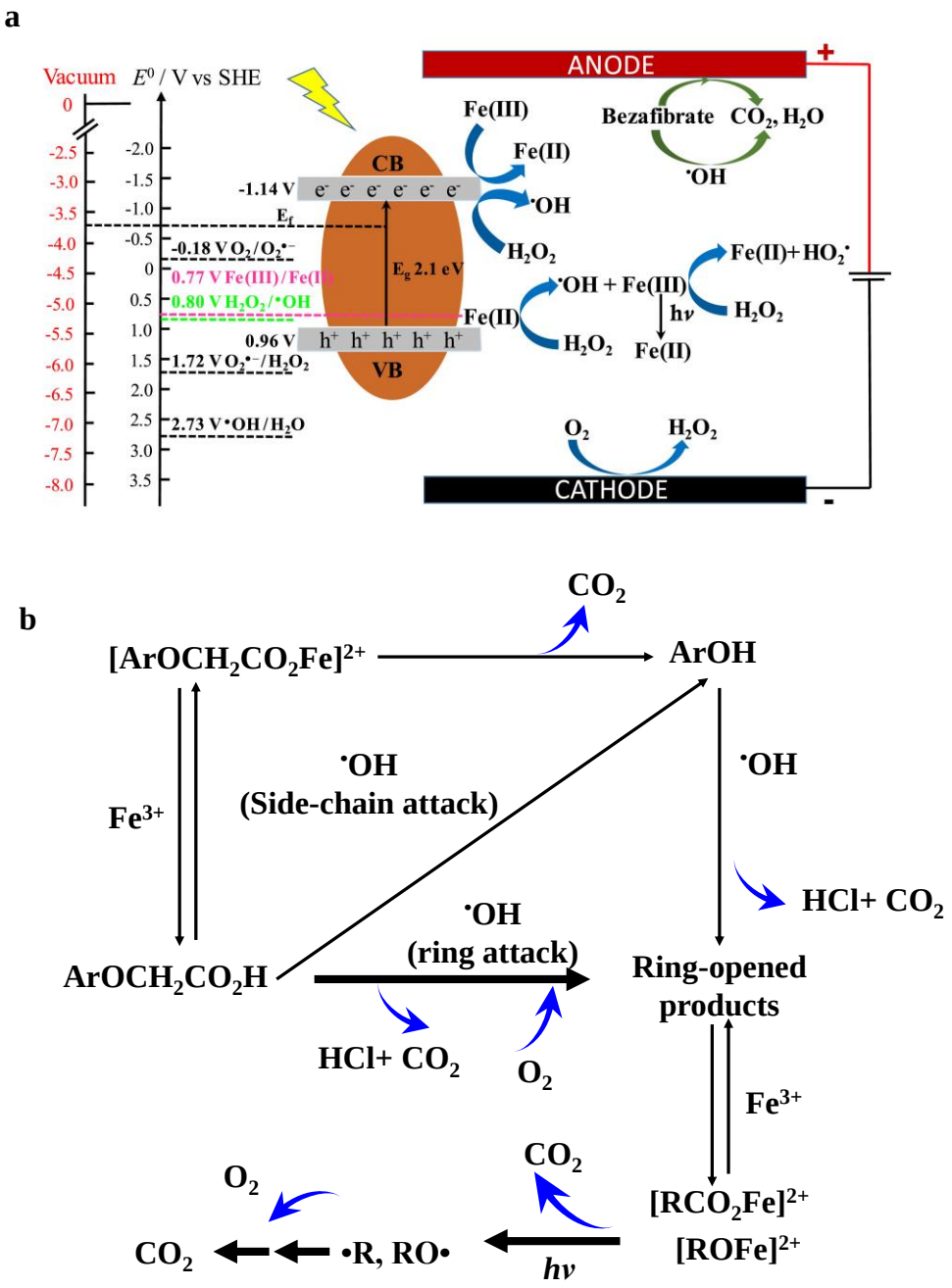

Figure 17. (a) Photosensitive Fe^{3+} ions are directly reduced to Fe^{2+} via photon absorption. Reproduced with permission from ref 194. Copyright 2020 Elsevier. (b) Photolysis of Fe(III)-carboxylate complexes. Reproduced with permission from ref 196. Copyright 1993 American Chemical Society.

4.5. In-situ H^+ formation

Aside from the abovementioned methods for iron reduction, *in-situ* H^+ generation via the anodic oxygen reduction reaction (OER, reaction (69)) has also been reported as a strategy to enhance the iron mass transport in EF in an undivided two-electrode cell.[56] The OER is the bottleneck for H_2 evolution from water splitting, owing to its

high overpotential (1.23 V *vs.* SHE), which means that a high current is needed to drive the anodic H^+ generation via reaction (69). On the cathode surface, H_2 evolution tends to prevail over the iron reduction or the ORR at such high current. To tackle this issue, the cathodic current density should be lower than the anodic one, aiming to favor the iron reduction. To achieve this, modifications in the total surface area of the cathode have been reported, as depicted in Figure 18.[198] A larger number of cathodes was used in the EF cell, which resulted in a lower current density in each cathode, depressing H_2 evolution in favor of Fe^{3+} reduction. The H^+ formed via the OER can diffuse into the cathodic local area and prevent the iron precipitation. In this way, the mass transport of iron ions was enhanced. Analogously, Yuan et al.[199] proposed a divided EF system with one anode and two cathodes, where excessive H^+ exists in the system, resulting in an improvement of the Fe^{3+}/Fe^{2+} cycle. A recent study of Zhang et al.[56] also reported a similar strategy to boost the iron cathodic reduction.

$$2H_2O \rightarrow O_2 + 4H^+ + 4e^- \qquad E^0 = -1.229 \text{ V vs.SHE} \qquad (69)$$

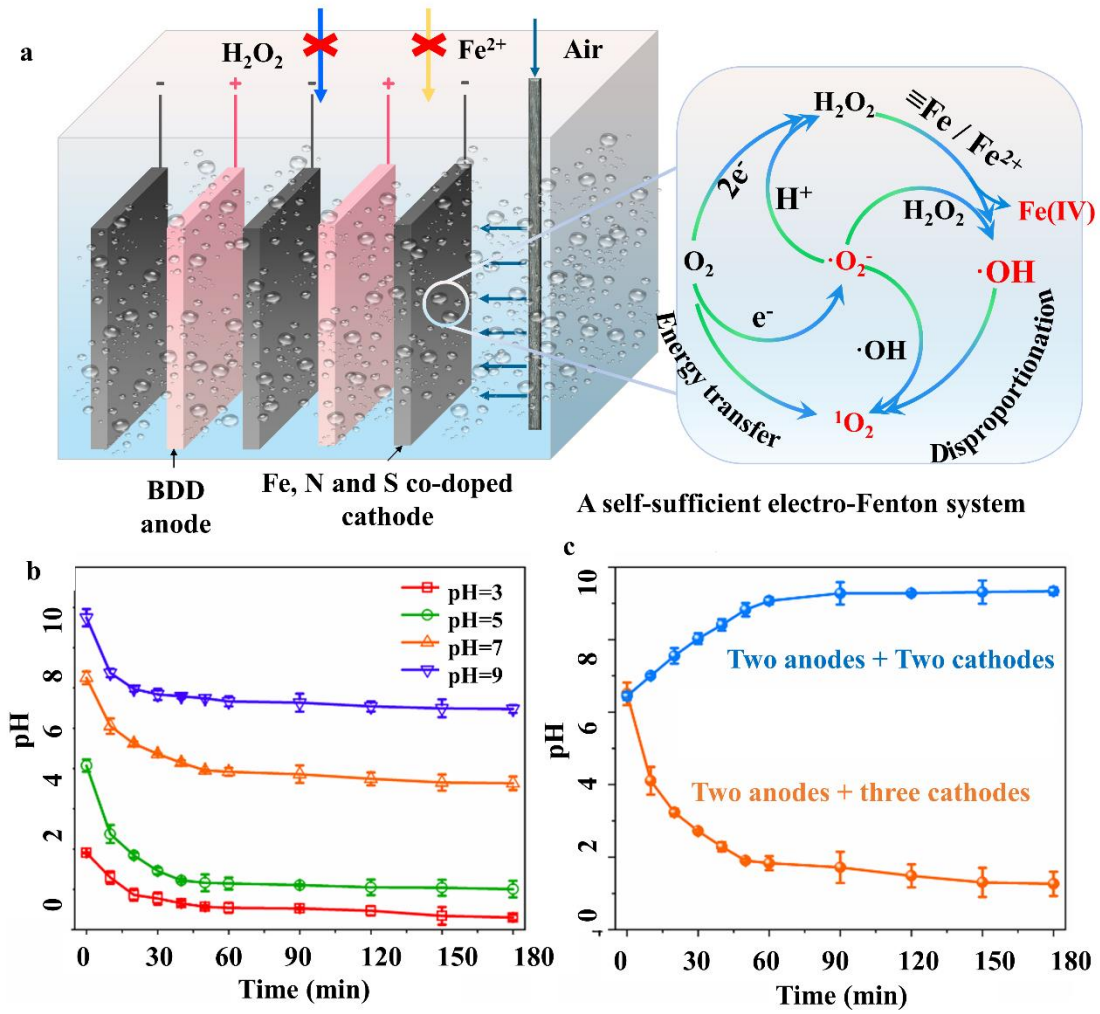

Figure 18. (a) Schematic diagram of a self-sufficient electro-Fenton system. Plot of pH versus time with different (b) initial pH and (c) number of cathodes. Reproduced with permission from ref 198. Copyright 2022 Elsevier.

5. Challenges and future prospects

Despite the achievements obtained so far to enhance the Fe^{2+} regeneration in EF, there are still some concerns regarding the Fe^{3+}/Fe^{2+} cycling that should be surmounted in future investigations to widen the implementation of EF in industrial applications.

(i) Cathodic iron reduction along with H_2O_2 formation via the 2-e^- ORR is triggered in active sites on the electrode surface. It is then of great importance to clarify the active sites for each specific reaction. This will help to design cathode materials with suitable active sites for each reaction to maximize the EF performance.

(ii) In general, hydrated Fe^{3+} is the main form taken into consideration when evaluating the Fe^{3+}/Fe^{2+} cycling. However, the speciation of Fe^{3+} at different pH values presents a series of aqueous Fe^{3+} species with different properties. For example, the electron-deficient Fe^{3+} is more susceptible to electronegative sites, but $[FeOH]^{2+}$ species can bind with electropositive sites via electron-rich oxygen.[67] In this regard, the speciation of Fe^{3+} at different pH values should be taken into consideration, including reactivity for iron recovery, H_2O_2 decomposition, and so on. It is well known that both homogeneous and heterogeneous iron reduction reactions are involved in EF,[200] and consequently, attention should be given to both types of processes.

(iii) The diffusion and double layer at the cathode side, whose length is in the millimeter range, are the main reaction zones for both H_2O_2 cathodic production and iron reduction. More fundamental investigations related to the processes taking place in this area are needed to lay down the mechanistic aspects involved, such as the spatial and temporal distributions of dissolved oxygen, H^+, Fe^{2+} and Fe^{3+} in such microenvironment. For instance, the active species formed in a local alkaline environment at the cathode may be different from the species in the bulk since the electric field can be as high as 10^9 V m^{-1}. Hence, operando spectroscopic or microscopic tools are crucial to analyze these phenomena, such as in-situ X-ray photoelectron spectroscopy, in-situ electrochemical attenuated total reflection Fourier-transform infrared spectroscopy or operando X-ray absorption spectra measurement.

(iv) Simulations are needed when in-situ *operando* spectroscopic or microscopic techniques fail to unveil the nature in the microenvironment. It is known that modeling in the EF process via density-functional theory (DFT) calculations is mainly based on the electronic effects in the cathode structure. Besides, in recent years, molecular dynamics simulations have been also used in EF to do the simulation from a large-scale

atomic view.[201] However, the cathodic iron reduction and H_2O_2 generation via ORR are controlled by both mass transport and electronic effects.[202] Hence, models that are closer to real conditions are needed. Among the proposed models, microkinetic modeling proposed by Huang, which incorporated the electronic effects, double-layer effect and mass transport, constitutes a good example.[203]

(v) The dominant role conferred to Fe^{2+} is the activation of the cathodic electrogenerated H_2O_2 into $^{\bullet}OH$ through Fenton's reaction (2). However, this is limited by the narrow operation pH and iron sludge production and hence, more cleaner ways must be developed to produce $^{\bullet}OH$. For example, the three-electron oxygen reduction reaction (O_2 - H_2O_2 -$^{\bullet}OH$), activated by atomic H*.[204]

(vi) Aside from the magnetic field, magnetohydrodynamics favoring iron reduction, its influence in the spin-dependent electrochemical behavior of Fe^{3+}/Fe^{2+}, and the electron-transfer process should be further investigated. Recent works have shown a magnetic field-controlled spin-dependent reduction reaction in Pd nanoparticles.[205] and Ni^{2+}/Ni^{0} .[206] The influence of formation and detachment of cathodic H_2 with magnetic fields should also be considered as it leaves more active sites for iron reduction.

(vii) Although many studies have reported the enhancement of iron mass transport via MHD in the presence of magnetic fields, more fundamental research is needed to clarify the changes in the inner and outer Helmholtz planes, as well as in the diffusion layer.

(viii) Aside from Fe^{3+} reduction, other factors altering the double-layer structure may have significant effects. For example, cations in the double layer might induce the cation promotion effect, consisting in the modification of the rate-determining electron transfer to O_2 following the order: $Cs^+ > K^+ > Li^+$.[207, 208] In addition, the common anions

present in the water like CO_3^{2-} and SO_4^{2-} may have a significant irreversible poisoning effect on the ORR as reported for Pt/C catalysts.[209] The influence of different ions on the structure of the double-layer and how they affect the cathodic iron reduction or ORR in EF have not been investigated in detail yet.

(ix) For the well-established H_2O_2 generation via ORR, the following unified key performance indicators are commonly used as benchmark: onset potential and reduction current (from voltammetric studies), yield and selectivity (from rotating ring-disk electrode measurements) and current efficiency (from bulk electrolysis). In contrast, there is a lack of such indicators for cathodic iron reduction. Several EF works have reported the evolution of total Fe, Fe^{2+} and Fe^{3+} during the treatment as a means to evaluate the cathodic iron reduction capacity. These measurements could be considered as plausible Fe^{3+} reduction performance indicators.[138] In addition, current efficiency for Fe^{3+} reduction could be another potential indicator that has not been explored. In this regard, unified benchmarks for the evaluation of the catalytic activity for Fe^{3+} reduction should be developed.

(x) Even though this review paper has focused on the fundamental aspects regarding the Fe^{2+} regeneration during EF, scale-up investigations using real wastewater samples are crucial for large-scale applications, since other organic and/or inorganic components of the actual matrices may have important effects on the performance. For instance, the presence of ions like Ca^{2+}, Mg^{2+} and CO_3^{2-} in water may result in cathodic salt precipitation (mostly $CaCO_3$ and $MgCO_3$) caused by local alkalization.[210] Salt precipitation may result in electrode passivation, leading to high energy consumption and additional maintenance costs. Besides, electrode passivation may be irreversible even after acid-washing recovery.[211] Several investigations have demonstrated the efficiency of EF in the treatment of real industrial wastewater,

generally at bench-scale,[212] whereas larger-scale reports are still scarce.[213] The readers are referred to recent review papers by authoritative groups on EF applications, advances and prospects for further details.[202, 214-216]

6. Conclusions

This work reviews the main mechanisms involved in the regeneration of Fe^{2+} ions from Fe^{3+} cathodic reduction during EF, as well as other strategies that have been implemented to enhance such process. The ideas presented here offer a critical point of view on the progress of Fe^{2+} regeneration in EF, aiming at drawing more attention to this essential process that ensures the availability of Fe^{2+} ions that allows maintaining the Fenton´s reaction (2). The main approaches that have been explored to boost the Fe^{3+} reduction to Fe^{2+} have been directed to enhance either the electron transfer or mass transport. Electron transfer strategies include the development of electron-rich materials, single-atom catalysts, materials with confinement effects, inorganic chelating agents and even microbial fuel cells. The use of magnetic fields, pulse electrolysis, the interfacial Joule heating effect, and photoirradiation with UVA light have been proposed as mass transport improvement approaches. More research is required in all these fields in the next future to achieve a better development and understanding of the processes considered in them.

This review paper gives the basis to better understand the Fe^{3+}-to-Fe^{2+} conversion in EF, which can guide scientists in the development of enhanced cathode materials for both H_2O_2 production and Fe^{2+} regeneration, as well as novel catalysts for higher efficiency, with the goal of designing highly effective EF systems for wastewater treatment at industrial scale. Regarding water disinfection, the spread of Covid-19 has awakened the awareness for the need of next-generation disinfection techniques, where

EF could find a great niche of opportunities. In this context, this manuscript provides some hints to boost the •OH production and hence, the disinfection performance, through the optimization of Fe^{2+} regeneration.

The ultimate goal of investigating the Fe^{2+} regeneration efficiency during EF is to encourage the EF application at large scale. One of the major challenges of EF is its high energy consumption derived from its operation costs related to electricity, which could be a limitation, especially in rural areas with restricted access to the electricity grid. The use of renewable energy sources such as solar and wind could alleviate such issues, increasing at the same time the competitiveness of this technology.[10, 217] In the same line, EF could be easily scaled up for industrial applications in countries with accessible electricity prices such as Canada, where electricity cost is 50% lower than in the US.[218,219] On the other hand, the installation/initial capital costs are still elevated, estimated at approximately USD $27,000-$40,000 per m^3 of treated wastewater, establishing a COD removal rate of 85%.[220] Although there are still some challenges to scale-up the EF process, we do believe that it will find industrial applications in the near future if enough data on operation and equipment costs of larger-scale systems are proven to be competitive. From our perspective, the main niche of application is the treatment of hard-to-treat industrial wastewater employing devices powered by renewable energy sources with net zero carbon emissions. In this regard, solar PEF with solar collector-type photoreactors is one of the most promising EF alternatives for either centralized or on-site wastewater treatments in sunny locations.

Acknowledgements

This work is *in honor of Prof. Enric Brillas's life-long contribution to electrochemistry*. It has been supported by National Natural Science Foundation of

China (No. 52000052 and No. 52070056) and State Key Laboratory of Urban Water Resource and Environment (Harbin Institute of Technology, No. 2021TS26). The postdoctoral scholarship awarded to Fengxia. Deng. (State Scholarship Fund, CSC, China) is acknowledged. I. Sirés and E. Brillas are grateful to financial support from project PID2019-109291RB-I00 (MCIN/AEI/10.13039/501100011033, Spain). We appreciate kind suggestions given by Baojian Jing, Yingshi Zhu, Wei Zhou and Zhihong Ye.

AUTHOR BIOS

Fengxia Deng (Researcher ID: 0000-0001-8645-3876) is an assistant professor at the School of Environment, Harbin Institute of Technology, China. Currently, she is working as a post-doc at the *Universitat de Barcelona* (Spain), in the specialty of Electrochemistry under the supervision of Prof. Enric Brillas and Prof. Ignasi Sirés. She received her Ph.D. in Environmental Science and Engineering from the Harbin Institute of Technology in 2019. During her Ph.D. study, she obtained CSC scholarship and being as a joint Ph.D. candidate at the National University of Singapore (Singapore) under the joint supervision of Prof. Olivier Lefebvre and Prof. Fang Ma. Dr. Fengxia has won the Excellent Oral Presentation Award, and Best Poster Award three times in the international conference Currently, her research mainly focuses on the electro-Fenton process, including synergistic regulation of mass transfer and reactivity/selectivity of reactions (cathodic iron reduction and oxygen reduction reaction). She has published 44 peer-review papers in the electrochemistry (especially electro-Fenton, h-index=21 (December 2022)) and some of her works have been published in Chemical Society Reviews, Applied Catalysis B: Environmental, Journal of Materials Chemistry A, etc.

Hugo Olvera-Vargas (Researcher ID: 0000-0001-6320-2847) is a chemist from the Autonomous University of Mexico State (UAEMex), Mexico, where he also obtained a MSc degree in Chemical Sciences specializing in Environmental Analytical Chemistry (graduated with distinction). Dr. Hugo holds a joint PhD degree in Chemistry and Environmental Science by the University of Paris-Est, the UNESCO-IHE Institute for Water Education (The Netherlands), and the University of Cassino and Southern Lazio (Italy). His PhD project earned him the award for the best thesis in science and engineering by the University of Paris-Est in 2015. He conducted postdoctoral research at the University of Toulouse III Paul-Sabatier (France) and worked as a research fellow at the National University of Singapore (NUS). Currently, Dr. Hugo is an Assistant Professor at the Institute for Renewable Energy of the National Autonomous University of Mexico (UNAM). His research focuses on the development and application of sustainable electrochemical and photoelectrochemical processes for the treatment and valorization of industrial wastewater and pollutants of emerging concern. Dr. Hugo has published more than 30 scientific papers, 4 book chapters, and has participated in 4 patents (Scopus h-index 23, with 36 research items and 1492 citations as consulted in September 2022). He has presented his research work on several international conferences, some of them as invited speaker. He has mentored and supervised several BSc, MSc and PhD students. He is member of the Mexican National Research System, and part of the editorial board of the *Journal of Environmental Chemical Engineering*. He has participated in several scientific conferences as presenter, invited speaker, and seminar organizer.

Minghua Zhou (Researcher ID: 0000-0002-3311-0535) obtained his doctorate from Zhejiang University (China) in 2003. He was at College of Resource and Environment, Zhejiang University as assistant and associate professor from 2003 to 2006. After his postdoctoral stay at the University of Sydney, he joined in Nankai University as full Professor in 2008. He has undertaken Marie Curie More Experienced Research Fellow at University of Kuopio, Finland and invited professor at Université Paris-Est in France. He is currently Professor and Associate Dean of College of Environmental Science and Engineering at Nankai University, director of Tianjin Advanced Water Treatment Technology International Joint Research Center and vice director of Tianjin Key Laboratory of Environmental Technology for Complex Trans-Media Pollution. His current research interest includes water pollution control technology, environmental catalysis, and advanced oxidation processes (AOPs) and particularly Electrochemical Advanced Oxidation Processes (EAOPs) including electro-Fenton process. He has published more than 250 peer-review papers with about 14,000 citations in Scopus and h-index of 66, 4 books and 8 book chapters. He received 1 first-class research award and 3 second-class research awards of provincial and ministerial level in China and 2 international awards. He was awarded as "Ten thousand plan"- Leading Talents in Science and Technology Innovation, and "Most Cited Chinese Researchers" (Environmental Science) since 2014. He is vice-chair of Division 5: Electrochemical Process Engineering and Technology, International Society of Electrochemistry, and guest editor or member of Editorial Board of several scientific journals, such as Chemosphere, Separation Purification Technology, Chinese Chemical Letters, Catalyst and Journal of Chemistry.

Shan Qiu (Researcher ID: 0000-0001-8329-6852) obtained her Ph.D. degree in Environmental Engineering in 2010 from the Harbin Institute of Technology (HIT, China). In October 2010 he became a lecturer at the Department of Environmental Engineering in Harbin Institute of Technology, Since December 2021, she works as a professor in the same Department. She was also a National registered environmental protection engineer and became Assistant Director of the State Key Laboratory of Urban Water Resources and Environment (SKLUWRE) in 2018. She mainly focuses on electrochemistry and environmental microbiology. Her major efforts have been devoted to advanced oxidation processes in industrial wastewater and municipal wastewater treatment and reuse. She has presided over three sub-projects supported by the National Natural Science Foundation of China, six national major projects, and more than ten other provincial and ministerial level projects. She is a Young Editor of Chinese Chemical Letter, and published more than 50 indexed papers in A*pplied Catalysis B: Environmental*, *Journal of Hazardous Materials*, and others; got more than 20 patents. Design more than 40 wastewater actual engineering projects, like coking, petrochemical, refining, pharmaceutical, printing and dyeing, saccharin, and other types.

Ignasi Sirés (Researcher ID: C-7054-2013) obtained his Ph.D. degree in Chemistry in 2007 from the Universitat de Barcelona (UB, Spain). He also became a Materials' Engineer after conducting studies at the UB and the Universitat Politècnica de Catalunya. He has undertaken postdoctoral stays and professor-researcher positions at: Università degli Studi di Genova, Université Paris-Est, University of Southampton in the UK and Universidad de Guanajuato. Dr. Sirés was awarded the 'Oronzio and Niccolò De Nora Foundation Prize in Environmental Electrochemistry' in 2010 (International Society of Electrochemistry), the 'CIDETEC 2011 Prize for Young Researchers in Electrochemistry' (Spanish Electrochemistry Group of the Spanish Royal Society of Chemistry), the prestigious 'Carl Wagner Medal of Excellence in Electrochemical Engineering 2014' (Working Party on Electrochemical Engineering (WPEE) of the European Federation of Chemical Engineering (EFCE)) and the '1st Prize Dr. Alejandro J. Arvia for Young Researchers in Electrochemistry to the best under-40 researcher in electrochemistry by the Iberoamerican Society of Electrochemistry. In September 2009 he became an Assistant Professor at the Department of Physical Chemistry in the Faculty of Chemistry of the UB, carrying out his research with Prof. Enric Brillas at the *Laboratory of Materials' and Environmental Electrochemistry*. Since September 2014, he works as a Tenured Assistant Professor at the same Department. His research interests mainly focus on all aspects of environmental electrochemistry for wastewater treatment, although his major efforts have been devoted to the electrochemical advanced oxidation processes based on Fenton's reaction chemistry, having filed two patents and worked in industry-funded projects. With more than 180 indexed papers and more than 15000 citations (h-index = 58), he is currently among the 2% most cited and influencing authors in the world, being invited to give plenary and invited talks worldwide.

Enric Brillas (Barcelona, Spain, 1951, Researcher ID: 0000-0001-8147-4651) obtained his BS degree in Chemistry in 1974 from the *Universitat Autònoma de Barcelona* and received his Ph.D. degree in Chemistry in 1977 from the *Universitat Autònoma de Barcelona*, supervided by Prof. José M. Costa Torres. In 1980, he joined the *Universitat de Barcelona* as Associate Professor of Physical Chemistry and from 1987 to September 2022, as Full Professor of Physical Chemistry. At present, he is Honorific Professor of the *Universitat de Barcelona*. He made his post-doc in the *Università de Padova* (Italy) in 1982-1983, in the speciality of Electrochemistry upon the supervision of Prof. Elio Vianello. He was Headmaster of the Department of Physical Chemistry of the *Universitat de Barcelona* from 2000 to 2008. He was President of the Electrochemistry Group of the *Real Sociedad Española de Química* from 2004 to 2008 and Director of the *Laboratory of Electrochemistry of Materials and Environment* at the *Universitat de Barcelona* up to September 2022. His research mainly focuses on photocatalysis, photoelectrocatalysis, electrocatalysis and electrochemical advanced oxidation processes involving Fenton's reaction chemistry like electro-Fenton, photoelectro-Fenton with UV light and solar and peroxi-coagulation. He has received 4 national and international research awards. He is Editor of *Chemosphere* since 2008 and member of the Editorial Board of *Electrocatalysis*, *Journal of Hazardous Materials*, *Catalysts* and *Applied Catalysis B: Environmental*. He has supervised 22 PhD thesis, published 435peer-review papers with about 34,000 citations in Scopus and h-index = 95 (December 2022), six books and fifteen book chapters, and presented 367 communications to national and international congresses. He has participated in more than 70 research projects and has 8 patents.

References

(1) Tirado, L.; Gökkuş, Ö.; Brillas, E.; Sirés, I. Treatment of Cheese Whey Wastewater by Combined Electrochemical Processes. *J. Appl. Electrochem*. **2018**, *48*, 1307-1319.

(2) Dos Santos, P. R.; de Oliveira Dourados. M. E.; Sirés. I.; Brillas.E.; Cavalcante, R. P.; Cavalheri, P. S.; Paulo, P. L.; D.R.V. Guelfi, D. R. V.; Oliveira, S. C. D.; Gozzi, F.; Machulek Jr., A. Greywater Treatment by Anodic Oxidation, Photoelectro-Fenton and Solar Photoelectro-Fenton Processes: Influence of Relevant Parameters and Toxicity Evolution. *Process Saf. Environ. Prot*. **2023**, *169*, 879-895.

(3) Campos, S.; Lorca, J.; Vidal, J.; Calzadilla,W.; Toledo-Neira. C.; Aranda, M.; Miralles-Cuevas, S.; Cabrera-Reina, A.; Salazar, R. Removal of Contaminants of Emerging Concern by Solar Photo Electro-Fenton Process in a Solar Electrochemical Raceway Pond Reactor. *Process Saf. Environ. Prot*. **2023**, *169*, 660-670.

(4) Daniel, G.; Zhang, Y.; Lanzalaco, S.; Brombin, F.; Kosmala, T.; Granozzi, G.; Wang, A.; Brillas, E.; Sirés, I.; Durante, C. Chitosan-Derived Nitrogen-Doped Carbon Electrocatalyst for a Sustainable Upgrade of Oxygen Reduction to Hydrogen Peroxide in UV-Assisted Electro-Fenton Water Treatment. *ACS Sustain. Chem. Eng.* **2020**, *8*, 14425-14440.

(5) Poza-Nogueiras, V.; Rosales, E.; Pazos, M.; Sanromán, M. Á. Current Advances and Trends in Electro-Fenton Process Using Heterogeneous Catalysts-A Review. *Chemosphere* **2018**, *201*, 399-416.

(6) Nidheesh, P. V.; Zhou, M.; Oturan, M. A. An Overview on the Removal of Synthetic Dyes from Water by Electrochemical Advanced Oxidation Processes. *Chemosphere* **2018**, 197, 210-227.

(7) Sirés, I.; Brillas, E. Upgrading and Expanding the Electro-Fenton and Related Processes. *Curr. Opin. Electrochem.* **2021**, *27*, 100686.

(8) Moreira, F. C.; Boaventura, R. A. R.; Brillas, E.; Vilar, V. J. P. Electrochemical Advanced Oxidation Processes: A Review on Their Application to Synthetic and Real Wastewaters. *Appl. Catal. B: Environ.* **2017**, *202*, 217-261.

(9) Ganiyu, S.O.; Zhou, M.; Martínez-Huitle, C. A. Heterogeneous Electro-Fenton and Photoelectro-Fenton Processes: A Critical Review of Fundamental Principles and Application for Water/Wastewater Treatment. *Appl. Catal. B: Environ*. **2018**, *235*, 103-129.

(10) Ganiyu, S. O.; Martínez-Huitle, C. A.; Rodrigo, M.A. Renewable Energies Driven Electrochemical Wastewater/Soil Decontamination Technologies: A Critical Review of Fundamental Concepts and Applications. *Appl. Catal. B: Environ*. **2020**, *270*, 118857.

(11) Brillas, E. A Review on the Photoelectro-Fenton Process as Efficient Electrochemical Advanced Oxidation for Wastewater Remediation. Treatment with UV Light, Sunlight, and Coupling with Conventional and Other Photo-Assisted Advanced Technologies. *Chemosphere* **2020**, *250*, 126198.

(12) Martínez-Huitle, C. A.; Rodrigo, M. A.; Sirés, I.; Scialdone, O. Single and Coupled Electrochemical Processes and Reactors for the Abatement of Organic Water Pollutants: A Critical Review. *Chem. Rev.* **2015**, *115*, 13362-13407.

(13) Ganiyu, S. O.; Martínez-Huitle, C. A.; Oturan, M. A. Electrochemical Advanced Oxidation Processes for Wastewater Treatment: Advances in Formation and Detection of Reactive Species and Mechanisms. *Curr. Opin. Electrochem*. **2021**, *27*, 100678.

(14) Cornejo, O. M.; Sirés, I.; Nava, J. L. Cathodic Generation of Hydrogen Peroxide Sustained by Electrolytic O_2 in a Rotating Cylinder Electrode (RCE) Reactor, *Electrochim. Acta*. **2022**, *404*, 139621.

(15) Zhang, Y.; Daniel, G.; Lanzalaco, S.; Isse, A. A.; Facchin, A.; Wang, A.; Brillas, E.; Durante, C.; Sirés, I. H_2O_2 Production at Gas-Diffusion Cathodes Made from Agarose-Derived Carbons with Different Textural Properties for Acebutolol Degradation in Chloride Media. *J. Hazard. Mater.* **2022**, *423*, 127005.

(16) Ding, Y.; Zhou, W.; Gao, J.; Sun, F.; Zhao, G. H_2O_2 Electrogeneration from O_2 Electroreduction by N-Doped Carbon Materials: a Mini-Review on Preparation Methods, Selectivity of N Sites, and Prospects. *Adv. Mater. Interfaces* **2021**, *8*, 2002091.

(17) Zhou, W.; Xie, L.; Gao, J.; Nazari, R.; Zhao, H.; Meng, X.; Sun, F.; Zhao, G.; Ma, J. Selective H_2O_2 Electrosynthesis by O-Doped and Transition-Metal-O-Doped Carbon Cathodes via O_2 Electroreduction: A Critical Review. *Chem. Eng. J.* **2021**, *410*. 128368.

(18) Zhu, Y.; Zhu, R.; Xi, Y.; Zhu, J.; Zhu, G.; He, G. Strategies for Enhancing the Heterogeneous Fenton Catalytic Reactivity: A Review. *Appl. Catal. B: Environ*. **2019**, *255*, 117739.

(19) Zhou, H.; Zhang, Y.; He, B.; Huang, C.; Zhou, G.; Yao, B.; Lai, B. Critical Review of Reductant-Enhanced Peroxide Activation Processes: Trade-off Between Accelerated Fe^{3+}/Fe^{2+} Cycle and Quenching Reactions. *Appl. Catal. B: Environ*. **2021**, *286*, 119900.

(20) Bard, A. J.; Faulkner, L. R. *Electrochemical Methods: Fundamentals and Applications*, Wiley, 2000: p 61.

(21) Lei, Y.; Song, B.; van der Weijden, R, D.; Saakes, M.; Buisman, C. J. N. Electrochemical Induced Calcium Phosphate Precipitation: Importance of Local pH. *Environ. Sci. Technol.* **2017**, *51*, 11156-11164.

(22) An, J.; Li, N.; Wu, Y.; Wang, S.; Liao, C.; Zhao, Q.; Zhou, L.; Li, T.; Wang, X.; Feng, Y. Revealing Decay Mechanisms of H_2O_2-Based Electrochemical

Advanced Oxidation Processes after Long-Term Operation for Phenol Degradation. *Environ. Sci. Technol*. **2020**, *54*, 10916-10925.

(23) Zhang, Y.; Zhou, M. A. Critical Review of the Application of Chelating Agents to Enable Fenton and Fenton-Like Reactions at High pH Values. *J. Hazard. Mater*. **2019**, *362*, 436-450.

(24) Lipczynska-Kochany, E.; Kochany, J. Effect of Humic Substances on the Fenton Treatment of Wastewater at Acidic and Neutral pH. *Chemosphere* **2008**, *73*, 745-750.

(25) Madrid, E.; Lowe, J. P.; Msayib, K. J.; McKeown, N. B.; Song, Q.; Attard, G. A.; Düren, T.; Marken, F. Triphasic Nature of Polymers of Intrinsic Microporosity Induces Storage and Catalysis Effects in Hydrogen and Oxygen Reactivity at Electrode Surfaces. *ChemElectroChem* **2019**, 6, 252-259.

(26) Sudoh, M.; Kodera, T.; Sakai, K.; Zhang, J. Q.; Koide, K. Oxidative Degradation of Aqueous Phenol Effluent with Electrogenerated Fenton's Reagent. *J. Chem. Eng. Jap.* **1986**, *19*, 513-518.

(27) Brillas, E.; Sirés, I.; Oturan, M. A. Electro-Fenton Process and Related Electrochemical Technologies Based on Fenton's Reaction Chemistry. *Chem. Rev.* **2009**, *109*, 6570-6631.

(28) Brillas, E.; Mur, E.; Casado, J. Iron(II) Catalysis of the Mineralization of Aniline Using a Carbon- PTFE O_2 -Fed Cathode. *J. Electrochem. Soc*. **1996**, *143*, 49-53.

(29) Chou, S.; Huang, Y.; Lee, S.; Huang, G.; Huang, C. Treatment of High Strength Hexamine-Containing Wastewater by Electro-Fenton Method. *Water Res*. **1999**, *33*, 751-759.

(30) Xu, S.; Adhikari, D.; Huang, R.; Zhang, H.; Tang, Y.; Roden, E.; Yang, Y. Biochar-Facilitated Microbial Reduction of Hematite. *Environ. Sci. Technol*. **2016**, *50*, 2389-2395.

(31) Wang, W.; Chen, J.; Gao, J.; Meng, H.; Chai, S.; Jian, Y.; Shi, L.; Wang, Y.; He, C. Selective Electrochemical H_2O_2 Generation on the Graphene Aerogel for Efficient Electro-Fenton Degradation of Ciprofloxacin. *Sep. Purif. Technol*. **2021**, *272*, 118884.

(32) Chen, Y.; Ji, S.; Chen, C.; Peng, Q.; Wang, D.; Li, Y. Single-Atom Catalysts: Synthetic Strategies and Electrochemical Applications. *Joule* **2018**, *2*, 1242-1264.

(33) Wang, X.; Qiu, S.; Feng, J.; Tong, Y.; Zhou, F.; Li, Q.; Song, L.; Chen, S.; Wu, K.; Su, P.; Ye, S.; Hou, F.; Dou, S. X.;. Liu, H. K.; Max Lu, G. Q.; Sun, C.; Liu, J.; Liang, J. Confined Fe-Cu Clusters as Sub-Nanometer Reactors for Efficiently Regulating the Electrochemical Nitrogen Reduction Reaction. *Adv. Mater*. **2020**, *32*, 2004382.

(34) Qiu, S.; Tang, W.; Yang, S.; Xie, J.; Yu, D.; Garcia-Rodriguez, O.; Qu, J.; Bai, S.; Deng, F. A microbubble-Assisted Rotary Tubular Titanium Cathode for Boosting Fenton's Reagents in the Electro-Fenton Process. *J. Hazard. Mater*. **2022**, *424*, 127403.

(35) Nikolas, H.; Kurt, S.; Hans-Peter, S.; Ralf, K.; Marc, B.; Thomas, B. Activated Carbon, Biochar and Charcoal: Linkages and Synergies Across Pyrogenic Carbon's ABCs. *Water* **2018**, *10*, 182-198.

(36) Lu, Q.; Wang, H.; Liu, Y.; Hou, Y.; Li, H.; Zhang, Y. Graphitic Carbon Nitride Nanodots: As Reductant for the Synthesis of Silver Nanoparticles and its Biothiols Biosensing Application. *Biosens. Bioelectron*. **2017**, *89*, 411-416.

(37) Jia, C.; Dastafkan, K.; Ren, W.; Yang, W.; Zhao, C. Carbon-based Catalysts for Electrochemical CO_2 Reduction. *Sust. Energy Fuels* **2019**, 2890-2906.

(38) Zhang, Y.; Rhee, K. Y.; Hui, D.; Park, S. A Critical Review of Nanodiamond Based Nanocomposites: Synthesis, Properties and Applications, *Composites, B* **2018**, *143*, 19-27.

(39) Liu, Y.; Roy, S.; Sarkar, S.; Xu, J.; Zhao, Y.; Zhang, J. A Review of Carbon Dots and Their Composite Materials for Electrochemical Energy Technologies. *Carbon Energy* **2021**, *3*, 795-826.

(40) Ding, Y.; Zhou, W.; Gao, J.; Sun, F.; Zhao, G. H_2O_2 Electrogeneration from O_2 Electroreduction by N-Doped Carbon Materials: A Mini-Review on Preparation Methods, Selectivity of N Sites, and Prospects. *Adv Mater Interfaces* **2021**, *8*, 2002091.

(41) Bach, A.; Semiat, R. The Role of Activated Carbon as a Catalyst in GAC/Iron Oxide/H_2O_2 Oxidation Process. *Desalination* **2011**, *273*, 57-63.

(42) Seo, J.; Lee, H.; Lee, H.; Kim, H.; Lee, J.; Kim, H. S.; Lee, C. Enhanced Production of Reactive Oxidants by Fenton-Like Reactions in the Presence of Carbon Materials. *Chem. Eng. J.* **2015,** *273*, 502-508.

(43) Yoo, S. H.; Jang, D.; Joh, H.; Lee, S. Iron Oxide/Porous Carbon as a Heterogeneous Fenton Catalyst for Fast Decomposition of Hydrogen Peroxide and Efficient Removal of Methylene Blue. *J. Mater. Chem. A* **2017**, *5*, 748-755.

(44) Yang, Z.; Yu, A.; Shan, C.; Gao, G.; Pan, B. Enhanced Fe(III)-Mediated Fenton Oxidation of Atrazine in the Presence of Functionalized Multi-walled carbon Nanotubes. *Water Res.* **2018**, *137*, 37-46.

(45) Qin, Y.; Zhang, L.; An, T. Hydrothermal Carbon-Mediated Fenton-Like Reaction Mechanism in the Degradation of Alachlor: Direct Electron Transfer from Hydrothermal Carbon to Fe(III). *ACS Appl. Mater. Inter*. **2017**, *9*, 17115-17124.

(46) Klüpfel, L.; Keiluweit, M.; Kleber, M.; Sander, M. Redox Properties of Plant Biomass-Derived Black Carbon (Biochar). *Environ. Sci. Technol*. **2014**, *48*, 5601-5611.

(47) Yang, Y.; Qiao, S.; Zhou, J.; Quan, X. Mitigating Membrane Fouling Based on in Situ •OH Generation in a Novel Electro-Fenton Membrane Bioreactor. *Environ. Sci. Technol.* **2020**, *54*, 7669-7676.

(48) Qin, X.; Zhao, K.; Quan, X.; Cao, P.; Chen, S.; Yu, H. Highly Efficient Metal-Free Electro-Fenton Degradation of Organic Contaminants on a Bifunctional Catalyst, *J. Hazard. Mater*. **2021**, *416*, 125859.

(49) Sirés, I.; Garrido, J. A.; Rodríguez, R. M.; Brillas, E.; Oturan, N.; Oturan, M. A. Catalytic Behavior of the Fe^{3}+/Fe^{2+} System in the Electro-Fenton Degradation of the Antimicrobial Chlorophene. *Appl. Catal. B: Environ*. **2007**, *72*, 382-394.

(50) Zhou, P.; Zhang, J.; Xiong, Z.; Liu, Y.; Huo, X.; Cheng, X.; Li, W.; Cheng, F.; Zhang, Y. C_{60} Fullerol Promoted Fe(III)/H_2O_2 Fenton Oxidation: Role of Photosensitive Fe(III)-Fullerol Complex. *Appl. Catal. B: Environ*. **2020**, *265*, 118264.

(51) Guo, D.; Liu, Y.; Ji, H.; Wang, C.; Chen, B.; Shen, C.; Li, F.; Wang, Y.; Lu, P.; Liu, W. Silicate-Enhanced Heterogeneous Flow-Through Electro-Fenton System Using Iron Oxides Under Nanoconfinement. *Environ. Sci. Technol*. **2021**, *55*, 4045-4053.

(52) Zubir, N. A.; Yacou, C.; Motuzas, J.; Zhang, X.; Zhao, X. S.; Diniz Da Costa, J. C. The Sacrificial Role of Graphene Oxide in Stabilising a Fenton-Like Catalyst GO-Fe_3O_4. *Chem. Commun*. **2015**, *51*, 9291-9293.

(53) Ko, Y.; Kim, H.; Seid, M. G.; Cho, K.; Choi, J.; Lee, W.; Hong, S. W. Ionic-Liquid-Derived Nitrogen-Doped Carbon Electrocatalyst for Peroxide Generation and Divalent Iron Regeneration: Its Application for Removal of Aqueous Organic Compounds. *ACS Sustain. Chem. Eng* **2018**, *6* 14857-14865.

(54) McCreery, R. L. Advanced Carbon Electrode Materials for Molecular Electrochemistry. *Chem. Rev.* **2008**, *108*, 2646-2687.

(55) Choi, H. C.; Shim, M.; Bangsaruntip, S.; Dai, H. Spontaneous Reduction of Metal Ions on the Sidewalls of Carbon Nanotubes. *J. Am. Chem. Soc.* **2002**, *124*, 9058-9059.

(56) Zhang, Q.; Zhou, M.; Du, X.; Su, P.; Fu, W.; Song, G. Highly Efficient Dual-Cathode Electro-Fenton Process Without Aeration at a Wide pH Range: Simultaneously Enhancing Fe(II) Regeneration and Mineralization Efficiency. *Chem. Eng. J*. **2022**, *429*, 132436.

(57) Cheng, P.; Teng, H. Electrochemical Responses from Surface Oxides Present on HNO_3-Treated Carbons. *Carbon* **2003**, *41*, 2057-2063.

(58) Kou, K.; Zhou, W.; Chen, S.; Gao, J. Mechanism Investigation of Carboxyl Functional Groups Catalytic Oxidation in Coal Assisted Water Electrolysis Cell. *Energy* **2021**, *226*, 120243.

(59) Sun, B.; Skyllas-Kazacos, M. Modification of Graphite Electrode Materials for Vanadium Redox Flow Battery Application-I. Thermal Treatment. *Electrochim. Acta* **1992**, *37*,1253-1260.

(60) Huang, Z.; Song, J.; Dou, S.; Li, X.; Wang, J.; Wang, X. Strategies to Break the Scaling Relation Toward Enhanced Oxygen Electrocatalysis. *Matter* **2019**, *1*, 1494-1518.

(61) Pan, T.; Wang, Y.; Yang, X.; Huang, X.; Qiu, R. Gallic Acid Accelerated BDE47 Degradation in PMS/Fe(III) System: Oxidation Intermediates Autocatalyzed Redox Cycling of Iron. *Chem. Eng. J.* **2020**, *384*, 123248.

(62) Umeda, J.; Suzuki, M.; Kato, M.; Moriya, M.; Sakamoto, W.; Yogo, T. Proton Conductive Inorganic-Organic Hybrid Membranes Functionalized with Phosphonic Acid for Polymer Electrolyte Fuel Cell. *J. Power Sources* **2010**, *195*, 5882-5888.

(63) Nriagu, J. O. Stability of Vivianite and Ion-Pair Formation in the System $Fe_3(PO_4)_2$-$H_3PO_4H_3PO_4$-H_2O. *Geochim. Cosmochim. Acta* **1972**, *36*, 459-470.

(64) Mu, Y.; Ai, Z.; Zhang, L. Phosphate Shifted Oxygen Reduction Pathway on Fe@Fe_2O_3 Core-Shell Nanowires for Enhanced Reactive Oxygen Species Generation and Aerobic 4-Chlorophenol Degradation. *Environ. Sci. Technol*. **2017**, *51*, 8101-8109.

(65) Wang, Z.; Pu, Y.; Wang, D.; Wang, J.; Chen, J. Recent Advances on Metal-Free Graphene-Based Catalysts for the Production of Industrial Chemicals. *Front. Chem. Sci. Eng.* **2018**, *12*, 855-866.

(66) Wang, X.; Yang, C.; Li, J.; Chen, X.; Yang, K.; Yu, X.; Lin, D.; Zhang, Q.; Wang, S.; Wang, J.; Xia, Z.; Jin, H. Insights of Heteroatoms Doping-Enhanced Bifunctionalities on Carbon Based Energy Storage and Conversion. *Adv. Funct. Mater*. **2021**, *31*, 2009109.

(67) Liu, M.; Feng, Z.; Luan, X.; Chu, W.; Zhao, H.; Zhao, G. Accelerated Fe^{2+} Regeneration in an Effective Electro-Fenton Process by Boosting Internal Electron Transfer to a Nitrogen-Conjugated Fe(III) Complex. *Environ. Sci. Technol*. **2021**, *55*, 6042-6051.

(68) Ma, J.; Xu, L.; Shen, C.; Hu, C.; Liu, W.; Wen, Y. Fe-N-Graphene Wrapped Al_2O_3/Pentlandite from Microalgae: High Fenton Catalytic Efficiency from Enhanced Fe^{3+} Reduction. *Environ. Sci. Technol*. **2018**, *52*, 3608-3614.

(69) Gorski, C. A.; Edwards, R.; Sander, M.; Hofstetter, T. B.; Stewart, S. M. Thermodynamic Characterization of Iron Oxide-Aqueous Fe^{2+} Redox Couples. *Environ. Sci. Technol*. **2016**, *50*, 8538-8547.

(70) Huang, D.: Zhao, J. Speeding up Fenton Reactions with a Heterogeneous Inorganic Co-Catalyst. *Chem-Us* **2020**, 6, 1512-1514.

(71) Dong, C.; Ji, J.; Shen, B.; Xing, M.; Zhang, J. Enhancement of H_2O_2 Decomposition by the Co-Catalytic Effect of WS_2 on the Fenton Reaction for the Synchronous Reduction of Cr(VI) and Remediation of Phenol. *Environ. Sci. Technol*. **2018**, *52*, 11297-11308.

(72) Tian, Y.; Zhou, M.; Pan, Y.; Du, X.; Wang, Q. MoS_2 as Highly Efficient Co-Catalyst Enhancing the Performance of Fe^0 Based Electro-Fenton Process in Degradation of Sulfamethazine: Approach and Mechanism. *Chem. Eng. J*. **2021**, *403*, 126361.

(73) Shen B.; Dong C.; Ji J.; Xing M.; Zhang J. Efficient Fe(III)/Fe(II) Cycling Triggered by MoO_2 in Fenton Reaction for the Degradation of Dye Molecules and the Reduction of Cr(VI). *Chin. Chem. Lett*. **2019**, *30*, 2205-2210.

(74) Zhao, Y.; Jia, Y.; Xu, J.; Han, L.; He, F.; Jiang, X. The Antibacterial Activities of MoS_2 Nanosheets Towards Multi-Drug Resistant Bacteria. *Chem. Commun*. **2021**, *57*, 2998-3001.

(75) Xiao, S.; Zhou, C.; Ye, X.; Lian, Z.; Zhang, N.; Yang, J.; Chen, W.; Li, H. Solid-Phase Microwave Reduction of WO_3 by GO for Enhanced Synergistic Photo-Fenton Catalytic Degradation of Bisphenol A. *ACS Appl. Mater. Inter*. **2020**, *12*, 32604-32614.

(76) Zhu, L.; Ji, J.; Liu, J.; Mine, S.; Matsuoka, M.; Zhang, J.; Xing, M. Designing 3D-MoS_2 Sponge as Excellent Cocatalysts in Advanced Oxidation Processes for Pollutant Control. *Angew. Chem. Int. Ed*. **2020**, *59*, 13968-13976.

(77) Deng, F.; Garcia-Rodriguez, O.; Olvera-Vargas, H.; Qiu, S.; Lefebvre, O.; Yang, J. Iron-Foam as a Heterogeneous Catalyst in the Presence of Tripolyphosphate Electrolyte for Improving Electro-Fenton Oxidation Capability. *Electrochim. Acta* **2018**, *272*, 176-183.

(78) Zhang, C.; Zhou, M.; Ren, G.; Yu, X.; Ma, L.; Yang, J.; Yu, F. Heterogeneous Electro-Fenton Using Modified Iron–Carbon as Catalyst for 2,4-Dichlorophenol Degradation: Influence Factors, Mechanism and Degradation Pathway. *Water Res*. **2015**, *70*, 414-424.

(79) Du, X.; Fu, W.; Su, P.; Cai, J.; Zhou, M. Internal-Micro-Electrolysis-Enhanced Heterogeneous Electro-Fenton Process Catalyzed by Fe/Fe_3C@PC Core–Shell Hybrid for Sulfamethazine Degradation. *Chem. Eng. J*. **2020**, *398*, 125681.

(80) Deng, F.; Olvera-Vargas, H.; Garcia-Rodriguez, O.; Qiu, S.; Yang, J.; Lefebvre, O. The Synergistic Effect of Nickel-Iron-Foam and Tripolyphosphate for Enhancing the Electro-Fenton Process at Circum-Neutral pH. *Chemosphere* **2018**, *201*, 687-696.

(81) Li, J.; Ai, Z.; Zhang, L. Design of a Neutral Electro-Fenton System with Fe@Fe_2O_3/ACF Composite Cathode for Wastewater Treatment. *J. Hazard. Mater*. **2009**, *164*, 18-25.

(82) Ai, Z.; Lu, L.; Li, J.; Zhang, L.; Qiu, J.; Wu, M. Fe@Fe_2O_3 Core-Shell Nanowires as Iron Reagent. 1. Efficient Degradation of Rhodamine B by a Novel Sono-Fenton Process. *J. Phys. Chem.* C **2007**, *111*, 4087-4093.

(83) Zhao, H.; Qian, L.; Guan, X.; Wu, D.; Zhao, G. Continuous Bulk FeCuC Aerogel with Ultradispersed Metal Nanoparticles: An Efficient 3D Heterogeneous

Electro-Fenton Cathode Over a Wide Range of pH 3-9. *Environ. Sci. Technol*. **2016**, *50*, 5225-5233.

(84) Qiu, S.; Wang, Y.; Wan, J.; Ma, Y.; Yan, Z.; Yang, S. Enhanced Electro-Fenton Catalytic Performance with In-Situ Grown Ce/Fe@NPC-GF as Self-Standing Cathode: Fabrication, Influence Factors and Mechanism. *Chemosphere* **2021**, *273*, 130269.

(85) Xu, L.; Wang, J. Magnetic Nanoscaled Fe_3O_4/CeO_2 Composite as an Efficient Fenton-Like Heterogeneous Catalyst for Degradation of 4-Chlorophenol. *Environ. Sci. Technol*. **2012**, *46*, 10145-10153.

(86) Wang, Y.; Zhang, H.; Li, B.; Yu, M.; Zhao, R.; Xu, X.; Cai, L. γ-FeOOH Graphene Polyacrylamide Carbonized Aerogel as Air-Cathode in Electro-Fenton Process for Enhanced Degradation of Sulfamethoxazole. *Chem. Eng. J*. **2019**, *359*, 914-923.

(87) Mi, X.; Li, Y.; Ning, X.; Jia, J.; Wang, H.; Xia, Y.; Sun, Y.; Zhan, S. Electro-Fenton Degradation of Ciprofloxacin with Highly Ordered Mesoporous $MnCo_2O_4$-CF Cathode: Enhanced Redox Capacity and Accelerated Electron Transfer. *Chem. Eng. J*. **2019**, *358*, 299-309.

(88) Dong, P.; Chen, X.; Guo, M.; Wu, Z.; Wang, H.; Lin, F.; Zhang, J.; Wang, S.; Zhao, C.; Sun, H. Heterogeneous Electro-Fenton Catalysis with Self-Supporting CFP@MnO_2-Fe_3O_4/C Cathode for Shale Gas Fracturing Flowback Wastewater. *J. Hazard. Mater*. **2021**, *412*, 125208.

(89) Ghasemi, M.; Khataee, A.; Gholami, P.; Soltani, R. D. C.; Hassani, A.; Orooji, Y. In-Situ Electro-Generation and Activation of Hydrogen Peroxide Using a CuFeNLDH-CNTs Modified Graphite Cathode for Degradation of Cefazolin. *J. Environ. Manage.* **2020**, *267*, 110629.

(90) Deng, D.; Yu, L.; Chen, X.; Wang, G.; Jin, L.; Pan, X.; Deng, J.; Sun, G.; Bao, X. Iron Encapsulated Within Od-Like Carbon Nanotubes for Oxygen Reduction Reaction. *Angew. Chem. Int. Ed.* **2013**, *52*, 371-375.

(91) Xiao, F.; Wang, Z.; Fan, J.; Majima, T.; Zhao, H.; Zhao, G. Selective Electrocatalytic Reduction of Oxygen to Hydroxyl Radicals via 3-Electron Pathway with FeCo Alloy Encapsulated Carbon Aerogel for Fast and Complete Removing Pollutants. *Angew. Chem. Int. Ed*. **2021**, *60*, 10375-10383.

(92) Cheng, L.; Men, Y.; Wang, J.; Wang, H.; An, W.; Wang, Y.; Duan, Z.; Liu, J. Crystal Facet-Dependent Reactivity of α-Mn_2O_3 Microcrystalline Catalyst for Soot Combustion. *Appl. Catal. B: Environ*. **2017**. *204*, 374-384.

(93) Huang, X.; Hou, X.; Zhang, X.; Rosso, K. M.; Zhang, L. Facet-Dependent Contaminant Removal Properties of Hematite Nanocrystals and Their Environmental Implications. *Environ. Sci: Nano* **2018**, *5*, 1790-1806.

(94) Hu, S.; Wu, Y.; Ding, Z.; Shi, Z.; Li, F.; Liu, T. Facet-Dependent Reductive Dissolution of Hematite Nanoparticles by *Shewanella putrefaciens* CN-32. *Environ. Sci. Nano* **2020**, 7, 2522-2531.

(95) Zhu, G.; Yu, X.; Xie, F.; Feng, W. Ultraviolet Light Assisted Heterogeneous Fenton Degradation of Tetracycline Based on Polyhedral Fe_3O_4 Nanoparticles with Exposed High-Energy {110} Facets. *Appl. Surf. Sci*. **2019**, *485*.

(96) Huang, X.; Hou, X.; Zhao, J.; Zhang, L. Hematite Facet Confined Ferrous Ions as High Efficient Fenton Catalysts to Degrade Organic Contaminants by Lowering H_2O_2 Decomposition Energetic Span. *Appl. Catal. B: Environ*. **2016**, *181*, 127-137.

(97) Zhou, Z.; Tian, N.; Li, J.; Broadwell, I.; Sun, S. Nanomaterials of High Surface Energy with Exceptional Properties in Catalysis and Energy Storage. *Chem. Soc. Rev*. **2011**, *40*, 4167-4185.

(98) Wang, S.; Liu, G.; Wang, L. Crystal Facet Engineering of Photoelectrodes for Photoelectrochemical Water Splitting. *Chem. Rev*. **2019**, *119*, 5192-5247.

(99) Liu, X.; Fan, J.; Liu, Z.; Yu, Y.; You, J.; Zhu, X.; Zhong, X.; Ma, S.; Lin, Z. Elimination of 4-Chlorophenol in Aqueous Solution by the Novel Pd/MIL-101(Cr)-Hydrogen-Accelerated Catalytic Fenton System. *Appl. Organomet. Chem*. **2019**, *33*, 5194-5213.

(100) Chen, M.; Bi, J.; Huang, X.; Wang, T.; Wang, Z.; Hao, H. Bi_2O_3 Nanosheets Arrays In-Situ Decorated on Carbon Cloth for Efficient Electrochemical Reduction of Nitrate. *Chemosphere* **2012**, *278*, 130386.

(101) Liu, X.; He, C.; Shen, Z.; Li, W.; Chen, N.; Song, J.; Zhou, X.; Mu, Y. Mechanistic Study of Fe(III) Chelate Reduction in a Neutral Electro-Fenton Process. *Appl. Catal. B: Environ*. **2020**, *278*, 119347.

(102) Liu, Z.; Dong, S.; Zou, D.; Ding, J.; Yu, A.; Zhang, J.; Shan, C.; Gao, G.; Pan, B. Electrochemically Mediated Nitrate Reduction on Nanoconfined Zero Valent Iron: Properties and Mechanism. *Water Res*. **2020**, *173*, 115596.

(103) Zeng, H.; Zhao, X.; Zhao, F.; Park, Y.; Sillanpää, M. Accelerated Fe^{3+}/Fe^{2+} Cycle Using Atomic H* on Pd/Al_2O_3: A Novel Mechanism for an Electrochemical System with Particle Electrode for Iron Sludge Reduction in the Fe^{2+}/Peroxydisulfate Oxidation Process. *Chem. Eng. J*. **2020**, *382*, 122972.

(104) Georgi, A.; Velasco Polo, M.: Crincoli, K.; Mackenzie, K.; Kopinke, F. Accelerated Catalytic Fenton Reaction with Traces of Iron: An Fe-Pd-Multicatalysis Approach. *Environ. Sci. Technol*. **2016**, *50*, 5882-5891.

(105) Liu, X.; Gao, S.; Fan, J.; Li, X.; Qin, H.; Wang, J.; Ma, S.; Liu, Z.; Yu, Y. The Construction of Accelerated Catalytic Fenton Reaction Based on Pd/MIL-101(Cr) and H_2. *New J. Chem*. **2019**, *43*, 8179-8188.

(106) Deng, F.; Olvera-Vargas, H.; Garcia-Rodriguez, O.; Qiu, S.; Ma, F.; Chen, Z.; Lefebvre, O. Unconventional Electro-Fenton Process Operating at a Wide pH Range with Ni Foam Cathode and Tripolyphosphate Electrolyte. *J. Hazard. Mater*. **2020**, *396*, 122641.

(107) Liu, X.; Li, W.; Wang, Y.; Zhou, G.; Wang, Y.; He, C.; Wang, G.; Mu, Y. Cathode-Introduced Atomic H* for Fe(II)-Complex Regeneration to Effective Electro-Fenton Process at a Natural pH. *Environ. Sci. Technol*. **2019**, *53*, 6927-6936.

(108) Han, Y.; Zhang, K.; Lu, Q.; Wu, Z.; Li, J. Performance and Mechanism of Nickel Hydroxide Catalyzed Reduction of N-Nitrosodimethylamine by Iron. *Sci. Total Environ.* **2021**, *772*, 145550.

(109) Tang, J.; Wang, J. Metal Organic Framework with Coordinatively Unsaturated Sites as Efficient Fenton-Like Catalyst for Enhanced Degradation of Sulfamethazine. *Environ. Sci. Technol*. **2018**, *52*, 5367-5377.

(110) Gao, C.; Su, Y.; Quan, X.; Sharma, V. K.; Chen, S.; Yu, H.; Zhang, Y.; Niu, J. Electronic Modulation of Iron-Bearing Heterogeneous Catalysts to Accelerate Fe(III)/Fe(II) Redox Cycle for Highly Efficient Fenton-Like Catalysis. *Appl. Catal. B: Environ*. **2020**, *276*, 119016.

(111) Yang, T.; Yu, D.; Wang, D.; Yang, T.; Li, Z.; Wu, M.; Petru, M., Crittenden, J. Accelerating Fe(III)/Fe(II) Cycle via Fe(II) Substitution for Enhancing Fenton-Like Performance of Fe-MOFs. *Appl. Catal. B: Environ*. **2021**, *286*, 119859.

(112) Shen, X.; Xiao, F.; Zhao, H.; Chen, Y.; Fang, C.; Xiao, R.; Chu, W.; Zhao, G. In situ-Formed PdFe Nanoalloy and Carbon Defects in Cathode for Synergic Reduction-Oxidation of Chlorinated Pollutants in Electro-Fenton Process. *Environ. Sci. Technol*. **2020**, *54*, 4564-4572.

(113) Zhou, Y.; Liu, X.; Zhao, Y.; Luo, S.; Wang, L.; Yang, Y.; Oturan, M. A.; Mu, Y. Structure-Based Synergistic Mechanism for the Degradation of Typical Antibiotics in Electro-Fenton Process Using Pd–Fe_3O_4 Model Catalyst: Theoretical and Experimental Study. *J. Catal.* **2018**, *365*, 184-194.

(114) Zheng, W.; Liu, Y.; Liu, F.; Wang, Y.; Ren, N.; You, S. Atomic Hydrogen in Electrocatalytic Systems: Generation, Identification, and Environmental Applications. *Water Res.* **2022**, *223*, 118994.

(115) Hayyan, M.; Hashim, M. A.; AlNashef, I. M. Superoxide Ion: Generation and Chemical Implications. *Chem. Rev*. **2016**, *116*, 3029-3085.

(116) Dedushko, M. A.; Pikul, J. H.; Kovacs, J. A. Superoxide Oxidation by a Thiolate-Ligated Iron Complex and Anion Inhibition. *Inorg. Chem*. **2021**, *60*, 7250-7261.

(117) Zhu, Y.; Qiu, S.; Deng, F.; Zheng, Y.; Li, K.; Ma, F.; Liang, D. Enhanced Degradation of Sulfathiazole by Electro-Fenton Process Using a Novel Carbon Nitride Modified Electrode. *Carbon* **2019**, *145*, 321-332.

(118) Zhang, Y.; Li, J.; Bai, J.; Li, L.; Xia, L.; Chen, S.; Zhou, B. Dramatic Enhancement of Organics Degradation and Electricity Generation via Strengthening Superoxide Radical by Using a Novel 3D AQS/PPy-GF cathode. *Water Res*. **2017**, *125*, 259-269.

(119) Jiang, Y.; Chen, Z.; Li, M.; Xiang, Q.; Wang, X.; Miao, H.; Ruan, W. Degradation of Diclofenac Sodium Using Fenton-Like Technology Based on Nano-Calcium Peroxide. *Sci. Total Environ*. **2021**, *773*, 144801.

(120) Liu, W.; Ai, Z.; Zhang, L. Design of a Neutral Three-Dimensional Electro-Fenton System with Foam Nickel as Particle Electrodes for Wastewater Treatment. *J. Hazard. Mater*. **2012**, *243*, 257-264.

(121) Fang, G.; Gao, J.; Liu, C.; Dionysiou, D. D.; Wang, Y.; Zhou, D. Key Role of Persistent Free Radicals in Hydrogen Peroxide Activation by Biochar: Implications to Organic Contaminant Degradation. *Environ. Sci. Technol*. **2014**, *48*, 1902-1910.

(122) Maschmeyer, T.; Rey, F.; Sankar, G.; Thomas, J. M. Heterogeneous Catalysts Obtained by Grafting Metallocene Complexes Onto Mesoporous Silica. *Nature* **1995**, *378*, 159-162.

(123) Li, R.; Ling, L.; Zhang, W. Single Iron Atom Catalysis: An Environmental Perspective. *Nano Today* **2021**, *38*, 101117.

(124) Yin, Y.; Shi, L.; Li, W.; Li, X.; Wu, H.; Ao, Z.; Tian, W.; Liu, S.; Wang, S.; Sun, H. Boosting Fenton-Like Reactions via Single Atom Fe Catalysis. *Environ. Sci. Technol*. **2019**, *53*, 11391-11400.

(125) An, S.; Zhang, G.; Wang, T.; Zhang, W.; Li, K.; Song, C.; Miller, J. T.; Miao, S.; Wang, J.; Guo, X. High-Density Ultra-Small Clusters and Single-Atom Fe Sites Embedded in Graphitic Carbon Nitride (g-C_3N_4) for Highly Efficient catalytic Advanced Oxidation Processes. *ACS Nano* **2018**, *12*, 9441-9450.

(126) Zuo, S.; Jin, X.; Wang, X.; Lu, Y.; Zhu, Q.; Wang, J.; Liu, W.; Du, Y.; Wang, J. Sandwich Structure Stabilized Atomic Fe Catalyst for Highly Efficient Fenton-Like Reaction at All pH Values. *Appl. Catal. B: Environ*. **2021**, *282*, 119551.

(127) Song, X.; Zhang, H.; Bian, Z.; Wang, H. In Situ Electrogeneration and Activation of H_2O_2 by Atomic Fe Catalysts for the Efficient Removal of Chloramphenicol. *J. Hazard. Mater.* **2012**, *412*, 125162.

(128) Seo, M.; Chung, T. D. Nanoconfinement Effects in Electrochemical Reactions. *Curr. Opin. Electrochem*. **2019**, *13*, 47-54.

(129) Qian, J.; Gao, X.; Pan, B. Nanoconfinement-Mediated Water Treatment: from Fundamental to Application. *Environ. Sci. Technol*. **2020**, *54*. 8509-8526.

(130) Derouane, E. G. The Energetics of Sorption by Molecular Sieves: Surface Curvature Effects. *Chem. Phys. Lett*. **1987**, *142*, 200-204.

(131) Khlobystov, A. N.; Britz, D. A.; Briggs, G. A. D. Molecules in Carbon Nanotubes. *Accounts Chem. Res*. **2005**, *38*, 901-909.

(132) Yang, Z.; Qian, J.; Yu, A.; Pan, B. Singlet Oxygen Mediated Iron-Based Fenton-Like Catalysis Under Nanoconfinement. *Proceed. Nat. Acad. Sci*. **2019**, *116*, 6659-6689.

(133) Chen, S.; Wu, G.; Sha, M.; Huang, S. Transition of Ionic Liquid [bmim][PF6] from Liquid to High-Melting-Point Crystal When Confined in Multiwalled Carbon Nanotubes. *J. Am. Chem. Soc*. **2007**, *129*, 2416-2417.

(134) Su, P.; Zhou, M.; Ren, G.; Lu, X.; Du, X.; Song, G. A. Carbon Nanotube-Confined Iron Modified Cathode with Prominent Stability and Activity for Heterogeneous Electro-Fenton Reactions. *J. Mater. Chem.* A. **2019**, *7*, 24408-24419.

(135) Zhang, S.; Sun, M.; Hedtke, T.; Deshmukh, A.; Zhou, X.; Weon, S.; Elimelech, M.; Kim, J. Mechanism of Heterogeneous Fenton Reaction Kinetics Enhancement Under Nanoscale Spatial Confinement. *Environ. Sci. Technol*. **2020**, *54*, 10868-10875.

(136) Shermukhamedov, S. A.; Nazmutdinov, R. R.; Bronshtein, M. D.; Probst, M. Confinement Effect on Heterogeneous Electron Transfer in Aqueous Solutions Inside Conducting Nanotubes. *ChemElectroChem* **2021**, *8*, 563-569.

(137) Ouyang, Q.; Kou, F.; Zhang, N.; Lian, J.; Tu, G.; Fang, Z. Tea Polyphenols Promote Fenton-Like Reaction: pH Self-Driving Chelation and Reduction Mechanism. *Chem. Eng. J*. **2019**, *366*, 514-522.

(138) Li, D.; Yu, J.; Jia, J.; He, H.; Shi, W.; Zheng, T.; Ma, J. Coupling Electrode Aeration and Hydroxylamine for the Enhanced Electro-Fenton Degradation of Organic Contaminant: Improving H_2O_2 Generation, Fe^{3+}/Fe^{2+} Cycle and N_2 Selectivity. *Water Res*. **2022**, *214*, 118167.

(139) Li, D.; Zheng, T.; Liu, Y.; Hou, D.; Yao, K. K.; Zhang, W.; Song, H.; He, H.; Shi, W.; Wang, L.; Ma, J. A Novel Electro-Fenton Process Characterized by Aeration from Inside a Graphite Felt Electrode with Enhanced Electrogeneration of H_2O_2 and Cycle of Fe^{3+}/Fe^{2+}. *J. Hazard. Mater*. **2020**, *396*, 122591.

(140) Cui, J.; Wang, X.; Zhang, J.; Qiu, X.; Wang, D.; Zhao, Y.; Xi, B.; Alshawabkeh, A. N.; Mao, X. Disilicate-Assisted Iron Electrolysis for Sequential Fenton-Oxidation and Coagulation of Aqueous Contaminants. *Environ. Sci. Technol*. **2017**, *51*, 8077-8084.

(141) Guan, X.; Dong, H.; Ma, J. Influence of Phosphate, Humic acid and Silicate on the Transformation of Chromate by Fe(II) Under Suboxic Conditions. *Sep. Purif. Technol*. **2011**, *78*, 253-260.

(142) Wang, L.; Cao, M.; Ai, Z.; Zhang, L. Dramatically Enhanced Aerobic Atrazine Degradation with $Fe@Fe_2O_3$ Core-Shell Nanowires by Tetrapolyphosphate. *Environ. Sci. Technol*. **2014**, *48*, 3354-3362.

(143) Deng, F.; Li, S.; Zhou, M.; Zhu, Y.; Qiu, S.; Li, K.; Ma, F.; Jiang, J. A. Biochar Modified Nickel-Foam Cathode with Iron-Foam Catalyst in Electro-Fenton for Sulfamerazine Degradation. *Appl. Catal. B: Environ*. **2019**, *256*, 117796.

(144) Olvera-Vargas, H.; Wee, V. Y. H.; Garcia-Rodriguez, O.; Lefebvre, O. Near-Neutral Electro-Fenton Treatment of Pharmaceutical Pollutants: Effect of Using a Triphosphate Ligand and BDD Electrode. *ChemElectroChem* **2019**, *6*, 937-946.

(145) Deng, F.; Qiu, S.; Zhu, Y.; Zhang, X.; Yang, J.; Ma, F. Tripolyphosphate-Assisted Electro-Fenton Process for Coking Wastewater Treatment at Neutral pH. *Environ. Sci. Pollut. Res*. **2019**, *26*, 11928-11939.

(146) Yang, Z.; Wu, S.; Sun, H.; Arhin, S. G.; Papadakis, V. G.; Goula, M. A.; Liu, G.; Zhang, Y.; Zhou, L.; Wang, W. Efficient Degradation of Organic Compounds in Landfill Leachate via Developing Bio-Electro-Fenton Process. *J. Environ. Manage.* **2022**, *319*, 115719.

(147) Kahoush, M.; Behary, N.; Cayla, A.; Nierstrasz, V. Bio-Fenton and Bio-Electro-Fenton as Sustainable Methods for Degrading Organic Pollutants in Wastewater. *Process Biochem.* **2018**, *64*, 237-247.

(148) Hassan, M.; Olvera-Vargas, H.; Zhu, X.; Zhang, B.; He, Y. Microbial Electro-Fenton: An Emerging and Energy-Efficient Platform for Environmental Remediation. *J. Power Sources* **2019**, 424, 220-244.

(149) Olvera-Vargas, H.; Trellu, C.; Oturan, N.; Oturan, M. A. *Bio-Electro-Fenton: A New Combined Process-Principles and Applications*, in: Zhou, M.; Oturan, M. A.; Sirés, I. (Eds.), Springer Singapore, Singapore, 2018, pp. 29-56.

(150) Feng, C.; Li, F.; Mai, H.; Li, X. Bio-Electro-Fenton Process Driven by Microbial Fuel Cell for Wastewater Treatment. *Environ. Sci. Technol*. **2010**, *44*, 1875-1880.

(151) Wang, X.; Liu, C.; Yuan, Y.; Li, F. Arsenite Oxidation and Removal Driven by a Bio-Electro-Fenton Process Under Neutral pH Conditions. *J. Hazard. Mater*. **2014**, *275*, 200-209.

(152) Jo, C.; Song, X.; Zhou, M. Enhanced Tetracycline Removal by Bioelectro-Fenton Through Boosting Fe^{2+}/Fe^{3+} Cycle from Microbial Iron Conversion. *J. Clean. Prod*. **2022**, *366*, 132905.

(153) Birjandi, N.; Younesi, H.; Ghoreyshi, A. A.; Rahimnejad, M. Electricity Generation Through Degradation of Organic Matters in Medicinal Herbs Wastewater Using Bio-Electro-Fenton System. *J. Environ. Manage*. **2016**, *180*, 390-400.

(154) Sathe, S. M.; Chakraborty, I.; Doki, M. M.; Dubey, B. K.; Ghangrekar, M. M. Waste-Derived Iron Catalyzed Bio-Electro-Fenton Process for the Cathodic Degradation of Surfactants. *Environ. Res*. **2022**, *212*, 113141.

(155) Li, X.; Chen, S.; Angelidaki, I.; Zhang, Y. Bio-Electro-Fenton Processes for Wastewater Treatment: Advances and Prospects. *Chem. Eng. J*. **2018**, *354*, 492-506.

(156) Ganiyu, S. O.; Martínez-Huitle, C. A. The Use of Renewable Energies Driving Electrochemical Technologies for Environmental Applications. *Curr. Opin. Electrochem*. **2020**, *22*, 211-220.

(157) Huang, L.; Wang, Q.; Jiang, L.; Zhou, P.; Quan, X.; Logan, B. E. Adaptively Evolving Bacterial Communities for Complete and Selective Reduction of Cr(VI), Cu(II), and Cd(II) in Biocathode Bioelectrochemical Systems. *Environ. Sci. Technol*. **2015**, *49*, 9914-9924.

(158) Wang, G.; Tang, K.; Jiang, Y.; Andersen, H. R.; Zhang, Y. Regeneration of Fe(II) from Fenton-Derived Ferric Sludge Using a Novel Biocathode. *Bioresour. Technol*. **2020**, *318*, 124195.

(159) Wang, G.; Jiang, Y.; Tang, K.; Zhang, Y.; Andersen, H. R. Efficient Recovery of Dissolved Fe(II) from Near Neutral pH Fenton via Microbial Electrolysis. *J. Hazard. Mater.* **2022**, *436*, 129196.

(160) Weber, K. A.; Achenbach, L. A.; Coates, J. D. Microorganisms Pumping Iron: Anaerobic Microbial Iron Oxidation and Reduction. *Nat. Rev. Microbiol*. **2006**, *4*, 752-764.

(161) Cui, Z.; Fu, L.; Zhao, Q.; Zhou, D. Iron-Reducing Bacteria in Water Regeneration and Energy Conversion. *Acta Microbiol*. **2021**, *61*, 2219-2235.

(162) Alves, M. N.; Neto, S. E.; Alves, A. S.; Fonseca, B. M.; Carrêlo, A.; Pacheco, I.; Paquete, C. M.; Soares, C. M.; Louro, R. O. Characterization of the Periplasmic Redox Network that Sustains the Versatile Anaerobic Metabolism of *Shewanella oneidensis* MR-1. *Front. Microbiol*. **2015**, *6*, 665.

(163) Richardson, D. J. Bacterial Respiration: A Flexible Process for a Changing Environment-1999 Fleming Lecture. *Microbiology* **2000**, *146*, 551-571.

(164) Nevin, K. P.; Lovley, D. R. Lack of Production of Electron-Shuttling Compounds or Solubilization of Fe(III) During Reduction of Insoluble Fe(III) Oxide by *Geobacter metallireducens*. *Appl. Environ. Microbiol*. **2000**, *66*, 2248-2251.

(165) Reguera, G.; McCarthy, K. D.; Mehta, T.; Nicoll, J. S.; Tuominen, M. T.; Lovley, D. R. Extracellular Electron Transfer via Microbial Nanowires. *Nature* **2005**, *435*, 1098-1101.

(166) Deng, F.; Li, S.; Cao, Y.; Fang, M.; Qu, J.; Chen, Z.; Qiu, S. A Dual-Cathode Pulsed Current Electro-Fenton System: Improvement for H_2O_2 Accumulation and Fe^{3+} Reduction. *J. Power Sources* **2020**, *466*, 228342.

(167) Burdyny, T.; Smith, W. A. CO_2 Reduction on Gas-Diffusion Electrodes and Why Catalytic Performance Must Be Assessed at Commercially Relevant Conditions. *Energy Environ. Sci*. **2019**, *12*, 1442-1453.

(168) Liang, J.; Xiang, Q.; Lei, W.; Zhang, Y.; Sun, J.; Zhu, H.; Wang, S. Ferric Iron Reduction Reaction Electro-Fenton with Gas Diffusion Device: A Novel Strategy for Improvement of Comprehensive Efficiency in Electro-Fenton. *J. Hazard. Mater.* **2021**, *412*, 125195.

(169) Singh, M.; Sahoo, A.; Yadav, K. I.; Sharma, Y. Role of Magnetism Present in the Cobaltites (ACo_2O_4 A = Co, Mn, and Fe) on the Charge Storage Mechanism in Aqueous Supercapacitor. *Appl. Surf. Sci*. **2021**, *568*, 150966.

(170) Tschöpe, A.; Franzreb, M. Influence of Non-Conducting Suspended Solids Onto the Efficiency of Electrochemical Reactors Using Fluidized Bed Electrodes. *Chem. Eng. J*. **2021**, *424*, 130322.

(171) Ren, J.; Zhu, Z.; Qiu, Y.; Yu, F.; Ma, J.; Zhao, J. Magnetic Field Assisted Adsorption of Pollutants from an Aqueous Solution: A Review. *J. Hazard. Mater*. **2021**, *408*, 124846.

(172) Coey, J. M. D.; Dunne, P. Patterning Metallic Electrodeposits with Magnet Arrays. *Phys. Rev*. *B* **2012**, *85*, 224411.

(173) Monzon, L. M. A.; Coey, J. M. D. Magnetic Fields in Electrochemistry: The Kelvin Force. A Mini-Review. *Electrochem. Commun*. **2014**, *42*, 42-45.

(174) Monzon, L. M. A.; Coey, J. M. D. Magnetic Fields in Electrochemistry: The Lorentz Force. A Mini-Review. *Electrochem. Commun*. **2014**, *42*, 38-41.

(175) Roy, K.; Devi, P.; Kumar, P. Magnetic-Field Induced Sustainable Electrochemical Energy Harvesting and Storage Devices: Recent Progress, Opportunities, and Future Perspectives. *Nano Energy* **2001**, *87*, 106119.

(176) Pan, Y.; Wang, Q.; Zhou, M.; Cai, J.; Tian, Y.; Zhang, Y. Kinetic and Mechanism Study of UV/Pre-Magnetized-Fe^0/Oxalate for Removing Sulfamethazine. *J. Hazard. Mater*. **2020**, *398*, 122931.

(177) Tian, Y.; Fu, W.; Wang, Q.; Tang, Y.; Zhou, M. High Electron Transfer Rate and Efficiency on Fe^0 Modified by Sulfidation and Pre-Magnetization for Carbamazepine Degradation by Heterogeneous Electro-Fenton in Wide pH Ranges. *Chem. Eng. J*. **2022**, *427*, 131694.

(178) Madsen, H. E. L. Influence of Magnetic Field on the Precipitation of Some Inorganic Salts. *J. Cryst. Growth* **1995**, *152*, 94-100.

(179) Dunne, P.; Coey, J. M. D, Influence of a Magnetic Field on the Electrochemical Double Layer. *J. Phys. Chem*. C **2019**, *123*, 24181-24192.

(180) Romero, J.; Prima-Garcia, H.; Varela, M.; Miralles, S. G.; Oestreicher, V.; Abellán, G.; Coronado, E. Giant Enhancement in the Supercapacitance of NiFe-Graphene Nanocomposites Induced by a Magnetic Field. *Adv. Mater*. **2019**, *31*, 1900189-1900213.

(181) Tian, Y.; Zhou, M.; Pan, Y.; Cai, J.; Ren, G, Pre-Magnetized Fe^0 as Heterogeneous Electro-Fenton Catalyst for the Degradation of p-Nitrophenol at Neutral pH. *Chemosphere* **2020**, *240*, 124962.

(182) Yang, L. Effect of Rapid Cathode Rotation and Magnetic Fields on Crystal Orientation in Electrodeposited Metals. *J. Electrochem. Soc*. **1954**, *101*, 456-469.

(183) Jiang, X.; Qiao, J.; Lo, L. M. C.; Wang, L.; Guan, X.; Lu, Z.; Zhou, G.; Xu, C. Enhanced Paramagnetic Cu^{2+} Ions Removal by Coupling a Weak Magnetic Field with Zero Valent Iron. *J. Hazard. Mater*. **2015**, *283*, 880-887.

(184) Ding, Y.; Zhou, W.; Xie, L.; Chen, S.; Gao, J.; Sun, F.; Zhao, G.; Qin, Y. Pulsed Electrocatalysis Enables an Efficient 2-Electron Oxygen Reduction Reaction for H_2O_2 Production. *J. Mater. Chem. A* **2021**, *9*, 15948-15954.

(185) Ding, Y.; Xie, L.; Zhou, W.; Sun, F.; Gao, J.; Yang, C.; Zhao, G.; Qin, Y.; Ma, J. Pulsed Electrocatalysis Enables the Stabilization and Activation of Carbon-Based Catalysts Towards H_2O_2 Production. *Appl. Catal. B: Environ*. **2022**, *316*, 121688.

(186) Liu, T.; Wang, J.; Yang, X.; Gong, M. A Review of Pulse Electrolysis for Efficient Energy Conversion and Chemical Production. *J. Energy Chem.* **2021**, *59*, 69-82.

(187) Qiang, Z.; Chang, J.; Huang, C. Electrochemical Regeneration of Fe^{2+} in Fenton Oxidation Processes. *Water Res.* **2003**, *37*, 1308-1319.

(188) Pei, S.; Teng, J.; Ren, N.; You, S. Low-Temperature Removal of Refractory Organic Pollutants by Electrochemical Oxidation: Role of Interfacial Joule Heating Effect. *Environ. Sci. Technol.* **2020**, *54*, 4573-4582.

(189) Zhang, Q.; Jing, B.; Qiu, S.; Cui, C.; Zhu, Y.; Deng, F. A Mechanism in Boosting H_2 Generation: Nanotip-Enhanced Local Temperature and Electric Field with the Boundary Layer. *J. Colloid Interface Sci.* **2023**, *629*, 755-765.

(190) Ping, Z. Y.; Guo, W. Y.; Hua, Q. B.; Chun, Y. H. Cathode-Control Alloying at an Au-ZnSe Nanowire Contact via in Situ Joule Heating. *Chin. Phys. Lett*. **2012**, *29*, 88105.

(191) Pei, S.; Shen, C.; Zhang, C.; Ren, N.; You, S. Characterization of the Interfacial Joule Heating Effect in the Electrochemical Advanced Oxidation Process. *Environ. Sci. Technol*. **2019**, *53*, 4406-4415.

(192) Coria, G.; Pérez, T.; Sirés, I.; Brillas, E.; Nava, J. L. Abatement of the Antibiotic Levofloxacin in a Solar Photoelectro-Fenton Flow Plant: Modeling the Dissolved Organic Carbon Concentration-Time Relationship. *Chemosphere* **2018**, *198*, 174-181.

(193) Xu, J.; Olvera-Vargas, H.; Teo, F. Y. H.; Lefebvre, O. A Comparison of Visible-Light Photocatalysts for Solar Photoelectrocatalysis Coupled to Solar Photoelectro-Fenton: Application to the Degradation of the Pesticide Simazine. *Chemosphere* **2021**, *276*, 130138.

(194) Ye, Z.; Schukraft, G. E. M.; Hermitte, A. L.; Xiong, Y.; Brillas, E.; Petit, C.; Sirés, I. Mechanism and Stability of an Fe-Based 2D MOF During the Photoelectro-Fenton Treatment of Organic Micropollutants under UVA and Visible Light Irradiation. *Water Res*. **2020**, *184*, 115986.

(195) Xu, A.; Brillas, E.; Han, W.; Wang, L.; Sirés, I. On the Positive Effect of UVC Light During the Removal of Benzothiazoles by Photoelectro-Fenton with UVA Light. *Appl. Catal. B: Environ.* **2019**, *259*, 118127.

(196) Sun, Y.; Pignatello, J. J. Photochemical Reactions Involved in the Total Mineralization of 2,4-D by Iron/Pydrogen peroxide/UV. *Environ. Sci. Technol.* **1993**, *27*, 304-310.

(197) Bates, H. G. C.; Uri, N. Oxidation of Aromatic Compounds in Aqueous Solution by Free Radicals Produced by Photo-excited Electron Transfer in Iron Complexes. *J. Am. Chem. Soc.* **1953**, *75*, 2754-2759.

(198) Zhu, Y.; Deng, F.; Qiu, S.; Ma, F.; Zheng, Y.; Gao, L. A self-Sufficient Electro-Fenton System with Enhanced Oxygen Transfer for Decontamination of Pharmaceutical Wastewater. *Chem. Eng. J.* **2022**, *429*, 132176.

(199) Yuan, S.; Fan, Y.; Zhang, Y.; Tong, M.; Liao, P. Pd-Catalytic in Situ Generation of H_2O_2 from H_2 and O_2 Produced by Water Electrolysis for the Efficient Electro-Fenton Degradation of Rhodamine B. *Environ. Sci. Technol*. **2011**, *45*, 8514-8520.

(200) Qiu, S.; He, D.; Ma, J.; Liu, T.; Waite, T.D. Kinetic Modeling of the Electro-Fenton Process: Quantification of Reactive Oxygen Species Generation. *Electrochim. Acta* **2015**, *176*, 51-58.

(201) Yu, D.; Wu, F.; He, J.; Bai, L.; Zheng, Y.; Wang, Z.; Zhang, J. Tuned Layered Double Hydroxide-based Catalysts Inducing Singlet Oxygen Evolution: Reactive Oxygen Species Evolution Mechanism Exploration, Norfloxacin Degradation and Catalysts Screen Based on Machine Learning. *Appl. Catal. B: Environ.* **2023**, *320*, 121880.

(202) Deng, F.; Jiang, J.; Sirés, I. State-of-the-Art Review and Bibliometric Analysis on Electro-Fenton Process. *Carbon Lett*. **2022**.

(203) Zhang, L.; Cai, J.; Chen. Y.; Huang, J. Modelling Electrocatalytic Reactions with a Concerted Treatment of Multistep Electron Transfer Kinetics and Local Reaction Conditions. *J. Phys. Condens. Matter* **2021**, 33, 504002.

(204) Zeng, H.; Zhang, G.; Ji, Q.; Liu, H.; Hua, X.; Xia, H.; Sillanpää, M.; Qu, J. pH-Independent Production of Hydroxyl Radical from Atomic H*-Mediated Electrocatalytic H_2O_2 Reduction: A Green Fenton Process Without Byproducts. *Environ. Sci. Technol*. **2020**, *54*, 14725-14731.

(205) Mondal, P. C.; Fontanesi, C.; Waldeck, D. H.; Naaman, R. Spin-Dependent Transport Through Chiral Molecules Studied by Spin-Dependent Electrochemistry. *Accounts Chem. Res*. **2016**, *49*, 2560-2568.

(206) Mishra, D.; Markus, T. Z.; Naaman, R.; Kettner, M.; Göhler, B.; Zacharias, H.; Friedman, N.; Sheves, M.; Fontanesi, C. Spin-Dependent Electron Transmission Through Bacteriorhodopsin Embedded in Purple Membrane. *Proceed. Nat. Acad. Sci.* **2013**, *110*, 14872-14898.

(207) Lee, J.; Lim, J. S.; Yim, G.; Jang, H.; Joo, S. H.; Sa, Y. J. Unveiling the Cationic Promotion Effect of H_2O_2 Electrosynthesis Activity of O-Doped Carbons. *ACS Appl Mater Interfaces* 2021, *13*, 59904-59914.

(208) Zhang, X.; Zhao, X.; Zhu, P.; Adler, Z.; Wu, Z.; Liu, Y.; Wang, H. Electrochemical Oxygen Reduction to Hydrogen Peroxide at Practical Rates in Strong Acidic Media. *Nat Commun*. **2022**, *13*, 2880.

(209) Zhu, S.; Hu, X.; Shao, M. Impacts of Anions on the Oxygen Reduction Reaction Kinetics on Platinum and Palladium Surfaces in Alkaline Solutions. *Phys. Chem. Chem. Phys*. **2017**, *19*, 7631-7641.

(210) Salmerón, I.; Oller; I.; Plakas, K. V.; Malato, S. Carbon-based Cathodes Degradation during Electro-Fenton Treatment at Pilot Scale: Changes in H_2O_2 Electrogeneration. *Chemosphere* **2021**, *275*, 129962.

(211) An, J.; Li, N.; Wan, L.; Zhou, L.; Du, Q.; Li, T.; Wang, X. Electric Field Induced Salt Precipitation into Activated Carbon Air-Cathode Causes Power Decay in Microbial Fuel Cells. *Water Res*. **2017**, *123*, 369-377.

(212) Olvera-Vargas, H.; Gore-Datar, N.; Garcia-Rodriguez, O.; Mutnuri, S.; Lefebvre, O. Electro-Fenton Treatment of Real Pharmaceutical Wastewater Paired with a BDD Anode: Reaction Mechanisms and Respective Contribution of Homogeneous and Heterogeneous OH. *Chem. Eng. J*. **2022**, *402*, 126524.

(213 Salmerón, I.; Plakas, K. V.; Sirés, I.; Oller, I.; Maldonado, M.; Karabelas, I.; Anastasios, J.; Sixto, M. Optimization of Electrocatalytic H_2O_2 Production at Pilot Plant Scale for Solar-assisted Water Treatment. *Appl. Catal. B: Environ*. **2019**, *242*, 327-336.

(214) Nidheesh, P. V.; Ganiyu, S. O.; Martínez-Huitle, C. A.; Mousset, E.; Olvera-Vargas, H.; Trellu, C.; Zhou, M.; Oturan, M. A. Recent Advances in Electro-Fenton Process and its Emerging Applications. *Crit. Rev. Environ. Sci. Technol*. **2022**, 1-27.

(215) Nidheesh, P. V.; Ganiyu, S. O.; Kuppam, C.; Mousset, E.; Samsudeen, N.; Olvera-Vargas, H.; Kumar, G. Bioelectrochemical Cells as a Green energy Source for Electrochemical Treatment of Water and Wastewater. *J. Water Process. Eng.* **2022**, *50*, 103232.

(216) Nidheesh, P. V.; Trellu, C.; Olvera Vargas, H.; Mousset. E.; Ganiyu, S. O.; Oturan, M. A. Electro-Fenton process in Combination with Other Advanced Oxidation Processes: Challenges and Opportunities. *Curr. Opin. Electrochem.* **2023**, *37*, 1-1171.

(217) Zhao, X.; Chen, J.; Guo, M.; Li, C.; Hou, N.; Bai, S. Constructed Wetlands Treating Synthetic Wastewater in Response to Day-Night Alterations: Performance and Mechanisms. *Chem. Eng. J*. **2022**, *446*, 137460, 1385-8947.

(218) Olvera-Vargas, H.; Dubuc, J.; Wang, Z.; Coudert, L.; Neculita, C. M.; Lefebvre, O. Electro-Fenton beyond the Degradation of Organics: Treatment of Thiosalts in Contaminated Mine Water. *Environ. Sci. Technol*. **2021**, 55, 2564-2574.

(219) Qu. J. H.; Tian. X.; Zhang. X. B.; Yao. J. Y.; Xue. J. Q.; Li. K. G.; Zhang B.; Wang. L.; Zhang. Y. Free Radicals-Triggered Reductive and Oxidative Degradation

of Highly Chlorinated Compounds via Regulation of Heat-Activated Persulfate by Low-Molecular-Weight Organic Acids. *Appl. Catal. B: Environ*. **2022**, *310*, 121359.

(220) Ganiyu, S. O.; Sable, S.; Gamal El-Din, M. Advanced Oxidation Processes for the Degradation of Dissolved Organics in Produced Water: A Review of Process Performance, Degradation Kinetics and Pathway. *Chem. Eng. J*. **2022**, *429*, 132492.